

Ph.D. Thesis
Doctor of Philosophy

TUC/ School of
Production Engineering & Management

Topology optimization of polymorphic structures and mechanisms using global and multicriteria optimization

Nikos T. Kaminakis

Chania 2015



Technical
University
of Crete



This Ph.D thesis is approved by:

ADVISORY COMMITTEE

Stavroulakis E. Georgios (Supervisor)

Professor, School of Production Engineering & Management,
Technical University of Crete
.....

Marinakis Yannis (Co-supervisor)

Asst. Professor, School of Production Engineering & Management,
Technical University of Crete
.....

Papalambros Y. Panos (Co-supervisor)

Professor, Department of Mechanical Engineering,
University of Michigan
.....

THESIS EXAMINATION COMMITTEE

Bilalis Nikolaos

Professor, School of Production Engineering & Management,
Technical University of Crete
.....

Tsompanakis Yiannis

Assoc. Professor, School of Environmental Engineering,
Technical University of Crete
.....

Lagaros D. Nikos

Asst. Professor, Department of Civil Engineering,
National Technical University of Athens
.....

Mistakidis Euripidis

Professor, Department of Civil Engineering,
University of Thessaly
.....

Technical University of Crete
School of Production Engineering & Management

University Campus
Δ Building
731 00, Chania, Greece
Phone: +30 28210 37255 & 37305
info@pem.tuc.gr
<http://www.pem.tuc.gr>

This Ph.D research has been co-financed by the European Union (European Social Fund – ESF) and Greek national funds, through the Operational Program “Education and Lifelong Learning”, within the National Strategic Reference Framework (NSRF) – Research Funding Program: HERACLITOUS II. Investing in knowledge society through the European Social Fund.

Η παρούσα έρευνα έχει συγχρηματοδοτηθεί από την Ευρωπαϊκή Ένωση (Ευρωπαϊκό Κοινωνικό Ταμείο – ΕΚΤ) και από εθνικούς πόρους μέσω του Επιχειρησιακού Προγράμματος “Εκπαίδευση και Δια Βίου Μάθηση” του Εθνικού Στρατηγικού Πλαισίου Αναφοράς (ΕΣΠΑ) – Ερευνητικό Χρηματοδοτούμενο Έργο: ΗΡΑΚΛΕΙΤΟΣ II. Επένδυση στην κοινωνία της γνώσης μέσω του Ευρωπαϊκού Κοινωνικού Ταμείου.



Ευρωπαϊκή Ένωση
Ευρωπαϊκό Κοινωνικό Ταμείο



ΥΠΟΥΡΓΕΙΟ ΠΑΙΔΕΙΑΣ & ΘΡΗΣΚΕΥΜΑΤΩΝ, ΠΟΛΙΤΙΣΜΟΥ & ΑΘΛΗΤΙΣΜΟΥ
ΕΙΔΙΚΗ ΥΠΗΡΕΣΙΑ ΔΙΑΧΕΙΡΙΣΗΣ

Με τη συγχρηματοδότηση της Ελλάδας και της Ευρωπαϊκής Ένωσης



Summary

Topology optimization solves the basic engineering design problem of distributing a limited amount of material in a design space in order to form a structure or a mechanism that works in an optimal way. One of the most interesting applications is the synthesis of compliant mechanisms. A compliant mechanism is a flexible monolithic structure that transforms an external load to motion along a specific direction and the same time is stiff enough to bear with the applied forces. Multi-purpose compliant mechanisms are structures with all the above features that are able to deliver two or more different motions depending on the applied load case.

In this thesis a new hybrid algorithm is developed and used for the calculation of optimum structures and flexible mechanisms, which combines features of applicable global optimization, to avoid local minima, and classic topology optimization algorithms.

Topology optimization is used as a conceptual design tool for structures, compliant mechanisms and auxetic materials, etc. Following classical developments, several multi-objective topology optimization problems are first formulated. From numerical experiments it was noticed that when topology optimization starts from initial random material distributions, the resulted structures are different, meaning that local minima arise. Therefore, a hybrid algorithm utilizing the advantages of global optimization techniques, is proposed. The hybrid scheme uses topology optimization as the evaluation tool of the previously mentioned global optimization algorithms.

The majority of materials in nature when stretched in one direction, get thinner in the normal to loading direction, and vice versa. The opposite effect take place in auxetic materials. Auxetic materials are artificial microstructures with properties that may not be found in nature. Their mechanical properties are defined by their structure rather than their composition. The feature that describes them as auxetic, is the negative Poisson's ratio. This auxetic behavior occurs due to their specific internal structure and the way it deforms when the sample is uniaxially loaded. The design of auxetic materials can follow

similar techniques to the compliant mechanism and is presented as an application which leads to new designs of auxetic microstructures. Their effectiveness as well as their response to nonlinearities, are verified using numerical homogenization tools and CAD/CAE software.

Περίληψη

Η τοπολογική βελτιστοποίηση λύνει το βασικό πρόβλημα εύρεσης της καλύτερης κατανομής μιας περιορισμένης ποσότητας υλικού μέσα σε ένα προδιαγεγραμμένο χωρίο, προκειμένου η προκύπτουσα δομή να αποτελεί μια κατασκευή ή ένα μηχανισμό που θα λειτουργεί βέλτιστα. Μία από τις πιο ενδιαφέρουσες εφαρμογές είναι η σύνθεση εύκαμπτων μηχανισμών. Ένας εύκαμπτος μηχανισμός είναι ένα ελαστικό, μονολιθικό σώμα που μετατρέπει τις εξωτερικές φορτίσεις σε κίνηση μέσω της παραμόρφωσης του, κατά μήκος μιας συγκεκριμένης κατεύθυνσης και ταυτόχρονα είναι αρκετά άκαμπτο ώστε να αντέχει τις επιβαλλόμενες φορτίσεις. Οι πολυμορφικοί εύκαμπτοι μηχανισμοί είναι κατασκευές με όλα τα παραπάνω χαρακτηριστικά που είναι σε θέση να παρέχουν δύο ή περισσότερες διαφορετικές κινήσεις, ανάλογα με την επιβαλλόμενη φόρτιση.

Στην παρούσα διατριβή αναπτύσσεται και χρησιμοποιείται υβριδικός αλγόριθμος για τον υπολογισμό κατασκευών και εύκαμπτων μηχανισμών, ο οποίος συνδυάζει χαρακτηριστικά εφαρμόσιμης ολικής βελτιστοποίησης, για την αποφυγή τοπικών ελαχίστων, και κλασικών αλγορίθμων τοπολογικής βελτιστοποίησης. Η τοπολογική βελτιστοποίησης μπορεί να χρησιμοποιηθεί ως ένα εννοιολογικό εργαλείο σχεδιασμού κατασκευών, εύκαμπτων μηχανισμών και αυξητικών υλικών, κ.τ.λ. Η χρήση κλασικών τεχνικών σχεδιασμού βέλτιστων κατασκευών, οδηγεί στην διατύπωση πολυκριτήριων προβλημάτων τοπολογικής βελτιστοποίησης. Από αριθμητικά πειράματα παρατηρήθηκε ότι η έναρξη της τοπολογικής βελτιστοποίησης από τυχαίες αρχικές κατανομές υλικού οδηγεί σε διαφορετικές τελικές λύσεις, κάτι που σημαίνει ότι ο αλγόριθμος εγκλωβίζεται σε τοπικά ελάχιστα. Αυτό το φαινόμενο είναι ιδιαίτερα έντονο στα προβλήματα σχεδιασμού εύκαμπτων μηχανισμών. Ως εκ τούτου, προτείνεται ένας νέος υβριδικός αλγόριθμος που αξιοποιεί τα πλεονεκτήματα τεχνικών ολικής βελτιστοποίησης και χρησιμοποιεί την τοπολογική βελτιστοποίηση ως εργαλείο αξιολόγησης.

Για την πλειοψηφία των υλικών στη φύση, όταν σε αυτά ασκούνται

εφελκυστικές δυνάμεις τότε αυτά γίνονται λεπτότερα στην κάθετα προς τη φόρτιση κατεύθυνση, και το αντίστροφο. Το αντίθετο αποτέλεσμα λαμβάνει χώρα για τα αυξητικά υλικά. Τα αυξητικά υλικά είναι τεχνητές μικροδομές με ιδιότητες που δεν μπορούν να βρεθούν στη φύση. Οι μηχανικές τους ιδιότητες καθορίζονται από τη δομή τους και όχι από τη σύνθεσή τους. Το χαρακτηριστικό που τα περιγράφει ως αυξητικά, είναι ο αρνητικός λόγος Poisson. Η αυξητική συμπεριφορά προκύπτει λόγω της ειδικής εσωτερικής δομής τους και του τρόπου που παραμορφώνονται όταν φορτιστούν μονοαξονικά. Τα αυξητικά υλικά μπορούν να σχεδιαστούν όπως οι εύκαμπτοι μηχανισμοί και ο σχεδιασμός τους παρουσιάζεται στην εργασία αυτή ως εφαρμογή, η οποία οδηγεί σε νέες μορφές αυξητικών μικροδομών. Η αποτελεσματικότητά τους καθώς και η απόκρισή τους σε μη γραμμική περιοχή επαληθεύονται με τη χρήση αριθμητικής ομογενοποίησης και εργαλείων CAD/CAE.

Preface

This Ph.D thesis was prepared at the School of Production Engineering & Management of Technical University of Crete as a partial fulfillment of the requirements for the degree of Doctor of Philosophy.

Chania, October 29, 2015

Nikos T. Kaminakis

Acknowledgements

Firstly, I would like to express my sincere gratitude to my advisor Prof. Stavroulakis Georgios for the continuous support of my Ph.D study and related research, for his patience, motivation, and immense knowledge. His guidance helped me in all the time of research and writing of this thesis. I could not have imagined having a better advisor and mentor for my Ph.D study.

Besides my advisor, I would like to thank the rest of my advisory thesis committee: Prof. Papalambros Panos and Prof. Marinakis Yannis, and my thesis committee: Professors, Bilalis Nikos, Tsompanakis Yannis, Lagaros Nikos, and Mistakidis Euripidis, for their insightful and interesting comments, but also for the hard questions which motivated me to widen my research from various perspectives.

My sincere thanks also goes to Dr. Drosopoulos Georgios, newly elected professor, for all the support, encouragement, advices that he offered me, and for all the stimulating discussions we had the last two, most difficult years. I deeply thank my Colleague, PhD candidate Tairidis George for his very interesting comments regarding my thesis defence (because PAOK we are). I greatly thank my fellow officemate Dr. Spiliopoulou Anastasia for her support, help and interesting chats we had the last six years. Without their precious support it would not be possible to conduct and finally complete this research.

Last but not the least, I would like to thank my family: my parents and my sisters for supporting me spiritually throughout this thesis from and my life in general and my wife Elena for being a continuous source of support, energy and strength, giving me always the courage and will to carry on regardless the difficulties, without her I would not have been able to accomplish this goal.

Contents

Summary	i
Περίληψη	iii
Preface	v
Acknowledgements	vi
Contents	vii
List of Figures	ix
List of Tables	xiii
1 Introduction	1
1.1 Motivation	1
1.2 Objectives and approach	3
1.3 Thesis outline	4
2 Literature Review	5
2.1 Structural optimization	5
2.2 Topology optimization	8
2.3 SIMP alternatives	8
2.4 Application of Topology optimization	10
3 Topology Optimization for structures and compliant mechanisms	14
3.1 Problem formulation for structures	14
3.2 Topology optimization numerical problems	22
3.3 Multiplicity of solutions	25
3.4 Multiple load cases	25
3.5 Topology optimization for the design of compliant mechanisms	30

3.6	Output control	36
4	The Hybrid Scheme	41
4.1	The hybrid solution algorithm	41
4.2	Evolutionary Algorithms	43
4.3	Differential Evolution (DE)	48
4.4	Swarm Intelligence	56
4.5	The hybrid scheme	64
5	Case Study: Compliant mechanisms	68
5.1	Classic compliant mechanisms: Single load case	68
5.2	Polymorphic compliant mechanisms: Two load cases	84
6	Auxetic materials	100
6.1	Auxetic materials	100
6.2	Results: Trusses	103
6.3	Results: Continuous formulation	111
6.4	Using homogenization to verify topology optimization	114
6.5	CAD-CAE Verification	121
6.6	Mechanical behaviour of auxetic structures using nonlinearities	129
7	Conclusions & Future work	134
7.1	Achievements of the thesis	134
7.2	Conclusions	134
7.3	Future work	135
	Bibliography	139

List of Figures

1.1	Design optimization of a cantilever beam.	1
2.1	Galileo's Shape Optimization	6
2.2	Structural optimization categories	7
2.3	An comparison between topology optimized and Michell type optimal structures	9
3.1	Topology Optimization Definition	15
3.2	Graphical representation of the SIMP approach for various penalty coefficients p	16
3.3	The left image indicates the discretization of the design domain into finite elements. Each element is equipped with a density design variable. The right image shows a final topology. White elements indicate absence of material $x_e = 0$. Black cells show presence of material $x_e = 1$. For gray elements the density is $0 < x_e < 1$	17
3.4	Topology optimization iterative local search algorithm.	23
3.5	Checker board regions appears in the classic MBB problem.	24
3.6	Mesh dependency phenomena	24
3.7	Graphic representation of the filter for the mesh dependency problem	26
3.8	Multiple Load cases. On the left: domain definition. In the middle: the resulted structure for one load case. On the right: the resulted structure for two load cases.	26
3.9	A force inverter. One load case definition problem	31
3.10	Two loads case compliant mechanism problem	34
3.11	Maximize $u_{out}^{@X}$ & minimize $u_{out}^{@Y}$	37
3.12	Graphical representation of the domain for the design of a polymorphic compliant mechanism	38
3.13	Two loads case compliant mechanism problem	39

4.1	Multiplicity of solution. First row: several random material distributions used as starting points for the iterative process of topology optimization. Second row: the resulted material distributions. the two from the left for the single load case problem. Two from the right for the multiple load case problem.	42
4.2	A population of 4 individuals, represented as row vectors	46
4.3	One point crossover operator applied to two members of the population	46
4.4	Mutation operator applied to two offsprings that was generated from the crossover operator	47
4.5	Initialization of DE population	50
4.6	Generating the difference: $(\mathbf{b} - \mathbf{c})$	51
4.7	Create the trial vector $\mathbf{u}_i = \mathbf{a} + \beta(\mathbf{b} - \mathbf{c})$	52
4.8	Crossover	53
4.9	Selection	54
4.10	DE differentiations based on a) the base vector selection b) the number of differences used in the mutation operator, and c) the type of the random distribution used for exchanging parameters during crossover.	55
4.11	Particle $\mathbf{x}_i^{(t)}$ with its velocity $\mathbf{v}_i^{(t)}$	59
4.12	Calculations of $\omega_t \mathbf{v}_i^{(t)}$, $(\hat{\mathbf{x}}_i - \mathbf{x}_i^{(t)})$ and $(\hat{\mathbf{g}} - \mathbf{x}_i^{(t)})$	60
4.13	Composition of $c_1 \mathbf{r}_1 (\hat{\mathbf{x}}_i - \mathbf{x}_i^{(t)})$ and $c_2 \mathbf{r}_2 (\hat{\mathbf{g}} - \mathbf{x}_i^{(t)})$	61
4.14	Composition of temporary vector \mathbb{A}	61
4.15	Composition of a new velocity vector $\mathbf{v}_i^{(t+1)}$	62
4.16	Update of position and velocity of particle i for time increment $t + 1$	62
4.17	Initialization of the hybrid scheme	65
4.18	Evolution & evaluation inside the hybrid scheme	66
4.19	The hybrid scheme	67
5.1	Results: Hybrid Scheme, One Load Case, No output control, using DE	70
5.2	Intermediate material distributions for One load case using Differential Evolution	71
5.3	Results for one load case using Particle Swarm Optimization	73
5.4	Intermediate material distributions for One load case using Particle Swarm Optimization	74
5.5	Four Final material distributions using Hybrid Scheme using Differential Evolution for one load case	75

5.6	Four Final material distributions using Hybrid Scheme using PSO for one load case	76
5.7	Results for one load case using Differential Evolution and output control	80
5.8	Results for one load case using Particle Swarm Optimization and output control	82
5.9	Results for two loads case using Differential Evolution	85
5.10	Intermediate material distributions for Two loads case using Differential Evolution	86
5.11	Results for two loads case using Particle Swarm Optimization	88
5.12	Intermediate material distributions for Two loads case using Particle Swarm Optimization	89
5.13	Four Final material distributions using Hybrid Scheme using Differential Evolution for two loads case	91
5.14	Four Final material distributions using Hybrid Scheme using PSO for two loads case	92
5.15	Results for two loads case using Differential Evolution and featuring output control	95
5.16	Results for two loads case using Particles Swarm Optimization and featuring output control	97
6.1	a) Star shaped, two dimensional representative cell using beam elements. Finite element discretization and node numbering. b) The star-shaped cell deformed. Thin lines represents the undeformed shape [TSP97].	101
6.2	Regular and auxetic behaviour of microstructures based on their internal substructure. Blue dotted arrows show the displacements aligned with the applied force direction, while red dotted arrows show the displacements normal to the applied force.	101
6.3	Negative Poisson's ratio resulting from topology optimization of a compliant mechanism.	102
6.4	Auxetic material problem definition	104
6.5	Results: 3x3 subcells, Volume fraction: 40%	105
6.6	Results: 3x3 subcells, Volume fraction: 30%	106
6.7	Results: 6x6 subcells, Volume fraction: 21.3% (3x3: 40%)	107
6.8	Results: 6x6 subcells, equivalent to 3x3 mesh volume 30% volume fraction: 15.9% (3x3: 30%)	108
6.9	Results: 12x12 subcells, Volume fraction: 11.0% (3x3: 40%)	109
6.10	Results: 12x12 subcells, Volume fraction: 8.3% (3x3: 30%)	110

6.11	Continuous formulation with 30x30 elements and volume fraction at $\phi = 20\%$. Poisson's ratio $\nu = -0.192$	112
6.12	Continuous formulation with 30x30 elements and volume fraction at $\phi = 30\%$. Poisson's ratio $\nu = -0.223$	113
6.13	Geometry and mesh of the structure with 3600 plane stress elements.	116
6.14	General loading and boundary conditions applied to the heterogeneous model of the first example.	117
6.15	Initial and deformed position of the hard material for the loading of figure 6.14. Appearance of auxetic behaviour.	118
6.16	Initial and deformed position of the hard material obtained by numerical homogenization (with linear displacement boundary conditions). Appearance of auxetic behaviour.	119
6.17	The effective Poisson's ratio versus Young's modulus of the soft material obtained from the homogenization procedure.	119
6.18	(a) Initial configuration of the hard material (b) A slightly different configuration of the hard material: The circles indicate that the hard material is not in contact with these boundaries.	120
6.19	Initial and deformed position for the case of figure 6.18(b) Top left figure: the hard and the soft material - load direction 1. Top right figure: hard material only - load direction 1. Bottom left figure: hard and soft material - load direction 2. Bottom right figure: hard material only - load direction 2.	121
6.20	Final material distributions for run1 and run2 respectively	123
6.21	Displacements for run1 and run2 respectively	124
6.22	Displacements for case 1 and case 2 respectively	125
6.23	2d CAD modles created in Mechanical CAD softwareCreo 3.0	126
6.24	Finite element setup of case 1	127
6.25	Stress results for each case	128
6.26	Displacement results for each case	128
6.27	Meshes for each case	129
6.28	Mesh of the auxetic material distribution	130
6.29	Auxetic behaviour obtained by linear analysis - von Mises stress distribution (MPa)	130
6.30	Effective Poisson's ratio-external force diagram for non-linear finite element analysis of the auxetic microstructure	131
6.31	Equivalent plastic strain at the end of the auxetic behaviour	132
6.32	Equivalent plastic strain at the end of analysis (no auxetic behaviour)	133

List of Tables

5.1	Topology Optimization Algorithm parameters	69
5.2	Differential Evolution configuration parameters	69
5.3	Particles Swarm Optimization configuration parameters	72
5.4	Results for One load case using Hybrid scheme with DE	76
5.5	Results for One load case using Hybrid scheme with PSO	77
5.6	Running parameters: topology optimization for the design of compliant mechanism using DE, and featuring output control, with a single load case.	78
5.7	Differential Evolution configuration parameters	78
5.8	Results: topology optimization for the design of compliant mechanism using DE, and featuring output control, with a single load case.	79
5.9	Particles Swarm Optimization configuration parameters	81
5.10	Results: topology optimization for the design of compliant mechanism using PSO, and featuring output control, with a single load case.	81
5.11	Results DE vs PSO. Topology optimization for the design of compliant mechanism, featuring output control, with a single load case.	83
5.12	Results for Two loads case using Hybrid scheme with DE	90
5.13	Results for Two loads case using Hybrid scheme with PSO	90
5.14	Running parameters: topology optimization for the design of compliant mechanism using DE, and featuring output control, with a single load case.	93
5.15	Differential Evolution configuration parameters	93
5.16	Numerical Results for two load cases, DE and output control	94
5.17	PSO configuration parameters	96
5.18	Numerical Results for two load cases, PSO and output control	96
5.19	Results DE vs PSO. Topology optimization for the design of compliant mechanism, featuring output control, with two load cases.	99

6.1	Numerical data for several cell configurations	104
6.2	Effective material properties obtained by numerical homogenization, for the hard and soft material distribution given by topology optimization.	118
6.3	Topology Optimization Algorithm configuration parameters for the auxetic mechanism problem with mesh 120×120	122
6.4	Differential Evolution configuration parameters for the auxetic mechanism problem with mesh 120×120	123
6.5	Comparison between	123
6.6	Aluminum Alloy AL6061-T6 mechanical properties.	126
6.7	Numerical results for each case FEA study.	127

CHAPTER 1

Introduction

1.1 Motivation

Seeking the optimum design is not always easy. Actually it is very difficult. For any design process, the engineer firstly drafts the outlines of the product and later tries to optimize it by finding the best design parameters that satisfy project requirements. There are always questions that must be answered and decisions that must be taken. For example in figure 1.1 a load F must be supported using a cantilever beam, with the minimum of material. The questions that may arise are: how big the hole must be in order to save weight and where should be placed?, is it better to place two or more smaller holes instead of one?, which material should be used?, should the borders (in blue) be curves instead of lines?, is it necessary the shape of the hole to be circular?, can the final design be manufactured? Design optimization's goal is to find answer to all above questions.

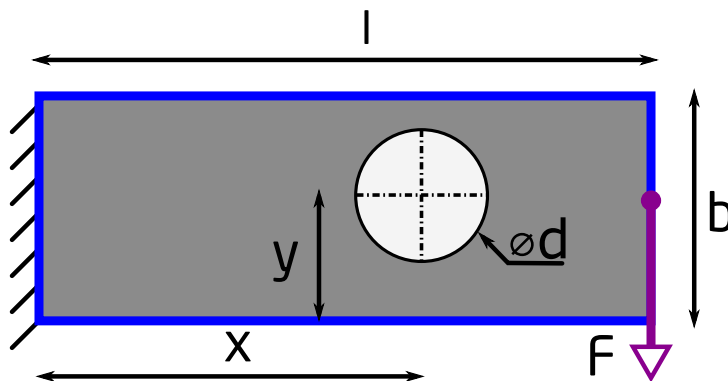


Figure 1.1: Design optimization of a cantilever beam.

Topology optimization seeks to find solution to the problem of what is the optimum way to distribute material inside a predefined area in order for

the resulted structure to behave the best under a given set of loads and constraints. The optimal structure is created without the restrictions concerning its topology, like the assumption that we are looking for a cantilever with holes like in the previous example. Topology optimization is an incredibly powerful tool in many areas of design such as architecture, structural and fluid mechanics, optics and electronics, etc. The basic idea is to optimize a structure such us to use less material than before, but at the same time to be able to behave the same way or even better under the same conditions. Sometimes the resulted structures are very difficult or even impossible to be manufactured using conventional, subtractive procedures like machining a bulk or raw material. Additive manufacturing procedures, like 3D printing, gave the opportunity to build structures that are impossible to achieve otherwise. This method is derived from structural design and so topology optimization applied in this context is also known as structural optimization.

Applying topology optimization to structural design in general, involves considering concepts such as volume, weight, stresses, stiffness, displacements, buckling loads and resonant frequencies, with some of these defining the objective function and others constraining the structure. In other applications, aerodynamic performance, optical performance or conductance may be of interest, in which case the underlying state equations are very different to those considered in the structural case.

In structural design, topology optimization can be regarded as an extension of size and shape optimization. Size optimization considers a structure which can be decomposed into a finite number of members. Each member is then parametrised so that, for example, cross sectional area of the member is the only variable defining the member. Size optimization then seeks to find the optimal values of the parameters defining the members.

Shape optimization is an extension of size optimization in that it allows extra freedoms in the configuration of the structure such as the location of connections between members or location of the holes in the structure or even the shape of the hole. A hole actually may have any shape that does not always have to be a circle. In a more general sense a hole can be represented by a triangle or a polygon of any kind with fillets in its corners, or even a closed NURBS spline. The designs allowed are restricted to a fixed topology and thus can be written using a limited number of optimization variables that may be the number of holes or the size of the edges of the polygons and the value of the fillets.

Topology optimization extends size and shape optimization, by allowing the calculation of the optimal structure without any restriction related to its

type. Its purpose is to search for the optimal layout of material inside a 2- or 3-dimensional design domain. The material must be distributed in such a way that the structure must be feasible so that there are no islands of material inside the design domain. In simpler words, all particles of material must be connected, leaving areas inside the design domain empty as "holes". Furthermore, as Robert le Ricolais quoted "the art of structure is where to put the holes".

1.2 Objectives and approach

When starting to use topology optimization in any problem, one must define some basic concepts, like the design domain, the loads and the boundary conditions, as well as the amount of area or volume that are allowed to use (sometimes mentioned as a fraction of the 2D area or the 3d volume). But is the resulting structure really the optimal one? There are some drawbacks in this method. Checkerboard effects may appear (the resulting structure has areas that look like a checkerboard), the method is mesh-dependent and different final results appear when the method starts from different initial conditions meaning that the method falls into local minima. The later phenomenon appears often in the design of compliant mechanisms.

In order to search for global optima, one must use global optimization techniques, deterministic, stochastic (simulated annealing, Monte-Carlo sampling) or heuristic (genetic algorithms, swarm-based optimization algorithms, differential evolution, etc.). In any case, a large number of design variables must be used that makes the problem impossible to solve.

A new hybrid scheme is proposed, taking advantage from the use of evolutionary algorithms and local search methods. The algorithm creates random initial material distributions that are evaluated using topology optimization. The "initial" resulted structures are being developed according to the evolutionary strategy that is used, until termination criteria are met.

In this hybrid scheme two evolutionary algorithms are used: Differential Evolution (DE), and Particles Swarms Optimization (PSO). The hybrid scheme was used and compared applications such as simple and multifunctional compliant mechanisms, and auxetic materials.

1.3 Thesis outline

The thesis is organized as follows: chapter 2 presents some definitions of structural and topology optimization as well as auxetic materials. Chapter 3 refers to topology optimization, and its problem definition for structures and mechanisms, for one and multiple load case. There is also an implementation of motion control for compliant mechanisms. Chapter 4 presents the hybrid scheme algorithm. There is also a presentation Differential Evolution, and Particle Swarm Optimization. Chapter 5, presents results from the design of compliant mechanism. The example of the asymmetric compliant is used. It is also presented a multiple load case compliant mechanism. Both examples have been studied, initially without output control and subsequently with output control. Chapter 6 presents results for auxetic structures using truss and 2d plane stress elements. The auxetic behaviour of the later verified using modern CAD & CAE software. There is a brief description on the effects of geometric and elastoplastic nonlinearities on the auxetic structures. Finally chapter 7 summarizes the achievements of this work. Ideas for future work are set out as possible topics for further research.

CHAPTER 2

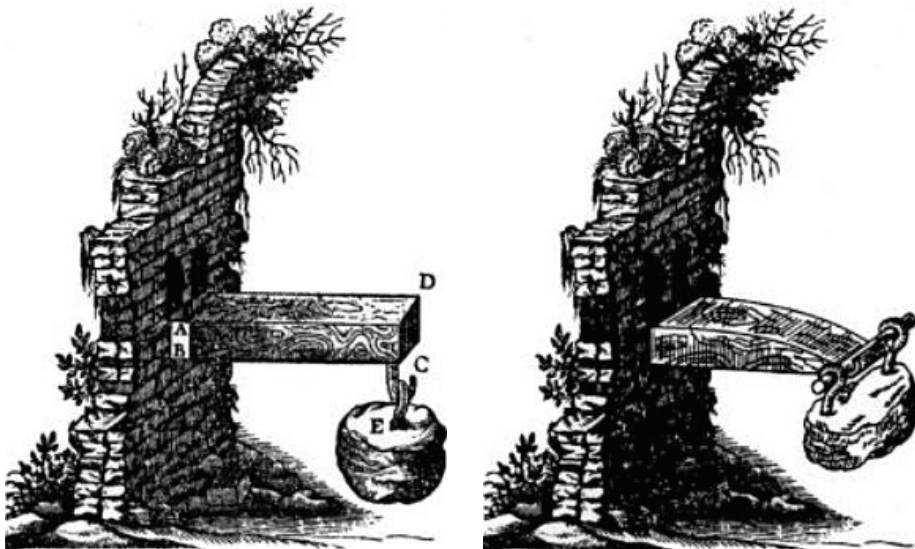
Literature Review

2.1 Structural optimization

A structure can be defined as *any assemblage of materials which is intended to sustain loads* [Gor78]. Optimization is a process of making things optimum. Design optimization is generally defined by Papalambros and Wilde [PW00] as the selection of the *best* design within the available means. Structural optimization is the design and manufacture of a structure that sustains the applied loads (static or dynamic, etc.) in the best way. Galileo Galilei was one of the pioneers in structural optimization. In the second part of his book *Discorsi* [Gal38] published in 1638, he investigated the fracture process of brittle bodies, whereas also the shape of bodies was considered with regard to strength. He also proved that the optimum shape for a beam supported at one end and bearing a load at the other is parabolic (see figure 2.1).

Structural optimization can be classified in three major categories:

- sizing optimization: is the simplest form of structural optimization. The main feature of the sizing optimization is that the shape of the structure (or the design domain) is known and fixed through the optimization process. The objective of the sizing problem is to optimize the structure by adjusting the sizes of the components. Here the design variables are the sizes of the structural elements, for example the diameter of a rod, the thickness or the cross section area of a beam. In any case the optimal values of the design variables minimizes (or maximizes) a physical quantity such as the mean compliance (external work), peak stress, deflection, etc., while equilibrium and other constraints on the state and design variables are satisfied. See 2.2(a) for an example of size optimization where the diameter of the rods are the design variables.
- shape optimization: As with sizing optimization the topology (number of holes, beams, etc.) of the structure is already known when using shape optimization, the shape optimization will not result in new holes

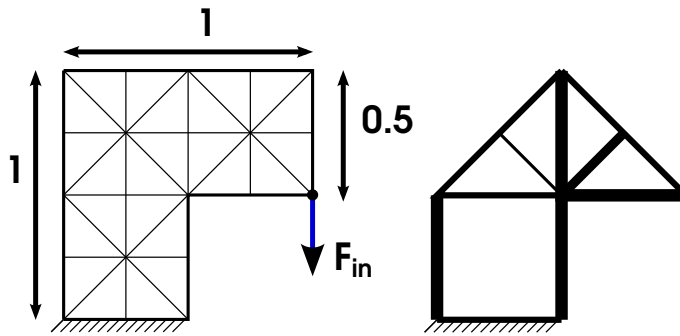


(a) Galileo's original cantilever beam's shape (b) Galileo's optimal cantilever beam's shape

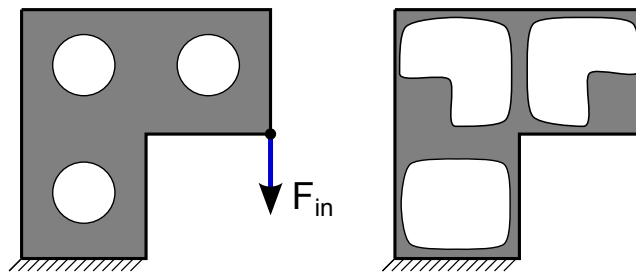
Figure 2.1: Galileo's Shape Optimization

or split bodies apart. In this case, the design variables can, for example, be thickness distribution along structural members, diameter of holes, radii of fillets or any other measure. See 2.2(b) for an example of shape optimization. A fundamental difference between shape vs. topology and size optimization is that instead of having one or more design variables for each element the design variables in shape optimization each affect many elements.

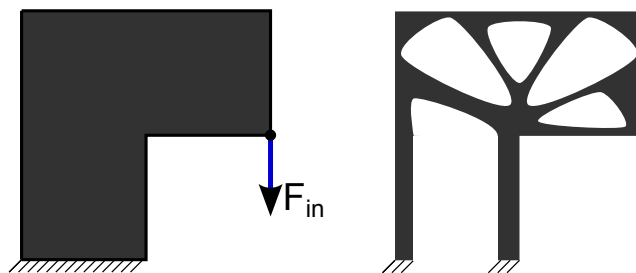
- topology optimization: is the most general form of structural optimization. The main purpose of topology optimization, is to find the optimum material distribution inside a fixed, predefined design domain, in order that, the resulting structure is able to bear with the external loads and satisfy the boundary conditions. See 2.2(c) for an example of topology optimization.



(a) Size Optimization



(b) Shape Optimization



(c) Topology Optimization

Figure 2.2: Structural optimization categories

2.2 Topology optimization

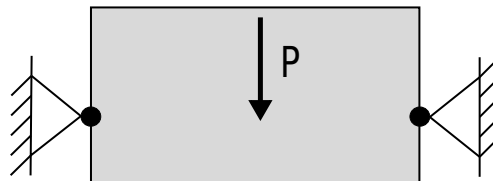
Topology optimization for truss structures has been studied first by Michell [MCE04] in 1904. In his work he presented analytical formulas for structures with minimum weight given stress constraints on various design domains.

Numerical topology optimization has been introduced by Bendsoe & Kikuchi in 1988 when they proposed a homogenization method [BK88]. The main idea of the homogenization method is that a material density is introduced by representing the material as a microstructure. The microstructure is a composite material with an infinite number of infinitely small voids. This leads to a porous composite that can have a density varying between 0% and 100%. In later works [Ben89] Bendsoe removed this discrete nature of the problem by introducing a density function that is a continuous design variable. The resulted shape of the optimized structure is defined by domains of high density [Ben89].

Rozvany *et al.* [RZB92] made a breakthrough by proposing a penalization scheme called SIMP: Solid Isotropic Microstructure with Penalty. Using the SIMP method, the resulted optimal structure is consisted of solid and empty material only. Due to the simplicity in the methodology, SIMP has become a popular approach to structural topology optimization.

2.3 SIMP alternatives

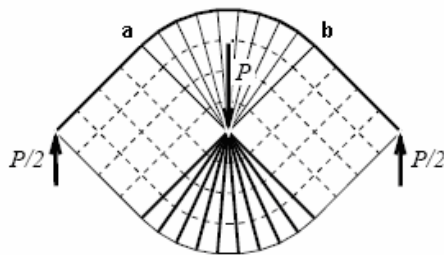
Except the SIMP method that is used widely in topology optimization, there are a lot of other methods that attempt to solve the problem of the optimal layout of material such like the alternative to SIMP method, Evolutionary Structural Optimization (ESO) proposed by Xie and Stevens [XS93], Bi-directional Evolutionary Structural Optimization (BESO) proposed by Querin *et al.* in 2000 [QX00],[Que+00], topological derivatives proposed by Sokolowski in 1999 [SZ99], level set method [OS88], a combination of level set method and ESO [Jia+11] and a new introduced hybrid method based on evolutionary algorithms and local search methods [KS12], [KDS15].



(a) Design domain



(b) Topology optimized solution



(c) Michell type optimal structure

Figure 2.3: An comparison between topology optimized and Michell type optimal structures

2.4 Application of Topology optimization

2.4.1 Compliant mechanisms

A compliant mechanism is a single-piece flexible structure that combines the mobility of a conventional mechanism with the stiffness of a conventional structure. A compliant mechanism utilizes the structural deformation, to transmit force or deliver motion. Due to the absence of joints, a compliant mechanism can also be seen as a structure that is stiff enough to bear the input loads along with the generated stresses.

The non-existence of joints results to compliant mechanisms free of phenomena like joint friction and backlash, while taking away the need for lubrication. Their system integration is easily achieved, and they can be coupled with modern actuators. Their design is scalable and can be equally effective at micro, meso or macro scale. They can be manufactured using a wide range of materials such as steel, aluminum, titanium, glass and carbon fiber reinforced plastics. Due to their monolithic structure there is no need to include springs, fasteners or hinges. The compliant mechanisms are fatigue resistant as a result of the even stress distribution to their through their deformation[Fle15].

A leading application of compliant mechanisms is its use in Micro Electro Mechanical Systems (MEMS) as pressure, acceleration, displacement sensors [KA08] or mechanical amplifiers for piezoelectric actuators [CF00]. Another great application of compliant mechanisms is in aerospace area where they are used to change the shape of an airfoil, and consequently the aerodynamic features of wings and other control areas of an aircraft [Kot+03]. This is referred with the term *airfoil morphing*. Just recently in 2014, the first plane with flexible wings that use compliant mechanisms took off [Ame14].

The major drawback of classical optimal structural design is that the resulting structure depends on the adopted structure and only parametrization gives some flexibility in the search for the optimum. In compliant mechanisms the topology of the structure is not always known from the beginning. Therefore topology optimization method must be applied [BK88; Ben95]. Some applications of the compliant mechanisms are the design force inverters [BS03], of micro-grippers [Sig96], micro-structures with negative thermal expansion ratio [ST99], or negative Poisson's ratio [LSB97], [KS12], structures with multiple output points [FKK99] and contact aided compliant mechanisms [MLF09; MA07].

Compliant mechanisms for single and multiple load cases have been pro-

posed in the past [Alo+13]. Nonconvexity appears with higher severity in the multiple loading case (polymorphic mechanisms), a fact that has already been observed in structural optimization [XS93] and gives no guarantee that simple heuristic iterative solution algorithms will work. For several reasons it would be more suitable to take advantage of the flexibility of general purpose global optimization algorithms (genetic algorithms, evolutionary algorithms etc). Unfortunately, due to the large scale of the arising optimization problems, the lack of experience for the tuning of the involved parameters (like the population size and the coding in genetic optimization, etc) and the huge computing power required [Sig11], the applicability of general purpose, unmodified, global optimization techniques, is not efficient. Several attempts have been published with appropriately modified algorithms, like the genetic algorithm with appropriate handling of design connectivity for structural topology optimization presented in [WT05; MRP06]. Single and multi-criteria optimization problems are formulated. A novel hybrid algorithm is proposed, which is based on the combination of classical, iterative solution algorithms, with evolutionary strategies such as genetic algorithms and particle swarm methods. The results of this work can be used for the design of optimal mechanisms and micromechanisms, for elastic mechanical problems or in multiphysics.

In order to find the best structure that utilizes the above demands (flexibility and stiffness), topology optimization is used. Similarly to structural topology optimization, topology optimization of compliant mechanisms can be performed based on continuum as well as truss and frame discretization. The continuum approach will be followed here. The mechanical modelling techniques are taken from reference [BS03] and it was based on the 99 lines MATLAB code [Sig01]. For the purposes of this thesis, linear finite elements has been used in order to benchmark the method in a much simpler problem which nevertheless leads to nonconvex optimization problems with multiple solutions. The difficulties are expected to be more severe in large deformation problems. Especially, if the design intent is the synthesis of a *path following* compliant mechanism, the use of nonlinear analysis is the only way [PBS01].

2.4.2 Auxetic materials

Auxetic materials have certain properties that make them suitable for a number of novel applications to defence and civil sectors [Liu06]. The negative Poisson's effect is attributed to the microstructure of the material. From experience and analytical investigations a number of auxetic microstructures have

been proposed and studied (re-entrant corners, nonconvex microstructures, nematic mechanisms, etc.). Automatic design of auxetic microstructures that go beyond the classical ones have been proposed using techniques from topology optimization of flexible mechanisms [KS12]. Nevertheless, due to limited ability of topology optimization to deal with all possible design goals, like dynamic behaviour or fatigue resistance, manufacturability, constraints, etc., the result still requires modification. Usage of classical design optimization techniques can be used at this step. The final verification, which indicates that the proposed microstructure has the required properties, is done with numerical homogenization.

Several analytical and numerical approaches have been proposed in the past for the investigation of heterogeneous structures, like composites. Analytical/mathematical methods, like asymptotic homogenization [San80], can be more accurate than numerical methods in the description of the microstructure, for relatively simple microscopic patterns and constitutive laws. On the other hand, numerical methods are suitable for the simulation of complex microscopic geometries, over a statistically defined representative amount of material [ZW08], thus the Representative Volume Element (RVE).

According to numerical homogenization, a unit cell is independently solved and the resulting average quantities are then used for the determination of the parameters of a macroscopic constitutive law [PS00; DBA08]. From another point of view, multi-scale computational homogenization incorporates a concurrent analysis of both the macro and the microstructure in a nested multi-scale approach, [SSB85; Kou02; DWS13a; DWS13b; MPG07; Kan+09; Pin+09; GKB10]. Within this method, the macroscopic response is determined during simulation, after solving the microscopic problem and transferring the necessary information on the macroscopic scale.

Some efforts towards coupling topology optimization and homogenization, have already been reported. In [AJM04] topology optimization and homogenization concepts have been used for a minimum stress design. In [ALS14] a homogenization procedure has been incorporated in the overall optimization procedure. In [NTN13] a multi-scale computational homogenization approach is used in order to take into account nonlinear effects.

The verification of the auxetic behaviour of a microstructure, which is initially obtained by topology optimization is achieved by using numerical homogenization. Verification [ASM06] stands for an independent procedure, according to which numerical homogenization is used to investigate in the microscopic level, the effective material behaviour for the heterogeneous material distribution given by topology optimization. Results regarding effective

Poisson's ratio are compared with the output given by optimization. The homogenization scheme has not been incorporated in the overall topology optimization algorithm, thus homogenization is considered independently of the optimization procedure. First, the material distribution, which is given by topology optimization, is considered. Then, the structure is treated as a heterogeneous one consisting of an existing, hard material and another soft material in the areas of voids. A classical numerical homogenization approach is finally used and the effective Poisson's ratio is estimated. Another way to testify the auxetic behaviour is to draft a 2d NURBS parametric model based on the outcome of the hybrid scheme. An bitmap image that describes the material distribution of the auxetic structure is imported into a CAD application so that a virtual two dimensional model is drafted. The resulted structure is analysed using FEA in order to confirm the auxetic behaviour.

The novelty of the presented work is focused on the combined use of state of the art techniques from the following areas: first the material design problem is solved by using topology optimization for compliant mechanisms design [LSB97]. Furthermore, the arising nonconvex optimization problems for several practical reasons are solved by means of a hybrid algorithm composed of evolutionary algorithms and local search iterations such as to ensure that integral structure appears in each step of the algorithm [KS12]. Finally, the arising microstructure is verified by using numerical homogenization [ZW08].

CHAPTER 3

Topology Optimization for structures and compliant mechanisms

3.1 Problem formulation for structures

3.1.1 Mathematical formulation of the continuum

The optimum material layout problem combines several features from the classic problems of structural optimization. The goal of topology optimization is to find the best material distribution inside a predefined design domain Ω . The body is constrained at its boundaries $^1\Gamma_u$ and $^2\Gamma_{tt}$, while body forces f are applied, along with traction forces t at boundary Γ_t . There are specific areas inside the domain Ω that material must be present and areas that must be void (see subfigure 3.1(a)). The only known parameters are the applied loads, material properties, and boundary conditions along with several side constraints such as areas that material is present or not inside the domain. The optimum distributed material inside the domain Ω is Ω^{mat} and is a fraction ϕ of the whole volume or area. In this problem, the size, shape and the connectivity of the material are the unknowns. Subfigure 3.1(b) shows the resulted material distribution Ω^{mat} inside the domain Ω .

3.1.2 Mathematical formulation of the topology optimization for structures

The topology optimization problem is a "0-1" integer optimization problem. First, the design domain Ω is discretized into N finite elements (figure 3.3). Each finite element represents a design variable of density x . This means that each finite element could or could not have material. If density is equal to

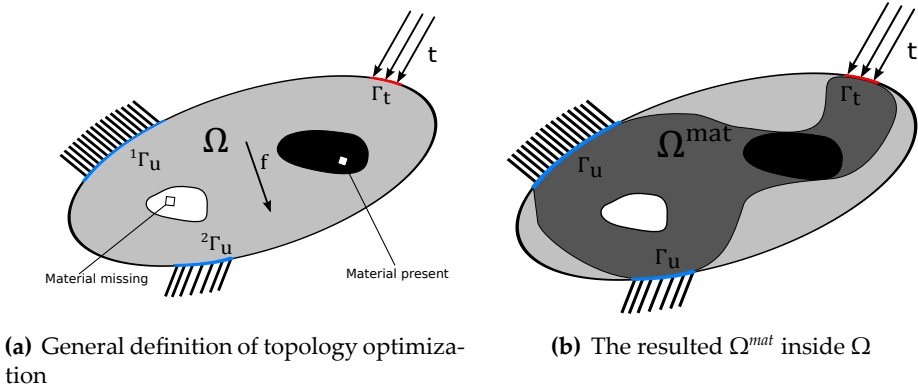


Figure 3.1: Topology Optimization Definition

unity, material is present in that area and the cell is painted in black. If density is equal to zero, no material is present in that area, and the cell is painted in white. The design variables can be combined in a vector $\mathbf{x} \in \mathbb{R}^N$. The global stiffness matrix of the structure $\mathbf{K}(\mathbf{x}) \in \mathbb{R}^{d \times d}$ depends on the design variables where d is the total number of degrees of freedom. The displacement vector $\mathbf{u} \in \mathbb{R}^d$ can be calculated by the governing equilibrium equations:

$$\mathbf{K}(\mathbf{x})\mathbf{u} = \mathbf{f} \quad (3.1)$$

where $\mathbf{f} \in \mathbb{R}^d$ is the external load vector that combines all applied body, surface, and point forces.

Assuming linear elasticity, the strain and stress tensors can be related to the displacement vector through the kinetic and constitutive equations:

$$\epsilon_{ij} = \frac{1}{2}(\mathbf{u}_{i,j} + \mathbf{u}_{j,i}), \quad (3.2)$$

$$\sigma_{ij} = \mathbf{E}_{ijkl}\epsilon_{kl}, \quad (3.3)$$

where \mathbf{E} is the constitutive matrix that is dependent upon that material's Poisson's ratio ν and Young's modulus \mathbf{E}_0 .

The density design variable should attain one of the limiting values, zero or one, such that the discretized domain results in a black and white solution, giving a rough description of the continuum structure boundaries. The "0-1" problem can be relaxed by substituting the integer variables of density with continuous variables powered in a penalty value $p \geq 3$ leading the design

variables near to the ideally desired discrete values 0 and 1. This approach is called SIMP (Solid Isotropic Material with Penalization) [Ben89; Roz09]. The material properties \mathbf{E}_e within each element e can be expressed as:

$$\mathbf{E}_e = x_e^p \mathbf{E}_0 \quad (3.4)$$

where \mathbf{E}_0 is the Young's modulus of the solid material, and p is the penalization power coefficient. Figure 3.2 illustrates the relation between relative stiffness $\frac{E_e}{E_0}$ and the element volume density x_e for various penalty values. It must be mentioned that for computational purposes a lower limit of the x_e must be set. That for the values of volume elements are set to:

$$0 < x_{min} < x_e \leq 1 \quad e = 1, 2, \dots, N \quad (3.5)$$

where x_{min} is usually set to 10^{-3} .

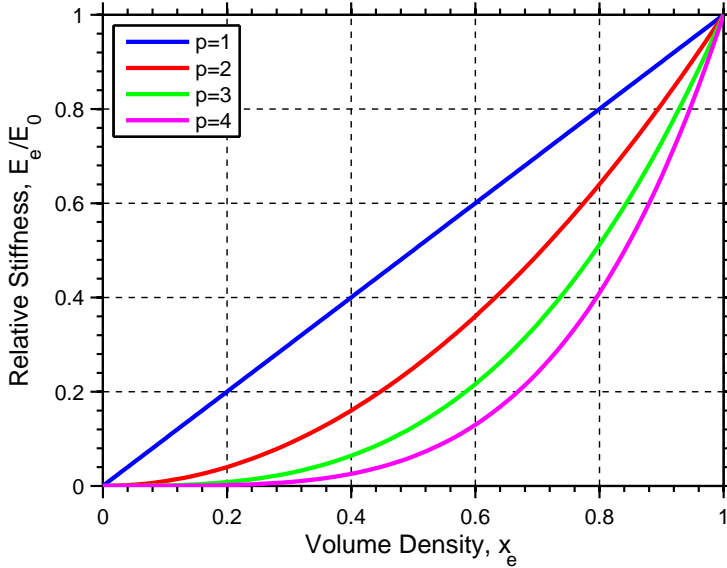


Figure 3.2: Graphical representation of the SIMP approach for various penalty coefficients p

Using SIMP the stiffness of each element \mathbf{K}_e can be set as:

$$\begin{aligned} \mathbf{K}_e &= x_e^p \mathbf{K}_0, \quad e = 1, \dots, N, \quad p > 1, \\ \mathbf{K}_e(x_e = 0) &= 0, \quad \mathbf{K}_e(x_e = 1) = \mathbf{K}_0. \end{aligned} \quad (3.6)$$

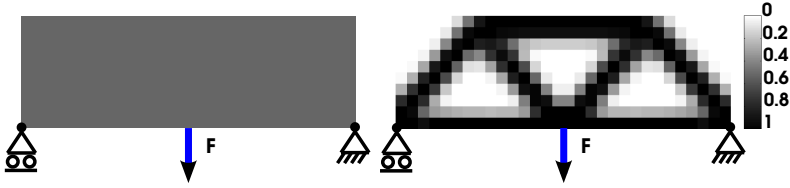


Figure 3.3: The left image indicates the discretization of the design domain into finite elements. Each element is equipped with a density design variable. The right image shows a final topology. White elements indicate absence of material $x_e = 0$. Black cells show presence of material $x_e = 1$. For gray elements the density is $0 < x_e < 1$.

where \mathbf{K}_0 is the element stiffness when $x_e = 1$ and p is the penalty factor, usually set $p \geq 3$. The global stiffness matrix \mathbf{K} is expressed as:

$$\mathbf{K} = \sum_{e=1}^N x_e^p \mathbf{K}_0 \quad (3.7)$$

The volume of the Ω^{mat} must be a percentage ϕ of the whole volume of Ω .

$$\begin{aligned} \frac{V}{V_0} \leq \phi &\Leftrightarrow V \leq \phi V_0 \\ V &= \sum_{e=1}^N v_e x_e \leq \phi V_0, \end{aligned} \quad (3.8)$$

where v_e is the volume of element e .

The objective function of the problem is the overall flexibility and it can be expressed as the compliance of the structure:

$$c = \mathbf{f}^T \mathbf{u} \quad (3.9)$$

All the above can express the mathematical formulation of topology opti-

mization problem for structures:

$$\begin{aligned}
 \min_{\mathbf{u}, x_e} c(x_e) &= \mathbf{f}^T \mathbf{u}, \\
 \text{subject to:} \\
 \mathbf{K}\mathbf{u} &= \mathbf{f}, \\
 \sum_{e=1}^N v_e x_e &\leq \phi V_0, \\
 0 < x_{min} &\leq x_e \leq 1, \quad e = 1, \dots, N, \\
 \text{SIMP:} \\
 \mathbf{K} &= \left(\sum_{e=1}^N x_e^p \mathbf{K}_0 \right), \quad p \geq 3
 \end{aligned} \tag{3.10}$$

3.1.3 Sensitivity analysis and Optimality Criteria

For a structure that must bear the applied loads, the objective function is the global flexibility that must be minimized. It is expressed in equation (3.9):

$$\begin{aligned}
 c &= \mathbf{f}^T \mathbf{u} = \mathbf{u}^T \mathbf{K}\mathbf{u} = \sum_{e=1}^N u_e \mathbf{K}_e u_e \\
 \mathbf{K}_e &= x_e^p \mathbf{K}_0
 \end{aligned} \tag{3.11}$$

and the global flexibility is expressed as:

$$c = \sum_{e=1}^N x_e^p u_e \mathbf{K}_0 u_e, \quad e = 1, \dots, N, \tag{3.12}$$

In order to solve the problem (3.9), the Lagrange multipliers method must be used. Then, a heuristic method is used to refresh the design variables while an iterative method is used to find the Lagrange multipliers. The Lagrange function is defined as:

$$\mathcal{L} = c + \lambda(V - \phi V_0) + \lambda_1^T (\mathbf{K}\mathbf{u} - \mathbf{f}) + \sum_{e=1}^N -\lambda_e (x_{min} - x_e) + \sum_{e=1}^N +\lambda_e (x_e - 1) \tag{3.13}$$

where λ and λ_1 are the Lagrange multipliers for the volume and equilibrium constraints, while ${}^-\lambda_e$ and ${}^+\lambda_e$ are the corresponding multipliers for the lower and upper constraints of the design variables. The Lagrange multiplier λ for the volume constraint is a scalar, while the coefficient λ_1 is a vector. The other multipliers ${}^-\lambda_e$ and ${}^+\lambda_e$ are scalars. The optimum is found when the partial derivatives of the Lagrange function are equal to zero:

$$\begin{aligned}\frac{\partial \mathcal{L}}{\partial x_e} &= 0, \quad \text{for } e = 1, \dots, N \\ \frac{\partial \mathcal{L}}{\partial x_e} &= \frac{\partial c}{\partial x_e} + \lambda \frac{\partial V}{\partial x_e} + \lambda_1^T \frac{\partial (\mathbf{K}\mathbf{u} - \mathbf{f})}{\partial x_e} - {}^-\lambda_e + {}^+\lambda_e\end{aligned}\quad (3.14)$$

Calculating the partial derivatives of *objective function* c inside the Lagrange function by using the chain rule, we get:

$$\begin{aligned}\frac{\partial c}{\partial x_e} &= \frac{\partial (\mathbf{f}^T \mathbf{u})}{\partial x_e} \\ &= \frac{\partial (\mathbf{u}^T \mathbf{K} \mathbf{u})}{\partial x_e} \\ &= \frac{\partial \mathbf{u}^T}{\partial x_e} \mathbf{K} \mathbf{u} + \mathbf{u}^T \frac{\partial \mathbf{K}}{\partial x_e} \mathbf{u} + \mathbf{u}^T \mathbf{K} \frac{\partial \mathbf{u}}{\partial x_e}\end{aligned}\quad (3.15)$$

Calculating the partial derivatives of *equilibrium constraint* inside the Lagrange function by using the chain rule, we get:

$$\lambda_1^T \frac{\partial (\mathbf{K}\mathbf{u} - \mathbf{f})}{\partial x_e} = \lambda_1^T \left(\frac{\partial \mathbf{K}}{\partial x_e} \mathbf{u} + \mathbf{K} \frac{\partial \mathbf{u}}{\partial x_e} \right) \quad (3.16)$$

For the volume constraint we get:

$$\begin{aligned}\lambda \frac{\partial V}{\partial x_e} &= \lambda \frac{\partial \left(\sum_{e=1}^N v_e x_e \right)}{\partial x_e} \\ &= \lambda v_e\end{aligned}\quad (3.17)$$

considering non active the constraints of space definition of the design variables ${}^-\lambda_e = {}^+\lambda_e = 0$ and that the load is independent of the design variables,

$\frac{\partial \mathbf{f}}{\partial x_e} = 0$, finally the partial derivatives of the Lagrange function are expressed as:

$$\begin{aligned}\frac{\partial \mathcal{L}}{\partial x_e} &= \frac{\partial \mathbf{u}^T}{\partial x_e} \mathbf{K} \mathbf{u} + \mathbf{u}^T \frac{\partial \mathbf{K}}{\partial x_e} \mathbf{u} + \mathbf{u}^T \mathbf{K} \frac{\partial \mathbf{u}}{\partial x_e} + \lambda v_e + \lambda_1^T \left(\frac{\partial \mathbf{K}}{\partial x_e} \mathbf{u} + \mathbf{K} \frac{\partial \mathbf{u}}{\partial x_e} \right) \\ \frac{\partial \mathcal{L}}{\partial x_e} &= \mathbf{u}^T \frac{\partial \mathbf{K}}{\partial x_e} \mathbf{u} + \lambda_1^T \frac{\partial \mathbf{K}}{\partial x_e} + \frac{\partial \mathbf{u}}{\partial x_e} (2\mathbf{u}^T \mathbf{K} + \lambda_1^T \mathbf{K}) + \lambda v_e\end{aligned}\quad (3.18)$$

Since the factor λ_1^T has been arbitrary defined, it can be chosen in such a way that the partial derivatives of the displacement over the design variables be zero, $\frac{\partial \mathbf{u}}{\partial x_e} = 0$. Having $\mathbf{K} \neq 0$ we get $\lambda_1^T = -2\mathbf{u}^T$, so that the factor $2\mathbf{u}^T \mathbf{K} + \lambda_1^T \mathbf{K}$ to be zero.

So the partial derivatives of the Lagrange function are expressed as:

$$\begin{aligned}\frac{\partial \mathcal{L}}{\partial x_e} &= -\mathbf{u}^T \frac{\partial \mathbf{K}}{\partial x_e} \mathbf{u} + \lambda v_e \\ &= -p x_e^{p-1} u_e \mathbf{K}_0 u_e + \lambda v_e \\ &= -p x_e^{p-1} q_c + \lambda v_e = 0\end{aligned}\quad (3.19)$$

where,

$$q_c = u_e \mathbf{K}_0 u_e \quad (3.20)$$

represents the energy of the element e , when that contains 100% material, meaning that the design variable $x_e = 1$. The refresh of the design variables is expressed from equation (3.20)

$$\frac{p x_e^{p-1} q_c}{\lambda v_e} = 1 \quad (3.21)$$

The physical significance of the equation (3.20) is that the energy density of the system must be constant in whole design domain. The Lagrange multiplier λ operates as a scaling factor so that the energy density to be constant. For the update of the design variables a heuristic scheme is used:

$$\begin{aligned}
x_{e,k+1} &= x_{e,k} \left(\frac{px_e^{p-1} q_c}{\lambda v_e} \right)^\zeta = x_{e,k} B_{e,k}^\zeta, \\
B_{e,k} &= \frac{px_e^{p-1} q_c}{\lambda v_e}, \\
\zeta &= 0.5, \quad 0 < \zeta < 1
\end{aligned} \tag{3.22}$$

where the $x_{e,k}$ stands of the relative density of element e at the k iteration. The ζ is an damping factor, usually set to 0.5, and it is used to stabilize the iterative process. In order not to have rapid changes in the values of the design variables in between two iterations, for example an element e first is solid and next is void, or the opposite effect, a limit of change of the design variable is set. This is done for stabilizing the iterative process as well. So for the heuristic scheme, the updated design variables are calculated such as:

$$x_{e,k+1} = \begin{cases} A_k & \text{if } x_{e,k} B_{e,k}^\zeta \leq A_k \\ x_{e,k} B_{e,k}^\zeta & \text{if } A_k \leq x_{e,k} B_{e,k}^\zeta \leq C_k, \\ C_k & \text{if } x_{e,k} B_{e,k}^\zeta \geq C_k \end{cases} \tag{3.23}$$

$$A_k = \max \{ (1 - m)x_{e,k}, x_{min} \} \tag{3.23a}$$

$$C_k = \min \{ (1 + m)x_{e,k}, 1 \} \tag{3.23b}$$

where m is the a motion limit usually set to 0.5, but lies between 0 and 1, $0 < m < 1$. Equation (3.23) adds material in elements where their energy is greater that the Lagrange multiplier λ , and that happens when $B_k > 1$, and removes material when the energy is lower than λ . This is happening only when the new values does not violate their limits $x_{min} \leq x_e \leq 1$. Equation (3.21) shows that the Lagrange multiplier is proportional to the average energy density in areas where the relative density takes intermediate values.

3.1.4 Topology Optimization: Iterative local search algorithm

Since topology optimization problems have many design variables one usually wants to avoid direct usage of general purpose optimization algorithms, since they can be computational expensive. For certain cases (mainly flexibility optimization without additional constraints) the construction of local

element-wise update techniques can be used for this purpose. Their origin is traced back to fully stressed design methods for trusses and optimality criteria methods [Roz89].

The steps of a schematic topology optimization algorithm are described below and further illustrated in figure 3.4

- Initialization
 - define design domain
 - apply loading and boundary condition
 - distribute randomly material inside the domain
- compute using Finite Elements Method (FEM) the structure
- run sensitivity analysis
- run low pass filtering (eliminate checkerboards effects)
- update design variables using a heuristic scheme (usually locally, element-wise)
- if convergence criteria are not satisfied repeat the loop else plot results

3.2 Topology optimization numerical problems

Several numerical problems appear during the topology optimization process. Most of these occur because of the:

- type and number of finite elements used
- optimization algorithm and it's tuning coefficients
- initial state that topology optimization start its iterative process.

One of the most frequent problems appearing are the checkerboard effects. The relative densities are between 0 and 1, therefore material distributions appear that look like checkerboards. Another numerical problem is the mesh dependency. The final material distributions are different if the design domain is meshed differently with different number of elements. In some

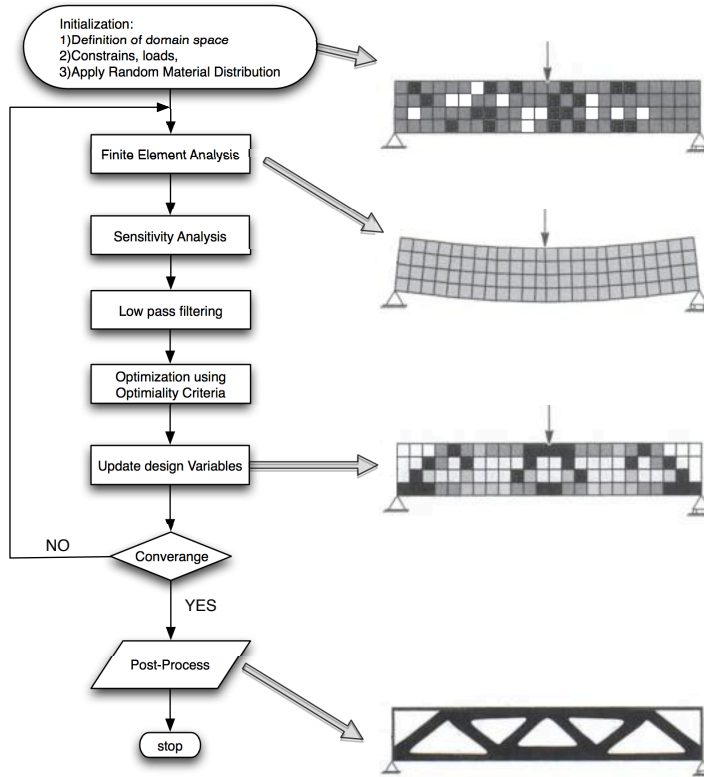


Figure 3.4: Topology optimization iterative local search algorithm.

cases different final material layouts appear if the topology optimization iterative process starts from different initial material distribution, using though the same mesh strategy. The iterative process is dependent of the starting point, meaning that the algorithm may stuck in local optima. This although, does not happen very often in structure problems. But when topology optimization is used for the design of compliant mechanisms, these phenomena appears frequently leading to different final distributions.

3.2.1 Checkerboard effects

Checkerboard effects shown in figure 3.5, are frequent in topology optimization and consists of areas in the final material distributions where solid and void elements are alternating. Initially checkerboard regions were believed to designate areas with higher stiffness. Works in the past [DS95],[JH96] have

shown that checkerboard patterns are due to bad numeric modelling on the stiffness of checkerboards. Several methods have been proposed in the past [SP98] in order to solve this problem. In our case the *mesh independent filter* has been used which solves the mesh dependency problem as well. The filter modifies the design sensitivity of a specific element based on the weighted average on the element sensitivities in a fixed neighbourhood.



Figure 3.5: Checker board regions appears in the classic MBB problem.

3.2.2 Mesh dependency

The mesh dependency problem is illustrated in figure 3.6. For the same problem illustrated in figure 3.5 and different mesh configurations, the final material distributions differ.

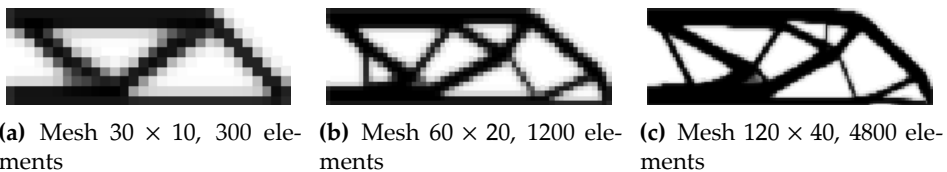


Figure 3.6: Mesh dependency phenomena

It is clear that even if the initial configuration is the same, when the mesh becomes more dense, the final layout differs. It must be mentioned that the proportion of elements in horizontal and vertical direction is the same. Making the mesh denser helps us find a better mapping of the final Ω^{mat} with much smoother boundaries.

Of course the resulted layout from the 120×40 mesh is considerably more detailed when compared with the other two. But a more detailed solution is not always applicable for manufacturing. One way to overcome this problem is to apply a filter that must be independent to the mesh. This method is heuristic, but gives very good results with a small computational cost. In the beginning a radius r_{min} is set and it may depend on the domain. It can be set for example the 4% to 5% of the horizontal dimension of the domain. Then a function $dist(e, i)$ that measures the distance between two elements, e and i . The filter can be applied on the sensitivities of the design variables or on the design variables itself. The filter can be applied as:

$$\hat{H}_i = r_{min} - dist(e, i), \{i \in N_r \mid dist(e, i) \leq r_{min}\}, \quad e = 1, \dots, N \quad (3.24)$$

where N_r is a set of elements, their distance from a element k is less or equal of r_{min} . Obviously, \hat{H} is zero for elements, their distance from element e is greater than r_{min} . Equations 3.25 and 3.26 show the effect of the filter on the design variables and their sensitivities respectively:

$$\hat{x}_e = \frac{1}{\left(\sum_{i=1}^{N_r} \hat{H}_f\right)} \sum_{i=1}^{N_r} \hat{H}_i x_i \quad (3.25)$$

$$\frac{\partial \hat{c}}{\partial x_e} = \frac{1}{x_e \left(\sum_{f=1}^{N_r} \hat{H}_f\right)} \sum_{i=1}^{N_r} \hat{H}_i x_i \frac{\partial c}{\partial x_e} \quad (3.26)$$

The effect of the filter is illustrated in figure 3.7

3.3 Multiplicity of solutions

3.4 Multiple load cases

3.4.1 Introduction to the problem with multiple load cases

The minimization of compliance of a structure can be extended for multiple load cases. The term *multiple load cases* refers to several forces being applied

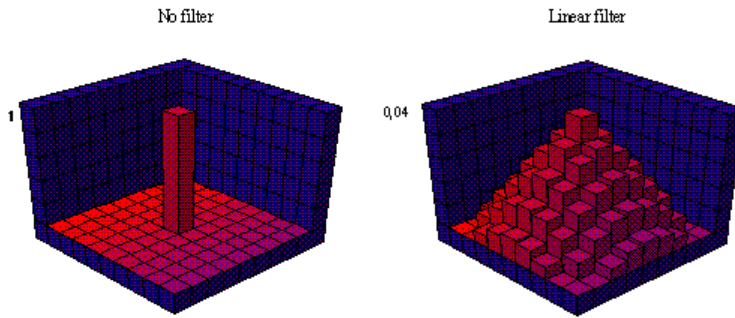


Figure 3.7: Graphic representation of the filter for the mesh dependency problem

on the a structure, but in different cases. If two or more loads are applied on the structure at the same time, it is referred to as *one load case*.

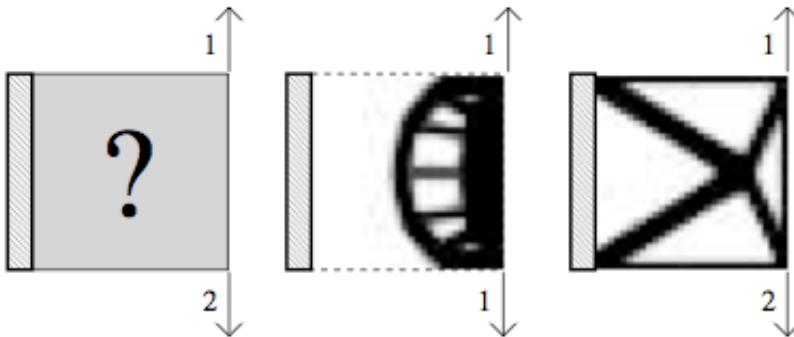


Figure 3.8: Multiple Load cases. On the left: domain definition. In the middle: the resulted structure for one load case. On the right: the resulted structure for two load cases.

3.4.2 Problem formulation

The objective function of the problem is the minimization of the flexibility of the structure for all load cases:

$$\begin{cases} \min_{\mathbf{u}_1, x_e} c_1(x_e) = \mathbf{f}_1^T \mathbf{u}_1, \\ \min_{\mathbf{u}_2, x_e} c_2(x_e) = \mathbf{f}_2^T \mathbf{u}_2, \\ \vdots \\ \min_{\mathbf{u}_m, x_e} c_m(x_e) = \mathbf{f}_m^T \mathbf{u}_m, \end{cases} \quad (3.27)$$

where m is the total number of the different load cases. The problem is multi-criteria since the structure must be optimized for each load case. The multicriteria problem can be converted to a single criteria problem taking the weighted sum of the compliances for each load case. [BK88]:

$$\min \sum_{i=1}^m w_i c_i = \sum_{i=1}^m w_i \mathbf{u}_i^T \mathbf{K} \mathbf{u}_i$$

subject to:

$$\left(\sum_{e=1}^N x_e^p \mathbf{K}_0 \right) \mathbf{u}_i = \mathbf{f}_i, \quad i = 1, \dots, m \quad (3.28)$$

$$\sum_{e=1}^N v_e x_e \leq \phi V_0,$$

$$0 < x_{min} \leq x_e \leq 1, \quad e = 1, \dots, N,$$

$$\sum_{i=1}^m w_i = 1$$

where w_i is the weight in each load case. Naturally all weights must be summed to unity. In this case the Lagrange function \mathcal{L} is expressed as following in accordance to equation (3.13):

$$\begin{aligned}
\mathcal{L} &= \sum_{i=1}^m w_i \mathbf{u}_i^T \mathbf{K} \mathbf{u}_i + \lambda (V - \phi V_0) \\
&+ \sum_{i=1}^m \lambda_i^T (\mathbf{K} \mathbf{u}_i - \mathbf{f}_i) \\
&+ \sum_{e=1}^N -\lambda_e (x_{min} - x_e) \\
&+ \sum_{e=1}^N +\lambda_e (x_e - 1)
\end{aligned} \tag{3.29}$$

The partial derivatives of \mathcal{L} are calculated just like the single load case (see equation (3.18)):

$$\begin{aligned}
\frac{\partial \mathcal{L}}{\partial x_e} &= 0, \quad \text{for } e = 1, \dots, N \\
\frac{\partial \mathcal{L}}{\partial x_e} &= \frac{\partial \left(\sum_{i=1}^m w_i \mathbf{u}_i^T \mathbf{K} \mathbf{u}_i \right)}{\partial x_e} + \lambda \frac{\partial V}{\partial x_e} + \sum_{i=1}^m \lambda_i^T \left(\frac{\partial (\mathbf{K} \mathbf{u}_i)}{\partial x_e} - \frac{\partial \mathbf{f}_i}{\partial x_e} \right) - \lambda_e + \lambda_e \Rightarrow \\
\frac{\partial \mathcal{L}}{\partial x_e} &= w_1 \frac{\partial \mathbf{u}_1^T}{\partial x_e} \mathbf{K} \mathbf{u}_1 + w_1 \mathbf{u}_1^T \frac{\partial \mathbf{K}}{\partial x_e} \mathbf{u}_1 + w_1 \mathbf{u}_1^T \mathbf{K} \frac{\partial \mathbf{u}_1}{\partial x_e} + \dots \\
&+ w_m \frac{\partial \mathbf{u}_m^T}{\partial x_e} \mathbf{K} \mathbf{u}_m + w_m \mathbf{u}_m^T \frac{\partial \mathbf{K}}{\partial x_e} \mathbf{u}_m + w_m \mathbf{u}_m^T \mathbf{K} \frac{\partial \mathbf{u}_m}{\partial x_e} + \lambda \frac{\partial V}{\partial x_e} \\
&+ \lambda_1^T \left(\frac{\partial \mathbf{K}}{\partial x_e} \mathbf{u}_1 + \mathbf{K} \frac{\partial \mathbf{u}_1}{\partial x_e} \right) + \dots + \lambda_m^T \left(\frac{\partial \mathbf{K}}{\partial x_e} \mathbf{u}_m + \mathbf{K} \frac{\partial \mathbf{u}_m}{\partial x_e} \right) \Rightarrow \\
\frac{\partial \mathcal{L}}{\partial x_e} &= \sum_{i=1}^m w_i \mathbf{u}_i^T \frac{\partial \mathbf{K}}{\partial x_e} \mathbf{u}_i + \sum_{i=1}^m w_i \lambda_i^T \frac{\partial \mathbf{K}}{\partial x_e} \mathbf{u}_i + \sum_{i=1}^m \frac{\partial \mathbf{u}_i}{\partial x_e} (2w_i \mathbf{u}_i^T \mathbf{K} + \lambda_i^T \mathbf{K}) + \lambda v_e
\end{aligned} \tag{3.30}$$

Since the coefficients λ_i^T have been set arbitrarily, they can be chosen in such a way that, the partial derivatives with respect to the design variables for

all load cases are equal to zero, $\frac{\partial \mathbf{u}_i}{\partial x_e} = 0$, $i = 1, \dots, m$. Moreover, since $\mathbf{K} \neq 0$ then $\lambda_i^T = -2\mathbf{u}_i^T$, in such a way $2\mathbf{u}_i^T \mathbf{K} + \lambda_i^T \mathbf{K}$, $i = 1, \dots, m$ equals to zero. So we get the partial derivatives of the Lagrange function:

$$\begin{aligned}
 \frac{\partial \mathcal{L}}{\partial x_e} &= - \sum_{i=1}^m w_i \mathbf{u}_i^T \frac{\partial \mathbf{K}}{\partial x_e} \mathbf{u}_i + \lambda v_e \\
 &= - \sum_{i=1}^m w_i (px_e^{p-1}) u_{e,i} \mathbf{K}_0 u_{e,i} + \lambda v_e \\
 &= -px_e^{p-1} \sum_{i=1}^m w_i u_{e,i} \mathbf{K}_0 u_{e,i} + \lambda v_e \\
 &= -px_e^{p-1} \hat{q}_c + \lambda v_e = 0
 \end{aligned} \tag{3.31}$$

where,

$$\hat{q}_c = \sum_{i=1}^m w_i u_{e,i} \mathbf{K}_0 u_{e,i} \tag{3.32}$$

that represents the energy for element e , when it is solid ($x_e = 1$) for all load cases. The heuristic scheme for updating the design variables is similar to that for a single load case (see equation 3.22):

$$\begin{aligned}
 x_{e,k+1} &= x_{e,k} \left(\frac{px_e^{p-1} \hat{q}_c}{\lambda v_e} \right)^\zeta = x_{e,k} B_{e,k}^\zeta \\
 B_{e,k} &= \frac{px_e^{p-1} \hat{q}_c}{\lambda v_e}, \\
 \zeta &= 0.5, \quad 0 < \zeta < 1
 \end{aligned} \tag{3.33}$$

while the heuristic scheme for the update of the design variables is similar to that in equation 3.23 by just replacing the q with \hat{q} .

3.5 Topology optimization for the design of compliant mechanisms

3.5.1 Description of a compliant mechanism

Compliant mechanisms are monolithic flexible structures that deliver motion according to predefined sets of loads and boundary conditions. The mechanisms must be as flexible as possible, but at the same time must be stiff enough to bear with loadings. The final shape of the flexible structure can be found using topology optimization, the same way as it is used to design structures. The flexible structure contains a fraction of volume of a predefined design domain. The structure is actuated with input loads at specific points or areas and delivers motion to specific output points or areas.

3.5.2 An example of a compliant mechanism

As an example of a compliant mechanism design problem we consider the displacement inverter of Figure 3.9. The goal of the topology optimization problem is to design a structure that converts an input displacement at point E to the opposite direction at point B. We define as positive X direction the rightwards direction and as positive Y direction the downwards one. At this point it should be mentioned that real life compliant mechanisms design will require the usage of large deformation theory. Nevertheless some of the representative difficulties arising during this study, and in particular nonconvexity and multiplicity of solutions, can also be demonstrated with the linear theory which is used here.

We assume that the input actuator is modelled by a spring with stiffness k_{in} and a force f_{in} . The goal of the optimization problem is to maximize the displacement u_{out} at point B, performed on the workpiece modelled by a spring with stiffness k_{out} (see figure 3.9). By specifying different values of k_{out} we can control the displacement amplification. If we specify a low value of k_{out} we get large displacement and vice versa. In order to maximize the work on the output spring, the available material must be distributed in the most efficient way. An optimization problem incorporating these ideas can be written as [BS03]:

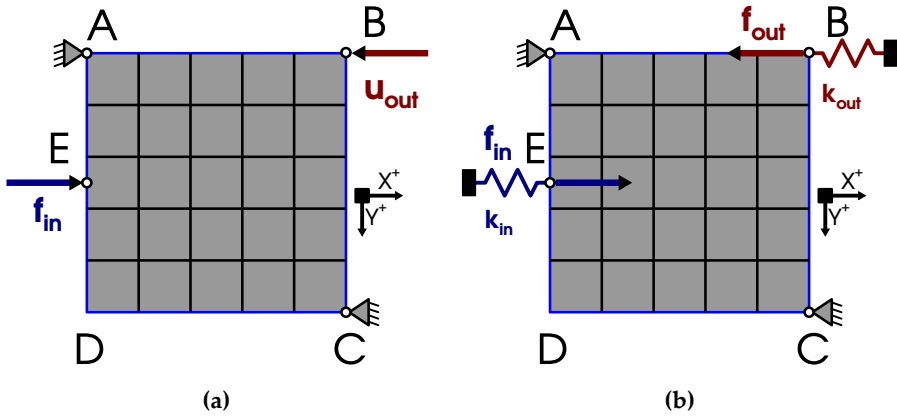


Figure 3.9: A force inverter. One load case definition problem

$$\begin{aligned}
 & \max_{\mathbf{u}, x_e} u_{out} = \mathbf{1}^T \mathbf{u}, \\
 & \text{s.t.} \\
 & \quad \mathbf{K}\mathbf{u} = \mathbf{f} \\
 & \quad \sum_{e=1}^N v_e x_e \leq \phi V_0 \\
 & \quad \mathbf{K} = \left(\sum_{e=1}^N x_e^p \mathbf{K}_0 \right), \quad p \geq 3 \\
 & \quad 0 < x_{min} \leq x_e \leq 1, \quad e = 1, \dots, N
 \end{aligned} \tag{3.34}$$

Here, u_{out} is the displacement at the output point B, x_e and v_e are the density and the volume of the element e . Moreover \mathbf{K} is the global stiffness matrix, \mathbf{u} is the displacement degrees of freedom vector, \mathbf{f} is the loading vector and ϕ is the maximum allowed covering of the available design space with material.

3.5.3 Sensitivity analysis for compliant mechanisms

The same iterative process that is used for solving the topology optimization problem for structures is used for the compliant mechanism problem as well.

The only difference is the calculation of the sensitivities of the problem. For that, the adjoint method is used.

For the objective function $u_{out} = \mathbf{1}^T \mathbf{u}$, the \mathbf{u} vector stands for the displacement vector that satisfies the equilibrium equation: $\mathbf{f} - \mathbf{K}\mathbf{u} = \mathbf{0}$. For any arbitrary vector $\boldsymbol{\omega}$ we get:

$$u_{out} = \mathbf{1}^T \mathbf{u} - \boldsymbol{\omega}^T (\mathbf{f} - \mathbf{K}\mathbf{u}) \quad (3.35)$$

When we differentiate equation with respect to the design variables we get:

$$\frac{\partial u_{out}}{\partial x_e} = \mathbf{1}^T \frac{\partial \mathbf{u}}{\partial x_e} - \frac{\partial \boldsymbol{\omega}^T}{\partial x_e} (\mathbf{f} - \mathbf{K}\mathbf{u}) - \boldsymbol{\omega}^T \left(\frac{\partial \mathbf{f}}{\partial x_e} - \frac{\partial \mathbf{K}}{\partial x_e} \mathbf{u} - \mathbf{K} \frac{\partial \mathbf{u}}{\partial x_e} \right) \quad (3.36)$$

Having in mind that the derivatives of the force vector \mathbf{f} (since the force is independent) and $\boldsymbol{\omega}$ had to be zero we get:

$$\frac{\partial u_{out}}{\partial x_e} = (\mathbf{1}^T + \boldsymbol{\omega}^T \mathbf{K}) \frac{\partial \mathbf{u}}{\partial x_e} + \boldsymbol{\omega}^T \frac{\partial \mathbf{K}}{\partial x_e} \mathbf{u} \quad (3.37)$$

where $\boldsymbol{\omega}$ is the solution that satisfies the adjoint problem $\mathbf{K}\boldsymbol{\omega} = -\mathbf{1}$, and $\mathbf{1}$ is a vector with the value 1 at the degree of freedom corresponding to the output point and zeros at all other places $\mathbf{1}^T = [0, 0, 0, \dots, 1, \dots, 0, 0, 0]$. Having in mind equation 3.7 and its derivative we get:

$$\frac{\partial u_{out}}{\partial x_e} = p x_e^{p-1} \boldsymbol{\omega}^T \mathbf{K}_0 \mathbf{u} \quad (3.38)$$

The solution of the adjoint problem $\mathbf{K}\boldsymbol{\omega} = -\mathbf{1}$ are the displacements when a force f_{out} is applied to the output point in the same but opposite direction with f_{in} when it is applied to the input point.

The optimization problem expressed in equation 3.34 is similar to the minimization of compliance problem. The optimality criteria method may be used for solving the problem along with the same heuristic scheme for the update of the design variables:

$$x_e^{k+1} = x_e^k \left(\frac{\max\left[0, -\frac{\partial u_{out}}{\partial x_e}\right]}{\lambda v_e} \right)^\eta \quad (3.39)$$

where η , is a damping factor between (0,1), and usually is set to 0.5 for the minimization of compliance, but in the case of compliant mechanisms is set to 0.2. According to bibliography, for optimum convergence of the iterative process, the Method of Moving Asymptotes (MMA) [Sva87] should be used.

3.5.4 Alternative problem definitions

The different requirements imposed on a compliant mechanism allow us to formulate the design problem in different alternative ways. Several formulations have been proposed. The weighted sum formulation, proposed by Anathasuresh, Kota and Kikuchi [AKK94] is a linear combination of the output displacement and the inverse of Strain Energy, also called compliance (described in equation 3.41). The multi-criteria formulation, proposed by Frecker in 1997 [Mar97], is based on a fraction of the Mutual Potential Energy (MPE) [SP70] over the Strain Energy (SE) (described in equation 3.42). Strain and Mutual Potential Energy are defined as follows [RS05]:

$$\begin{aligned} SE &= \mathbf{f}_{in} \mathbf{u}_{out}^1 \\ MPE &= \mathbf{f}_{out}^v \mathbf{u}_{out}^1 \end{aligned} \quad (3.40)$$

where \mathbf{u}_{out}^1 is the displacement at the output point due to the load \mathbf{f}_{in} applied at the input port, and \mathbf{f}_{out}^v is the virtual force at the output point specifying the direction of the desired output point displacement. For a given mechanism and input load \mathbf{f}_{in} the resulting MPE will typically be inversely related to the stiffness supplied at the output point. Hence when one refers to specific values of MPE both the input load \mathbf{f}_{in} and the output point stiffness should generally be stated. Another approach is based on the maximization of the output displacement, proposed by Bendsøe and Sigmund [BS03] and described in equation 3.43. The previously used definitions are summarized here:

$$\begin{aligned} \max \left\{ ad_{out} + (1-a) \frac{1}{SE} \right\} \\ \text{with predefined } F_{in} \text{ and } F_{out} \end{aligned} \quad (3.41)$$

$$\begin{aligned} \max \left\{ \frac{MPE}{SE} \right\} \\ \text{with predefined } F_{in} \text{ and output direction} \end{aligned} \quad (3.42)$$

$$\begin{aligned} \max \left\{ U_{out} \right\} \\ \text{with predefined } F_{in} \text{ and output direction} \end{aligned} \quad (3.43)$$

3.5.5 Compliant Mechanisms: Multiple loading cases-Polymorphic mechanisms.

We assume two load cases. The objective is to find the material distribution that allows for two different usages of the mechanism. In this case the objective is to maximise the displacements at the given output points. The problem is a genuine multiobjective optimization. One possible way to transform a multi-objective problem into a single one, is to take as an objective the weighted sum of all objectives. The graphic formulation of the problem is shown in figure 3.10:

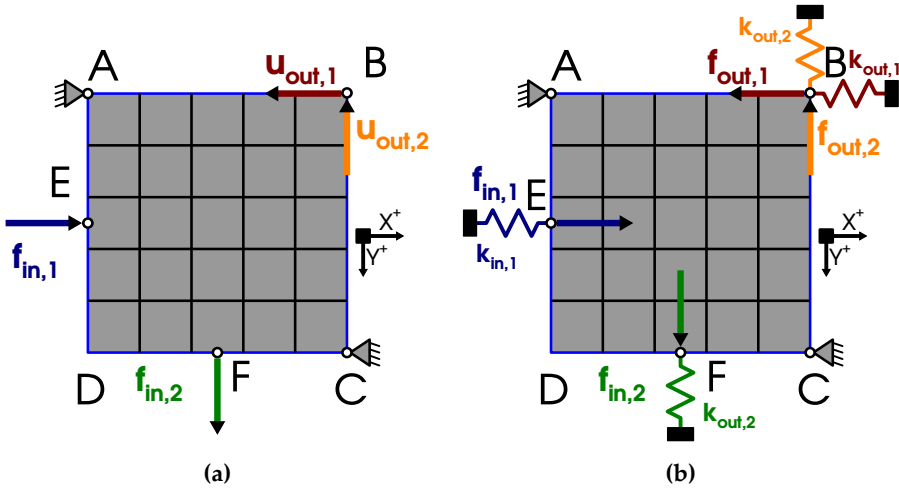


Figure 3.10: Two loads case compliant mechanism problem

In the case of the multi-purpose compliant mechanisms the problems that arise are multi-objective:

$$\left\{ \begin{array}{l} \max_{\mathbf{u}_1, x_e} c_1(x_e) = u_{out,1} \\ \max_{\mathbf{u}_2, x_e} c_2(x_e) = u_{out,2} \\ \vdots \\ \max_{\mathbf{u}_m, x_e} c_m(x_e) = u_{out,m} \end{array} \right. \quad (3.44)$$

where $u_{out,i}$ $i = 1, \dots, m$ are the separate displacements for each load case.

In order to transform a multi-objective problem into a single one, we take the weighted sum of all objectives:

$$\begin{aligned} \max \sum_{i=1}^m w_i c_i &= u_{out}^{(\Sigma)} = \sum_{i=1}^m w_i \mathbf{1}_i^T \mathbf{u}_i \\ \text{subject to:} \\ \mathbf{K} \mathbf{u}_i &= \mathbf{f}_i, \quad i = 1, \dots, m \\ \sum_{e=1}^N v_e x_e &\leq \phi V_0, \\ 0 < x_{min} &\leq x_e \leq 1, \quad e = 1, \dots, N, \\ \sum_{i=1}^m w_i &= 1 \end{aligned} \tag{3.45}$$

where $u_{out}^{(\Sigma)}$ is the sum of all displacements at the corresponding points, multiplied with weight factors w_i that sum to unity and $\mathbf{1}_i$ the corresponding unit vector for each load case.

The objective function is described as:

$$u_{out}^{(\Sigma)} = \sum_{i=1}^m w_i \left(\mathbf{1}_i^T \mathbf{u}_i - \omega_i (\mathbf{f} - \mathbf{K} \mathbf{u}_i) \right) \tag{3.46}$$

Differentiate with respect to the design variables we get:

$$\frac{\partial u_{out}^{(\Sigma)}}{\partial x_e} = \sum_{i=1}^m w_i \left((\mathbf{1}_i^T + \omega_i \mathbf{K}) \frac{\partial \mathbf{u}_i}{\partial x_e} + \omega_i \frac{\partial \mathbf{K}}{\partial x_e} \mathbf{u}_i \right) \tag{3.47}$$

where ω_i are the solution of the adjoint problems $\mathbf{K} \omega_i = -\mathbf{1}$, $i = 1, \dots, m$. In that case the derivatives are expressed as:

$$\begin{aligned} \frac{\partial u_{out}^{(\Sigma)}}{\partial x_e} &= \sum_{i=1}^m w_i (p x_e^{p-1} \omega_i \mathbf{K}_0 \mathbf{u}_i) \\ &= p x_e^{p-1} \sum_{i=1}^m w_i \omega_i \mathbf{K}_0 \mathbf{u}_i \end{aligned} \tag{3.48}$$

The heuristic update scheme is modified based on equation accordingly 3.39:

$$x_e^{k+1} = x_e^k \left(\frac{\max\left[0, -\frac{\partial u_{out}^{(\Sigma)}}{\partial x_e}\right]}{\lambda v_e} \right)^\eta \quad (3.49)$$

3.6 Output control

3.6.1 Output control for the "one load case" problem

The goal in this section is to design an asymmetric force inverter. The design domain is a rectangular "ABCD" with points "A" and "D" constraint. A force is acting to the middle of the edge "AD" in the horizontal direction. The goal is to maximize the displacement of the output point "B" in the X (but opposite) direction, $Xu_{out}^{@X}$, and the same time minimize the normal displacement in the Y direction $Xu_{out}^{@Y}$. One of the design goals may be the control of the output point. For the asymmetric force inverter problem the goal could be: the output point to moving in parallel to the input load. Therefore, that displacement, in the normal to the intended output direction, must be as minimum as possible. Two different criteria appear: (equation 3.50).

$$\begin{cases} \max_x |u_{out}^{@X}| \\ \text{and} \\ \min_x |u_{out}^{@Y}| \end{cases} \quad (3.50)$$

The second criteria in equation 3.50 could be expressed as: $\max \left| \frac{1}{u_{out}^{@Y}} \right|$. Consequently the two criteria can be written as:

$$\max_x \left| \frac{u_{out}^{@X}}{u_{out}^{@Y}} \right| \quad (3.51)$$

3.6.2 Output Control for the "multiple load cases" problem

The problem is graphically illustrated in figure 3.12. The domain is a rectangular "ABCD" with points "A" and "C" fixed. Two different load cases are present. Firstly, a horizontal force is applied to the middle of the edge "AD"

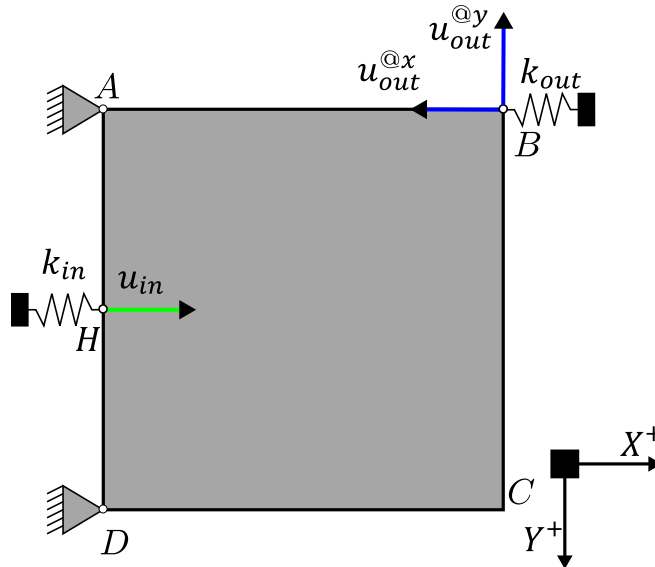


Figure 3.11: Maximize $u_{out}^{@X}$ & minimize $u_{out}^{@Y}$.

in a leftward direction and the objective is the output point "B" to move to the opposite direction. A second load is applied downwards in the middle of "DC" edge of the design domain and the objective is, the output point B to move to the opposite direction (upwards).

In this case, the multicriteria problem (without output control) is presented in equation 3.52.

$$\begin{cases} \max_x |u_{1,out}^{@X}| \\ \text{and} \\ \min_x |u_{2,out}^{@Y}| \end{cases} \quad (3.52)$$

In the resulted material distribution as well as in any load case, it is not initially established if output point "B" will move as intended. Output control must be applied.

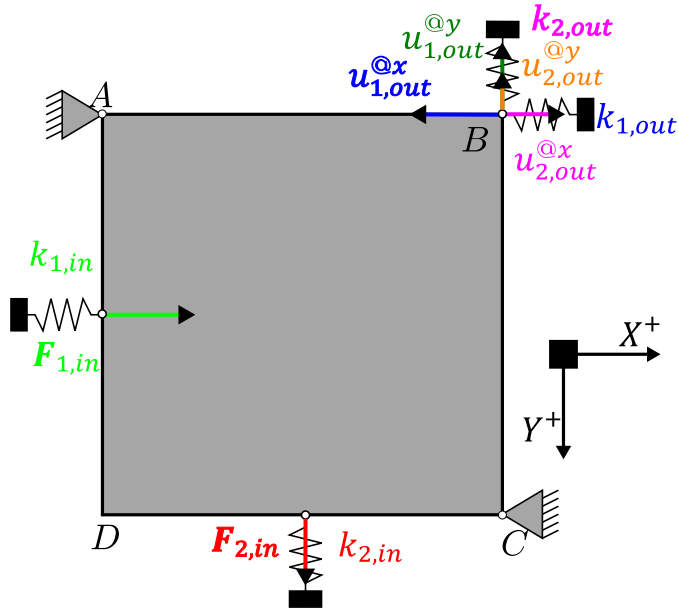
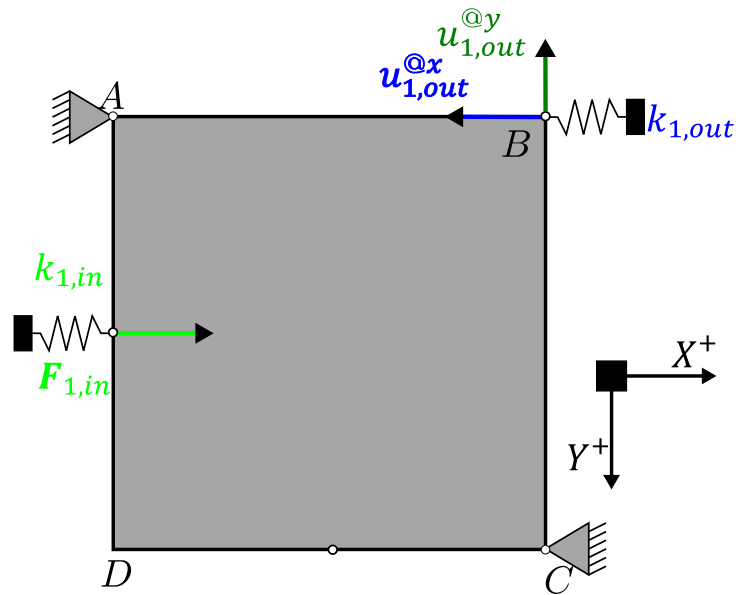


Figure 3.12: Graphical representation of the domain for the design of a polymorphic compliant mechanism

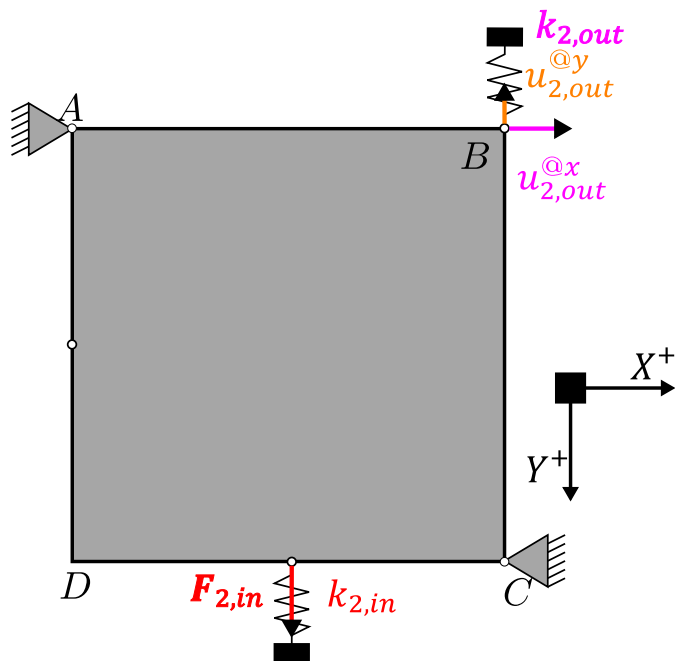
3.6.3 Motion control constraints

In any load case, point "B" may move in any direction. This may happen due to the final material distribution which is unknown from the beginning. It must be stated that it is not desirable to apply motion constraints to point "B" in any case. The goal is by leaving output point "B" free to move, to find the material distribution that satisfies both criteria: for the first load case point "B" must move leftwards $-X$, maximizing its displacement $u_{1,out}^{@X}$, minimizing the displacement in the Y direction $u_{1,out}^{@Y}$ (upwards or downwards) and in the second load case the same output point "B" must be moved downwards, minimizing the displacement in the horizontal direction (rightwards or leftwards).

Taking into account all the above, the problem is formulated as a twin multi-criteria problem:



(a) 1st load case



(b) 2nd load case

Figure 3.13: Two loads case compliant mechanism problem

$$\left\{ \begin{array}{l} \max_x |u_{1,out}^{@X}| \\ \min_x |u_{1,out}^{@Y}| \\ \text{and} \\ \max_x |u_{2,out}^{@Y}| \\ \min_x |u_{2,out}^{@X}| \end{array} \right. \quad (3.53)$$

Transforming each of the twin multi-criteria problem to a single criteria we get:

$$\left\{ \begin{array}{l} \max_x \left| \frac{u_{1,out}^{@X}}{u_{1,out}^{@Y}} \right| \\ \text{and} \\ \max_x \left| \frac{u_{2,out}^{@Y}}{u_{2,out}^{@X}} \right| \end{array} \right. \quad (3.54)$$

To convert all the above to a single criteria problem, maximization of the minimum of the two criteria is sufficient. Therefore, maximization of both criteria is accomplished. The problem is then formulated as:

$$\max_x \left\{ \min \left\{ \left| \frac{u_{1,out}^{@X}}{u_{1,out}^{@Y}} \right|, \left| \frac{u_{2,out}^{@Y}}{u_{2,out}^{@X}} \right| \right\} \right\} \quad (3.55)$$

CHAPTER 4

The Hybrid Scheme

4.1 The hybrid solution algorithm

4.1.1 Global and local Optimization Algorithms

All iterative techniques which are used in structural mechanism topology optimization are local iterative optimization methods or heuristics. In the case of nonconvex problems, they will stop at local minima. In fact, The topology optimization algorithm initial state dependent: when it starts from a different *initial point*, it may lead to completely different final topologies. An *initial point* is considered, either a uniform or a random distribution of material inside the design domain, that initially may violate or not the volume constraint, and taking into account various topological constraints such as presence or absence of material in specific areas. This effect appears more often in compliant mechanisms design and illustrated in figure 4.1. Therefore the need of using global optimization techniques arises.

The appearance of local minima in the topology optimization problem for structures and especially for mechanisms requires the usage of global optimization algorithms. Several works have been published in the past concerning the use of global optimization method *branch-and-bound* in topology optimization especially on the design of structures [Sto03; SB11]. Due to the large size of the problem, mathematical global optimization algorithms that work for small size problems are not suitable. The use of discrete variables in the brach-and-bound method, for large numbers of design variables makes the problem computationally extremely difficult to solve. In addition, special constraints must be considered in order to maintain the structural integrity in any iteration of the algorithm.

The only practically useful alternative seems to be the usage of genetic or evolutionary optimization algorithms. Several works has been published in the past making use of Genetic Algorithms in topology optimization problems [BRS08; BRS11; JS10; MPR10], swarm intelligence algorithms like Ant

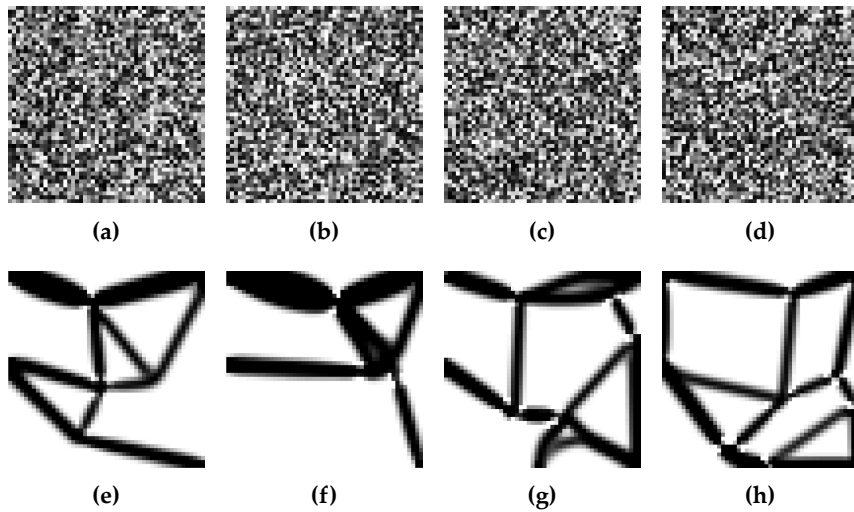


Figure 4.1: Multiplicity of solution. First row: several random material distributions used as starting points for the iterative process of topology optimization. Second row: the resulted material distributions. the two from the left for the single load case problem. Two from the right for the multiple load case problem.

Colonies [Kav+08; LL09] and Particle Swarms [LLL11], and evolutionary algorithms like Differential Evolution [WT10]. Provided that the algorithms are carefully tuned in order to cope with the large number of unknowns, one additional restriction makes usage of out-of-the-self algorithms difficult. In particular, the operators involved in evolutionary algorithms do not guarantee that at every step of the algorithm the value assigned to the vector of design variables represents a realizable structure or mechanism. It is possible that islands of materials may appear inside the design domain, something that make the structure with an invertible stiffness matrix. Therefore tailored operators are required to keep structural integrity or constraints and this makes every development case dependent [WT05; MRP06]. These comments are in accordance with published results [Sig11].

The following sections contain a brief description of the evolutionary algorithms, specifically Differential Evolution and Particle Swarm Optimization, as well as an outline of the hybrid scheme.

4.2 Evolutionary Algorithms

4.2.1 The definition of evolution

Evolution indicates all changes in the characteristics of living organisms over the years, including the appearance and new forms of life. In the 40s, the development was defined in great detail, as the changes in the sequence of alleles (different forms of a gene) in a population, from the current generation to the next. Biological evolution refers to all changes that appear in a population of organisms over time. These changes occur in organisms at the genetic level, when their genes are subject to mutation and/or recombination during the reproductive process, and that way they are transmitted to the next generations.

During the evolution, each member of the population inherits new features from its parents, something that increases its chances to survive and reproduce in comparison with the other similar individuals of population, inside their environment. The features that act positively, and thus incrementally to the probability to survive, tend to have great incidence in the population, while those that adversely affect or possess comparatively worse value, tend to diminish and disappear. This process of diversification of the survival and reproduction of individuals is known *natural selection*.

Charles Darwin (1809-1882) was the first to put forward the theory of evolution through natural selection and which supported the theory of organic evolution by sufficient evidence and determined how the process of natural selection brought about the adaptation of people in their environment, but avoided for years to publish his findings. Darwin's theory of natural selection claims that the diversity in organisms appears random in nature, while the survival or extinction of each organism is determined by its ability to adapt to its environment.

4.2.2 Evolutionary Algorithms

Inspired by the work and results of the Darwin's theories, many scientists and engineers apply the principles of natural evolution in research, resulting in a new kind of algorithms which are very useful in solving demanding and difficult problems. An example of use of the theory of evolution, for solving such problems is the Evolutionary Algorithms (Evolutionary Algorithms, EA). This kind of algorithms are useful in cases where the user is able to define a best solution among others, but finding the best is difficult, impossible

or requires a long time. In these cases an EA continuously produces better solutions until one which is sufficiently satisfactory in terms of requirements set, even if this is not the best of all.

Evolutionary algorithms are described as heuristic optimization algorithms, using mechanisms and techniques borrowed from biological evolution, such as reproduction, selection, crossover, recombination, mutation. Candidate solutions to a problem are individuals in a population and their value is described by a fitness function. The evolution of the population takes place after a repeated application of the above mentioned operators. The process of applying the operators to the individuals in the population is the factor that differentiate EA among each others, creating several variations.

Evolutionary algorithms are used for the solution of optimization problems because they are very easy to implement and use, and find application in a wide range of different problems in science and engineering. Ongoing research on this subject has led to the discovery of some of their weaknesses, such as slow convergence, but also to improvements of these, in order to overcome obstacles they may encounter. Users of EA's are very difficult to have a full overview of the best choice of tuning parameters of EA, since their performance is highly dependent upon the particular problem to be solved, and the respective parameters and constraints.

4.2.3 A brief history of EA's

The first one who referred to *genetical or evolutionary search* was Alan Turing in 1948. In 1962 Bremermann, programmed computer experiments on *optimization through evolution and recombination* [Bremermann1968]. In the 1960s, the main concept of the EA's was developed into three different implementations, which follow a distinct path, but having strong interactions between them:

- Evolution Strategies (ESs), proposed by Rechenberd and Schwefel [Rec73], [Sch93]
- Evolutionary Programming (EP), introduced by Fogel, Owens & Walsh [FOW66]
- Genetic Algorithms (GAs) presented in 1966 by Holland [Hol62; Hol92] and later developed by Goldberg [Gol89; Gol02] and Michalewicz [Mic96]

All three implementation were developed seperately for about 15 years, until the early 1990's where they considered as members of a greater ecosystem,

known as *Evolutionary Computing* (EC). Another branch of GA's, the Genetic Programming (GP), has been recently developed by Koza [Koz92; Koz94] and Banzhaf *et al* [Ban+98]. All four prementioned implementations are different branches of the EA's and can be viewed as different algorithm variants. More information regarding Evolutionary Computing can be found in reference [ES03].

4.2.4 EA's features

EA's introduce clear advantages in comparison with classical optimization methods. They do not require convexity, continuity or existence of the first or second derivatives of the objective function which is not always easily calculated. EA's differs from classical optimization methods in several aspects and present the following features that are borrowed from biology:

- **stochasticity:** the EA's are based on random sampling, which characterize them as a non-deterministic method, that may can result in usually quite close but different solutions for a repeated number of executions of the algorithm. In contrast with the deterministic methods that always result in the same solution.
- **population based:** unlike classical optimization methods that keep the best solution found up to the current step, the EA maintains a set of candidate solutions that form a population. The many different solutions are combined together by means of genetic operators to form additional solutions and thus to achieve evolution.
- **chromosomes:** in EA's each member of the population is a candidate solution that consists of chromosomes. For simplicity reasons, each member consists of one and only chromosome. Each chromosome is made by genes, and every gene represents a design variable. The chromosomes can be represented as a vectors or matrices that contain the values of each design variable. Different values in every design variable represent different members. Figure 4.2 illustrates four examples of individuals/chromosomes. Each chromosome consists of 9 genes, and each gene/design-variable can take 10 values, from 0 to 9.

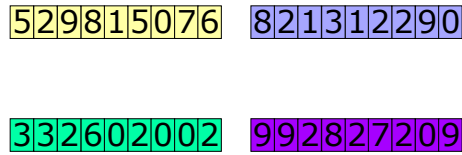


Figure 4.2: A population of 4 individuals, represented as row vectors

- recombination/crossover: in genetics, the recombination operator crosses the genetic material of two individuals in order to create new individuals. In EA's the recombination combines data from existing solutions in order to create new candidate solutions. The recombination operator plays a significant role in the process: exploration of the solution space in order to find the optimum solution. Figure 4.3 illustrates the procedure of the *one point crossover* operator: a cutoff point is selected randomly (position 5) and there is an exchange of the branches to yield two new individuals. There exists several kinds of recombination in the literature: *two points crossover* where, two cutoff points are selected randomly and anything that lies between the two points is exchanged between the parent individuals resulting two offsprings. Other kinds of recombination are the following [Cre15]:
 - cut and slice
 - multipoint recombination
 - uniform crossover
 - half uniform crossover

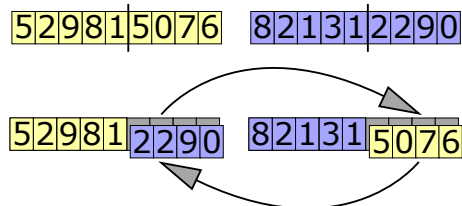


Figure 4.3: One point crossover operator applied to two members of the population

- mutation: this operators derives also from genetics. The mutation makes random changes or mutations in the genetic material (DNA) in one or more members of the population, differentiating the population. In EA's mutation accomplishes exactly the same job, randomly mutating one or more candidate solutions, which can be either better or worse than the existing ones. Mutation is equally important as crossover since it may help the algorithm to maintain genetic diversity and easily get away from local minima. The mutation can be applied either in parent or offspring members and there are many different ways to be implemented. Figure 4.4 describes the mutation procedure: one gene is randomly selected and a new value is set (randomly).

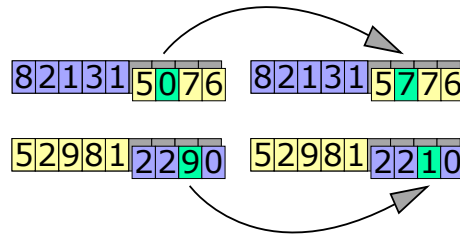


Figure 4.4: Mutation operator applied to two offsprings that was generated from the crossover operator

- evaluation: in life every new individual grows and competes with the other members in the population in order to survive. Some of the individuals die and some continue their life with ultimate aim to reproduce and give better offsprings. In EA's, each member competes with all other individuals in the population, therefore a value in each member must be set. This is accomplished by applying the *evaluation* operator to each member. This way all members are evaluated and sorted from the best to the worst. An example of a fitness function with many local minima is described in the following equation:

$$f(\mathbf{x}) = -x_1x_2^2 + e^{\left(\frac{x_3}{x_4 + 1}\right)} - \sin\left(\frac{x_5\pi}{x_7 + 1}\right) + \frac{\cos(x_5^3)}{x_6^2 + 1} \left(1 + \frac{x_8}{10} \cos(x_9\pi)\right)$$

- selection: after the evaluation of each member of the population a sorting is accomplished from the best to the worst. Some of the members

must be selected for elimination. The *selection* operator applied in each case depending on the strategy of each EA, some of worst members are vanished and new members are generated to take their place.

4.2.5 The EA procedure

Starting the algorithm, an initialization of the population is performed by generating random candidate solutions inside the solutions space. Each solution is evaluated and sorted from the best to the worst. Then an iterative process begins, where the operators of recombination-crossover and mutation, are applied to the population, generating a new intermediate population (offsprings). The new members of the intermediate population are evaluated and all of them (parents and offsprings) compete between each other. The selection operators is applied in order to create a new population that consists of some of the parents and some of the offsprings and eliminating the others. This depends on the strategy of each EA. It is also possible some of the best members of both population to be eliminated and some of the worst to be kept in the next generation in order to maintain a genetic diversity of the population. This is usually done in order to have the greatest possible diversity in population, so that the EA not to converge quickly and lead to a local optimum. On the other hand the diversity of the population should not be excessive because the algorithm may have slow convergence. The iterative process terminates when it met the convergence criteria. Algorithm 1 describes in pseudocode the structure of a typical EA:

4.3 Differential Evolution (DE)

Differential Evolution (DE) is a type of evolutionary algorithms. As every EA is a stochastic, population-based algorithm and was proposed by R. Storn and K. Price [SP95; PSL05], and further described, among others, in [Feo06]. One of the differences from evolutionary algorithms is that DE focuses in the distance and the direction information of the other candidate solutions. In the evolutionary algorithms, if a crossover operator is used, it is applied initially and then, the generated offsprings are mutated. Mutation operators are sampled from some probability distribution function. There are two basic differences in DE in comparison with other EA's:

Algorithm 1 Evolutionary Algorithm

```

set  $t = 0$ . Random initialization of 1st population  $G_0$  with  $N$  members
evaluate all candidate solutions
store best at  $\mathbf{g}^*$ 
repeat
  for  $t = 1$  : to  $T$  do
    Create intermediate population:  $\hat{G}_t$ 
    recombination/crossover
    mutation
    evaluation
    assembly of population  $G_t^* \leftarrow G_{t-1} + \hat{G}_t$ 
    select  $N$  members from population  $G_t^*$  to form population  $G_t$ 
    keep the best member of  $G_t$  at  $\mathbf{g}^*$ 
  end for
until Termination criteria is met
Now  $\mathbf{g}^*$  holds the best found solution.

```

- mutation is applied first to generate a trial vector, which is then used within the crossover operator to produce one offspring, and,
- mutation step sizes are not sampled from an a priori known probability distribution function but they are influenced by differences between some individuals of the current population.

4.3.1 Initialization of DE

DE follows all the steps of a classical EA. First there is an initialization of population. Every candidate solution can be represented by a vector (in bold letter) $\mathbf{x}_i = (x_{1,i}, x_{2,i}, \dots, x_{d,i})$, for $i = 1, \dots, N$, where N is the size of the population. Random vectors are generated so that they satisfy the lower and upper boundaries of each design variables that are already set. So that for each vector \mathbf{x}_i : $x_j^L \leq x_{j,i,0} \leq x_j^U$ where x_j^L and x_j^U the lower and upper boundaries of the design variable j . The index 0 in $x_{j,i,0}$ refers to the first generation. In general the parameter $x_{j,i,g}$ refers to the variable j of the i vector in generation g , $g = 1, \dots, G$. The initialization process is described by equation 4.1 where $r_{j,0}$ is a random number inside $(0, 1)$ and illustrated in figure 4.5. For this example 8 points that correspond to 8 2-dimensional vectors are generated inside the boundaries for each design variable.

$$x_{j,i,0} = x_j^L + r_{j,0}(x_j^U - x_j^L) \quad (4.1)$$

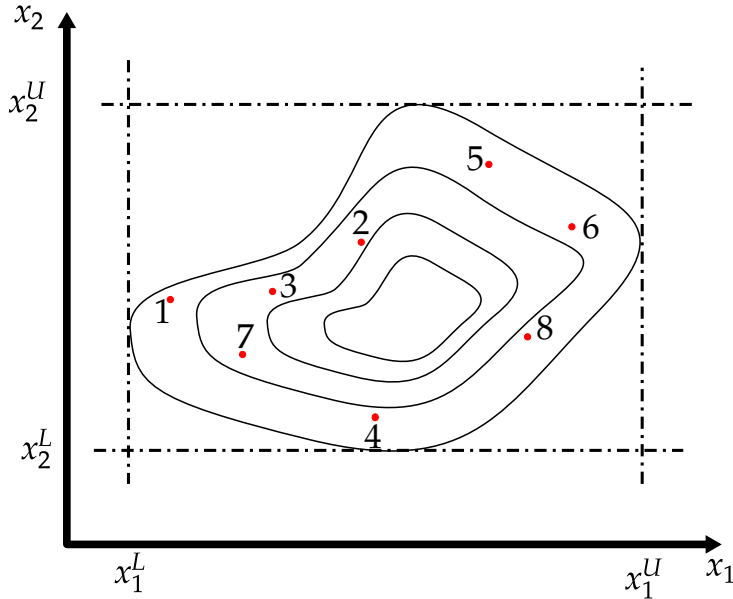


Figure 4.5: Initialization of DE population

4.3.2 The mutation operator

The mutation operator produces a trial individual \mathbf{u}_i for each individual \mathbf{x}_i of the current population by mutating it with a weighted differential. This trial individual will, then, be used by the crossover operator to produce an offspring. For each parent, \mathbf{x}_i , a trial individual \mathbf{u}_i , is generated as follows: three target individuals \mathbf{a} , \mathbf{b} , \mathbf{c} are selected from the population, such that $\mathbf{x}_i \neq \mathbf{a} \neq \mathbf{b} \neq \mathbf{c}$. Using these individuals, the trial vector is calculated by perturbing the target vector as follows:

$$\mathbf{u}_i = \mathbf{a} + \beta(\mathbf{b} - \mathbf{c}) \quad (4.2)$$

where $\beta \in (0, +\infty)$ is the scale factor, usually set equal to $\beta = 0.5$. The base vector \mathbf{a} can be determined either by selecting a random member of the population or by selecting the best member of the population. The vectors \mathbf{b} and \mathbf{c} are selected usually at random. Equation 4.3 presents a more sophisticated

mutation operators than the classical one, in which the parent is mutated using three different vectors and taking into account the best vector so far x_{opt} :

$$\mathbf{u}_i = \mathbf{a} + \beta(\mathbf{x}_{opt} - \mathbf{a}) + \beta \sum_{l=1}^2 (\mathbf{b}_l - \mathbf{c}_l) \quad (4.3)$$

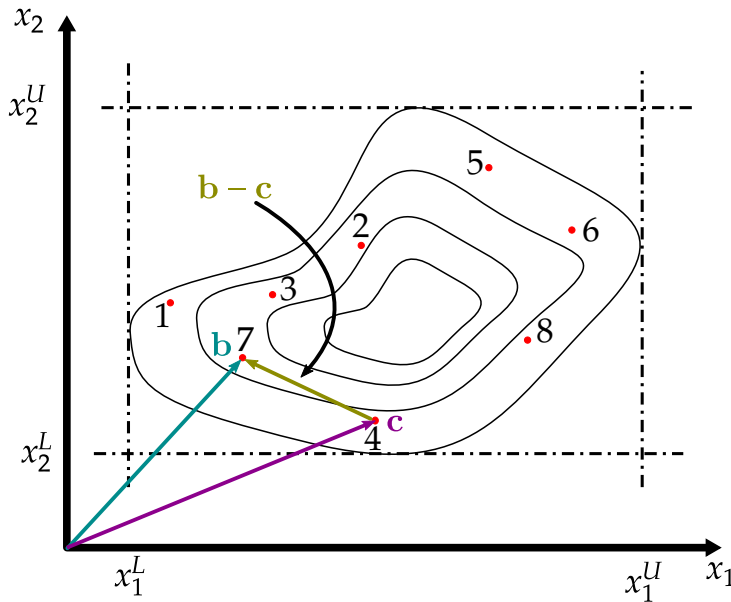


Figure 4.6: Generating the difference: $(\mathbf{b} - \mathbf{c})$

The trial vector \mathbf{u}_i competes with vector \mathbf{x}_i and if has better value of the fitness function it replaces it in the population.

4.3.3 DE crossover operator

After the completion of the mutation phase of the algorithm a crossover operator is, usually, applied. We used here binomial crossover where the points are selected randomly for the trial vector and for the parent. Initially, a crossover operator parameter C_r is selected that controls the fraction of d design variables that are selected from the trial vector. A random index is generated $k \in \{1, 2, \dots, d\}$. The C_r value is compared with the output of a random number generator, $r_k \in (0, 1)$. If the random number r_k is less or equal to the C_r , the

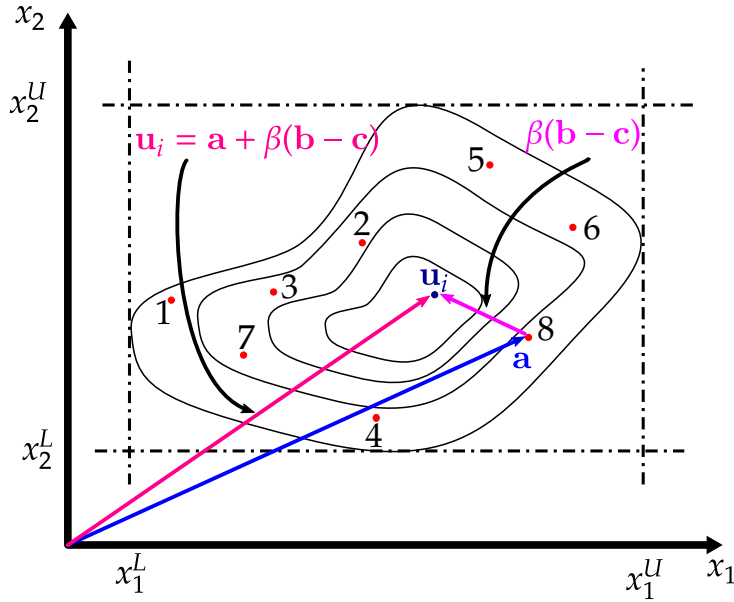


Figure 4.7: Create the trial vector $\mathbf{u}_i = \mathbf{a} + \beta(\mathbf{b} - \mathbf{c})$

corresponding value is inherited from the trial vector, otherwise it is selected from the parent:

$$\mathbf{v}_{i,g} = v'_{j,i,g} = \begin{cases} u_{j,i,g} & \text{If } r_k \leq C_r \text{ or } j = k \\ x_{j,i,g} & \text{otherwise} \end{cases} \quad (4.4)$$

Thus, the choice of the C_r is very significant because if the value is close or equal to 1, then, most of the values in the offspring are inherited from the trial vector (the mutant) but if the value is close to 0, then, the values are inherited from the parent. Figure 4.8 illustrates the crossover operator for two variables vectors. The vectors \mathbf{u}_i and \mathbf{x}_i are crossed over exchanging variables leading to two more possible vectors: \mathbf{u}'_i and \mathbf{u}''_i . Therefore after the crossover there are four possible trial vectors $\mathbf{v}_{i,g} \in \{\mathbf{x}_i, \mathbf{u}_i, \mathbf{u}'_i, \mathbf{u}''_i\}$.

4.3.4 Selection

After the crossover operator, the offspring vector $\mathbf{v}_{i,g}$ is evaluated by the fitness function and is compared with its parent $\mathbf{u}_{i,g}$. If the trial vector is better

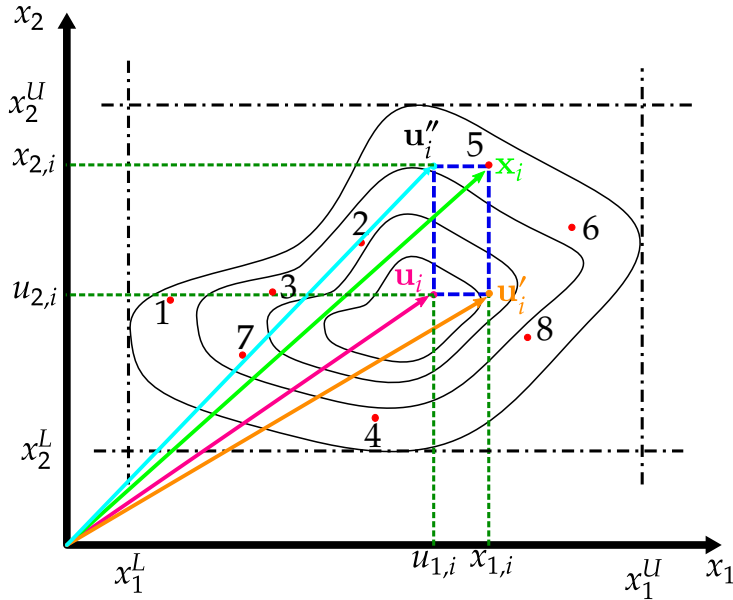


Figure 4.8: Crossover

from the parent, it is selected for the next generation, otherwise the parent survives for at least one more generation (see figure 4.9).

$$\mathbf{x}_{i,g+1} = \begin{cases} \mathbf{v}_{i,g} & \text{if } f(\mathbf{v}_{i,g}) \leq f(\mathbf{x}_{i,g}) \\ \mathbf{x}_{i,g} & \text{otherwise} \end{cases} \quad (4.5)$$

4.3.5 Differentiations of DE

The Differential Evolution algorithm can be differentiated based on three major features:

- the base vector selected for mutation whether is the best so far in the population or it is randomly selected or it is lied on a line connecting the best and a randomly selected vector
- one or more differences are added to the base vector
- the number of parameters donated by the mutant vector to the base vector follows binomial or exponential probability distribution

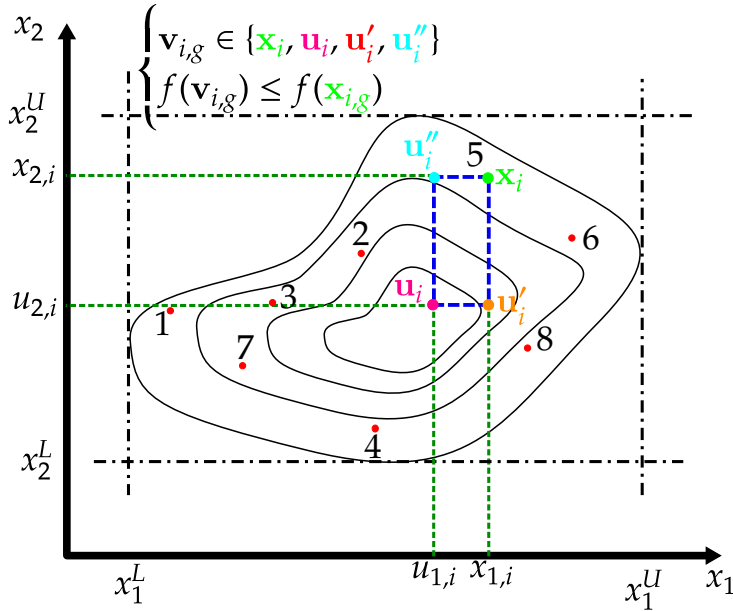


Figure 4.9: Selection

Based on the above mentioned possible options a DE can be characterized as: DE/rand/1/bin meaning that the based vector that is chosen for mutation is randomly selected, 1 difference (2 random vectors are selected) is added to the base vector (multiplied with the factor β) and the number of parameters donated from the mutant vector follows the binomial probability distribution. This strategy is defined as *classic DE*. Other possible options are illustrated in figure 4.10 and in more details in [PSL05].

4.3.6 The DE algorithm

Algorithm 2 describes in pseudocode the procedure of a classic DE.

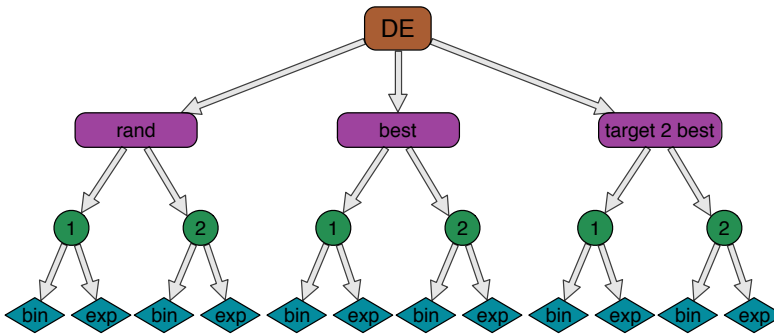


Figure 4.10: DE differentiations based on a) the base vector selection b) the number of differences used in the mutation operator, and c) the type of the random distribution used for exchanging parameters during crossover.

Algorithm 2 Differential Evolution

Initialize all candidate solutions randomly in the design-space

Evaluate all candidate solutions, store best at \mathbf{g}

repeat

for each solution $\mathbf{x}_i : i = 1$ to N **do**

 Pick three random solutions: $\mathbf{a}, \mathbf{b}, \mathbf{c}$, so that: $\mathbf{x}_i \neq \mathbf{a} \neq \mathbf{b} \neq \mathbf{c}$

 Create a trial individual \mathbf{u}_i : $\mathbf{u}_i \leftarrow \mathbf{a} + \beta(\mathbf{b} - \mathbf{c})$

 Generate a random index $k \in \{1, 2, \dots, d\}$

 Generate a random number $r_k \in (0, 1)$

if $r_k < C_r$ **then**

$x'_{k,i} \leftarrow u_{k,i}$

else

$x'_{k,i} \leftarrow x_{k,i}$

end if

if $f(\mathbf{x}'_i) < f(\mathbf{x}_i)$ **then**

$\mathbf{x}_i \leftarrow \mathbf{x}'_i$

end if

if $f(\mathbf{x}'_i) < f(\mathbf{g})$ **then**

$\mathbf{g} \leftarrow \mathbf{x}'_i$

end if

end for

until Termination criteria is met

Now \mathbf{g} holds the best found solution.

4.4 Swarm Intelligence

4.4.1 Introduction

The social behavior and education that an individual acquires in a social system, allows the individual to develop a knowledge that help the individual, together with other members to survive and evolve. People solve various problems by discussing about them with other people, sharing plans, thoughts, ideas and social behavior changes. These changes can be visualized as people move between them within their social environment. This is more evident in schools of fish and flocks of birds and insects when they are changing their three-dimensional formations in order to face a potential enemy-hunter, or to find food or to move from one place to another with the least loss of energy. This is an evidence that the swarm-group of individuals has developed a some kind of intelligence.

Swarm Intelligence was defined by Beni and Wang as a *collective behavior of decentralized, self-organized systems, natural or artificial* [BW89]. Swarm intelligence systems are groups of agents that communicate and interact with each other inside their environment without any centralized control over their behavior. The agents themselves follow very simple rules. However, through random interactions between them, unrelated to their individual behavior, an *intelligent* global behavior may appear. This phenomenon has been repeatedly observed in nature, in biological systems such as ant colonies, bird flocking, animal herding, bacterial growth, fish schooling.

Swarm Intelligence has been extensively used in solving optimization problems. Just like Evolutionary Algorithms, they are population based stochastic optimization algorithms that mimic the social behavior of groups of individuals inside their environment. In general, a swarm is a group of potential solutions that move inside the solution space, so as to find the optimum. There are several optimization algorithms:

- Particle Swarm Optimization
- Ant Colony Optimization
- Artificial Bee Colony Algorithm
- Bat Algorithm

4.4.2 Particle Swarm Optimization

Particle Swarm Optimization (PSO) was originally proposed by J. Kennedy and R. Eberhart, [KE95; EK95] as a simulation of the social behavior of social organisms such as bird flocking and fish schooling. PSO uses the physical movements of the individuals in the swarm and has a flexible and well-balanced mechanism to enhance and adapt to the global and local exploration abilities. Further material can be found in [KE01].

In PSO, each particle of the swarm, corresponds to a candidate solution that may move freely inside the solutions space. Every particle has a position and a velocity and can be represented as vector of design variables. In each iteration of the algorithm, every particle (candidate solution) is evaluated through a fitness function. The personal best positions of each particle are kept in memory along with the best position of the whole swarm. In that way, each particle knows as information the best positions of the other particles along with the best position of the swarm. In the next iteration, each particle is accelerated to a new position based on the information of its personal best and the global best position. Iterations continue until the termination criteria are met.

4.4.3 Comparison of PSO with EAs

The most important similarity between PSO and an EA is that both are based on the growth and the development of a population of candidate solutions. In both cases, the evolution of the population relies on stochasticity and an evaluation is applied to each candidate solution through a fitness function. Of course, due to the stochasticity, it is never sure that a global optimal is found. Another important similarity is the simplicity of the algorithms in both implementation and use. The number of the tuning parameters is small in both cases and both can be programmed easily in a few lines of code, with the PSO to excel a bit. The process of evaluation is easily parallelized, making both algorithms without difficulty tunned up to run on big clusters of CPU's.

The advantage of PSO, in relation to EA, is that it has memory. For each particle the best position that ever been is saved in memory, along with the best position of the whole swarm. In PSO there is no application of biological operators such as recombination, mutation and selection. Another difference between PSO and EA's, is that the particles are exchanging information (their best ever known position) with each other around their neighborhood (locally) but also with the best so far particle (globally) in the swarm, following

every time the best solutions so far. Usually the PSO is slower in progress and obviously in convergence than EAs but this is also an important advantage making PSO difficult to be trapped in local optima.

4.4.4 PSO modeling

4.4.4.1 Initialization

As it was prementioned before, a swarm consists of N particles, and each particle is represented by a vector $\mathbf{x}_i, i = 1, \dots, N$ of D design variables: $\mathbf{x}_i = (x_{1,i}, x_{2,i}, \dots, x_{D,i})^T$. A parameter t is set that corresponds to current motion of the swarm, where $t = 0, 1, \dots, T$ and T is the maximum number of motions the swarm is allowed to make. For each design variable there is a lower and upper bound: $x_j^L \leq x_{j,i,0} \leq x_j^U$. During initialization an initial (random) position for each particle is set inside the solution space, that satisfies the boundary conditions of each design variable, while the parameter t is set to 0. The initialization procedure is the same as in DE and is described by equation 4.1 and illustrated in figure 4.5.

Later an evaluation is taking place for all particles. A personal best $\hat{\mathbf{x}}_i$ is defined for each particle. The particle with the best fitness function value is saved in $\hat{\mathbf{g}}$:

$$\begin{aligned} \hat{\mathbf{x}}_i &\leftarrow \mathbf{x}_i \\ \hat{\mathbf{g}} &\leftarrow \mathbf{x}_k : f(\mathbf{x}_k) < f(\mathbf{x}_i), \quad k \neq i, \quad i = 1, \dots, N \end{aligned} \quad (4.6)$$

A velocity is defined of each particle as a vector of same size as \mathbf{x}_i : $\mathbf{v}_i = (v_{1,i}, v_{2,i}, \dots, v_{D,i})$ which describes a change of its position. The vector \mathbf{v}_i is initialized the same way \mathbf{x}_i is initialized.

4.4.4.2 Progress of PSO

The flying direction of each particle is the iteration by iteration interaction of individual and social flying experience. The algorithm completes the optimization through following the personal best solution of each particle and the global best value of the whole swarm. During evolution of the algorithm each particle updates its trajectory toward its own previous best position and the previous best position attained by any particle of the swarm, namely $\hat{\mathbf{x}}_i$ and $\hat{\mathbf{g}}$ respectively.

In time t a particle i has a position in the solution space represented by vector $\mathbf{x}_i^{(t)}$ and a velocity $\mathbf{v}_i^{(t)}$. Figure 4.11 illustrates the particle with its velocity along with its personal best and global best positions. The velocities and positions of particles are updated using the following formulas:

$$\begin{aligned}\mathbf{v}_i^{(t+1)} &= \omega_t \mathbf{v}_i^{(t)} + [c_1 \mathbf{r}_1 \circ (\hat{\mathbf{x}}_i - \mathbf{x}_i^{(t)})] + [c_2 \mathbf{r}_2 \circ (\hat{\mathbf{g}} - \mathbf{x}_i^{(t)})] \\ \mathbf{x}_i^{(t+1)} &= \mathbf{x}_i^{(t)} + \mathbf{v}_i^{(t+1)} \\ \omega_t &= \omega_{max} - \frac{(\omega_{max} - \omega_{min})t}{T}\end{aligned}\quad (4.7)$$

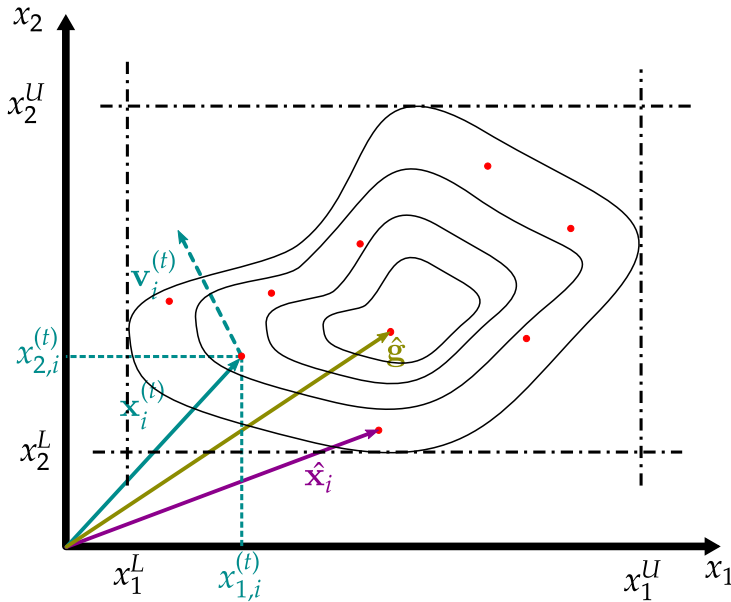


Figure 4.11: Particle $\mathbf{x}_i^{(t)}$ with its velocity $\mathbf{v}_i^{(t)}$

where t is the current time increment; c_1 and c_2 are the acceleration coefficients controlling how far a particle will move in a single iteration (typically set to 2.0); \mathbf{r}_1 , \mathbf{r}_2 are two random generated vectors using universal distribution inside $[0, 1]$, and ω_t is an inertia coefficient controlling the evolution of the algorithm for time step t . For high values of ω the algorithm facilitates a global search while for small values facilitates a local search. By linearly decreasing the inertia weight from a relatively large value to a small value through the course of the PSO run gives the best PSO performance compared with fixed

inertia weight settings. The symbol \circ represents the *Hadamard product* of vectors and matrices with same dimensions, where multiplication is based on element by element: $(\mathbf{A} \circ \mathbf{B})_{ij} = (\mathbf{A})_{ij} \cdot (\mathbf{B})_{ij}$.

Next, the velocity vector is scaled to $\omega_t \mathbf{v}_i^{(t)}$, and the vector differences, $(\hat{\mathbf{x}}_i - \mathbf{x}_i^{(t)})$ and $(\hat{\mathbf{g}} - \mathbf{x}_i^{(t)})$ are calculated and illustrated in figure 4.12.

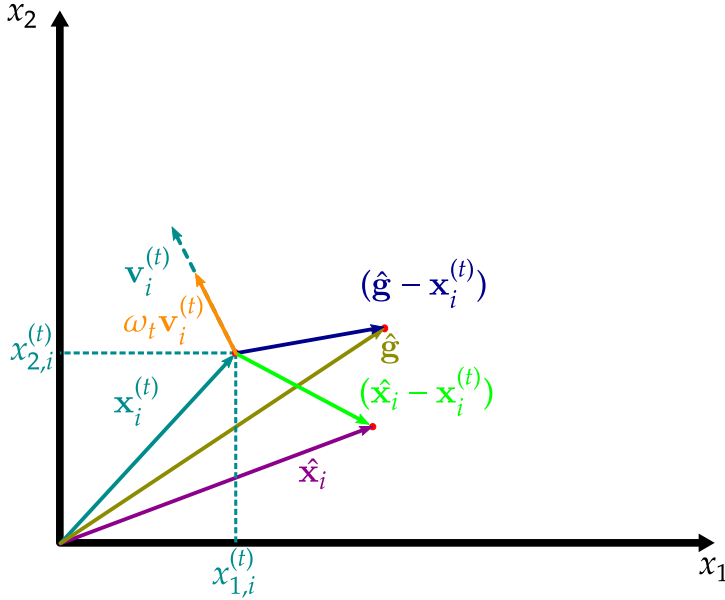


Figure 4.12: Calculations of $\omega_t \mathbf{v}_i^{(t)}$, $(\hat{\mathbf{x}}_i - \mathbf{x}_i^{(t)})$ and $(\hat{\mathbf{g}} - \mathbf{x}_i^{(t)})$

Subsequently, two new random vectors are generated r_1 and r_2 and two new vectors are composed: $c_1 r_1 \circ (\hat{\mathbf{x}}_i - \mathbf{x}_i^{(t)})$ and $c_2 r_2 \circ (\hat{\mathbf{g}} - \mathbf{x}_i^{(t)})$, which consequently formulate vector \mathbb{A} . This process is illustrated in figures 4.13 and 4.14 respectively. The two already composed vectors $\omega_t \mathbf{v}_i^{(t)}$ and \mathbb{A} are added to compose the new velocity vector $\mathbf{v}_i^{(t+1)}$ as presented in figure 4.15. The particle updates its new position by adding to its current position the new velocity vector: $\mathbf{x}_i^{(t+1)} = \mathbf{x}_i^{(t)} + \mathbf{v}_i^{(t+1)}$. This is described in figure 4.16. An evaluation is taking place and if the new $\mathbf{x}_i^{(t+1)}$ is better than the old $\mathbf{x}_i^{(t)}$, then it updates its personal best $\hat{\mathbf{x}}_i$. If it is even better than the global best $\hat{\mathbf{g}}$, then it becomes the global best.

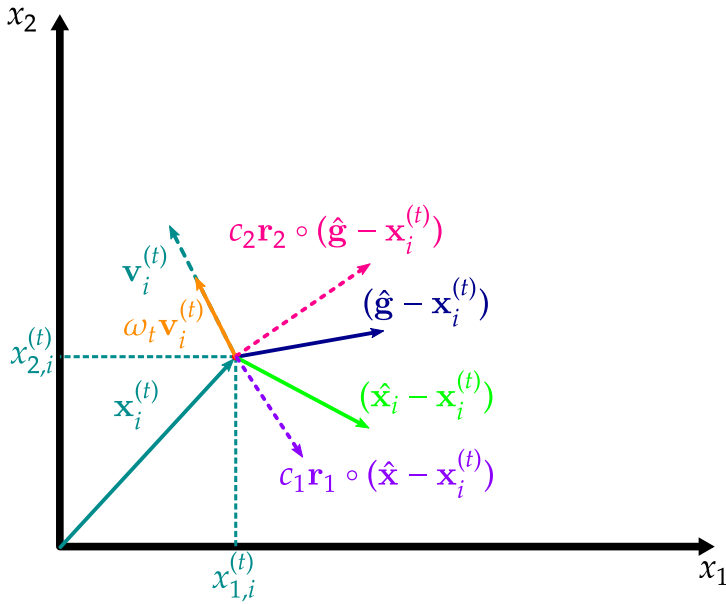


Figure 4.13: Composition of $c_1r_1(\hat{x}_i - x_i^{(t)})$ and $c_2r_2(\hat{g} - x_i^{(t)})$

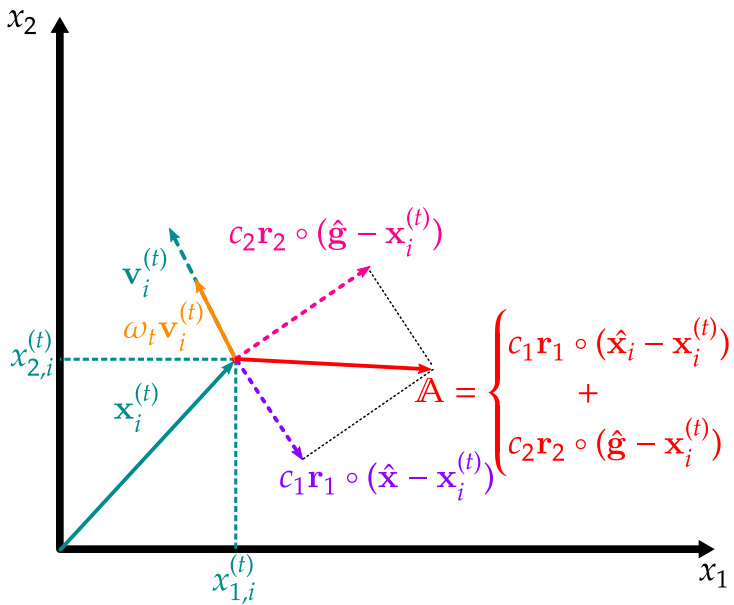


Figure 4.14: Composition of temporary vector \mathbb{A}

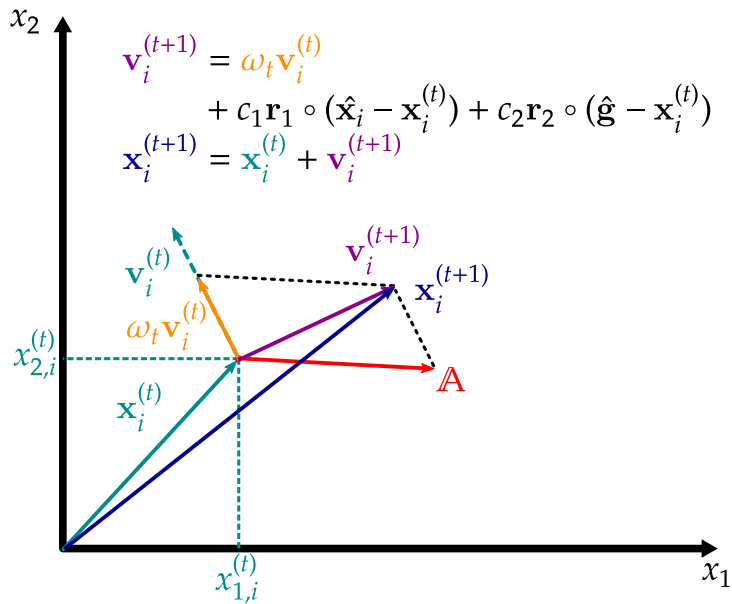


Figure 4.15: Composition of a new velocity vector $\mathbf{v}_i^{(t+1)}$.

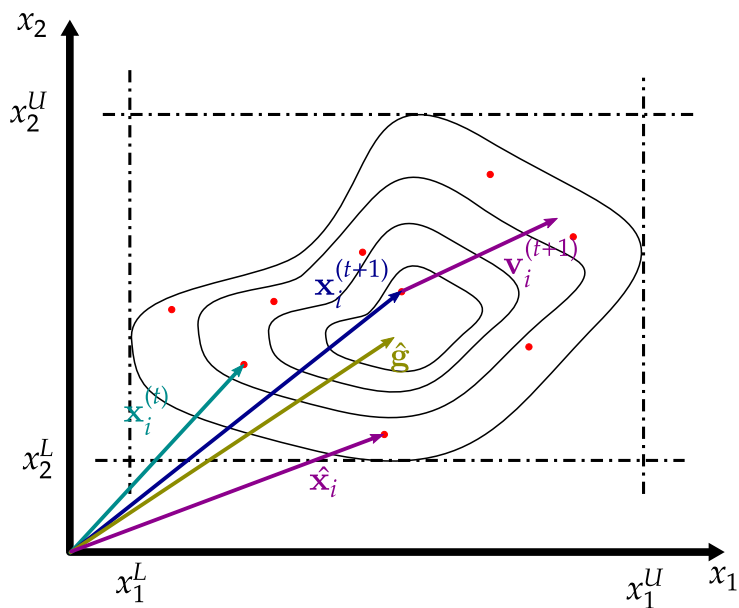


Figure 4.16: Update of position and velocity of particle i for time increment $t + 1$.

4.4.5 The PSO algorithm

Let N be the number of particles in the swarm, each has a position $\mathbf{x}_i \in \mathbb{R}^D$ and a velocity $\mathbf{v}_i \in \mathbb{R}^D$ where D the total number of design variables. Let $\hat{\mathbf{x}}_i$ be the best known position of particle i and let $\hat{\mathbf{g}}$ be the best known position of the entire swarm. A basic PSO algorithm is then:

Algorithm 3 Particle Swarm Optimization

```

for each particle:  $i = 1$  to  $N$  do
  Initialize particle's position:  $\mathbf{x}_i^{(0)} = \mathbf{x}^L + \mathbf{r}_x^{(0)} \circ (\mathbf{x}^U - \mathbf{x}^L)$ 
  Initialize the particle's best known position to its initial position:  $\hat{\mathbf{x}}_i \leftarrow \mathbf{x}_i$ 
  if  $f(\mathbf{p}_i) < f(\mathbf{g})$  then
    update the swarm's best known position:  $\hat{\mathbf{g}} \leftarrow \hat{\mathbf{x}}_i$ 
  end if
  Initialize the particle's velocity:  $\mathbf{v}_i^{(0)} = \mathbf{x}^L + \mathbf{r}_v^{(0)} \circ (\mathbf{x}^U - \mathbf{x}^L)$ 
end for
for  $t = 1$  to  $T$  do
  for each particle:  $i = 1$  to  $N$  do
    Generate random vectors:  $\mathbf{r}_1, \mathbf{r}_2 \in \mathbb{R}^D$  in  $[0, 1]$ 
    Update the particle's velocity:
    
$$\mathbf{v}_i^{(t+1)} \leftarrow \omega_t \mathbf{v}_i^{(t)} + [c_1 \mathbf{r}_1 \circ (\hat{\mathbf{x}}_i - \mathbf{x}_i)] + [c_2 \mathbf{r}_2 \circ (\hat{\mathbf{g}} - \mathbf{x}_i)]$$

    Update the particle's position:  $\mathbf{x}_i^{(t+1)} \leftarrow \mathbf{x}_i^{(t)} + \mathbf{v}_i^{(t+1)}$ 
    if  $f(\mathbf{x}_i^{(t+1)}) < f(\hat{\mathbf{x}}_i)$  then
      Update the particle's best known position:  $\hat{\mathbf{x}}_i \leftarrow \mathbf{x}_i^{(t+1)}$ 
      if  $f(\hat{\mathbf{x}}_i) < f(\hat{\mathbf{g}})$  then
        Update the swarm's best known position:  $\hat{\mathbf{g}} \leftarrow \hat{\mathbf{x}}_i$ 
      end if
    end if
  end for
  Update inertia parameter  $\omega_t \leftarrow \omega_{max} - \frac{(\omega_{max} - \omega_{min})t}{T}$ 
end for
Now  $\mathbf{g}$  holds the best found solution.

```

The vectors $\mathbf{r}_x, \mathbf{r}_v, \mathbf{r}_1, \mathbf{r}_2 \in \mathbb{R}^D$ and consists of uniformly distributed random numbers in the interval $[0, 1]$. The vectors $\mathbf{x}^L, \mathbf{x}^U \in \mathbb{R}^D$ and contain the lower and upper boundaries of each design variable.

4.5 The hybrid scheme

A hybrid scheme using evolutionary algorithms for structural optimization problems has been proposed in the past [Pap+96], [Pap+98]. The use of neural networks has also been applied [PLT98]. The hybrid scheme proposed here, due to the usage of classical local iterative topology optimization steps, guarantees structural integrity along every step of the algorithm. Furthermore the operators of the evolutionary algorithm remain unchanged. As a result the hybrid scheme is very general and allows for the usage of any evolutionary algorithm (genetic, particle swarm, etc) as well as every local iterative algorithm for the topology optimization. It must be mentioned that another hybrid scheme based on genetic algorithms for the design of structures, has been proposed recently [Car+13].

4.5.1 Initialization of the hybrid scheme

The hybrid algorithm starts by creating random initial material distributions. Each one of these does not represent a feasible structure or mechanism. Therefore an operator must be applied in order to evaluate them. This is achieved using topology optimization thus leading to a group of final material distributions. This process is illustrated in figure 4.17. Each of the final distributions has a value according to the fitness function used and sorted from the best to the worst. This group constitute the initial population used for the evolution process of the evolutionary algorithm used.

4.5.2 Progress of the hybrid scheme

The population of final material distributions generated in the previous step are used as generation 0 or swarm in time $t = 0$ for the purposes of DE and PSO respectively. The population is evolving according the parameters of each evolutionary algorithm used. Applying the evolutionary techniques used in Differential Evolution or Particle Swarm Optimization over the initial population of solutions, creates intermediate material distributions that are not feasible for two main reasons: either the resulted layout is not a structure (islands of material may appear) or the volume constraint is not satisfied. Thus the new intermediate distributions need to become "structures". Topology optimization is applied again in order to maintain structural integrity as well as to place a value to each resulted solution.

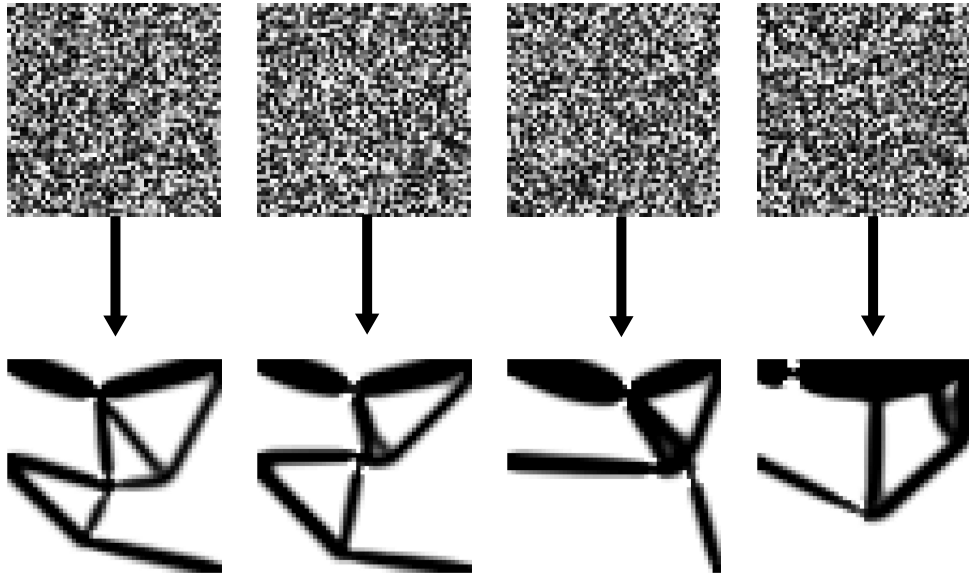


Figure 4.17: Initialization of the hybrid scheme

Figure 4.18 illustrates the prementioned process. The orange and magenta structures are combined together resulting to a different intermediate layout which is again evaluated in order to become a "structure". For the purposes of this example, the problem definition illustrated in figure 3.9(a) was used. The design domain was discretized in 2D square plain stress elements. The density of each element is represented as a design parameter which takes values in the $(0, 1]$.

The iterations of the hybrid algorithm stop when the termination criteria are met. The flow chart of the hybrid scheme is given in figure 4.19.

4.5.3 Advantages of the hybrid scheme

One of the great advantages of the proposed hybrid algorithm is that at the end of every step, due to internal steps of classical iterative topology optimization, the material distribution corresponds to a realistic structure. On the contrary, simple application of classical evolutionary algorithms in topology optimization, due to the drastic change of variables involved, does not guarantee that every material distribution resulted along the steps of the algorithm corresponds to a real structure (with invertible stiffness matrix). It should be

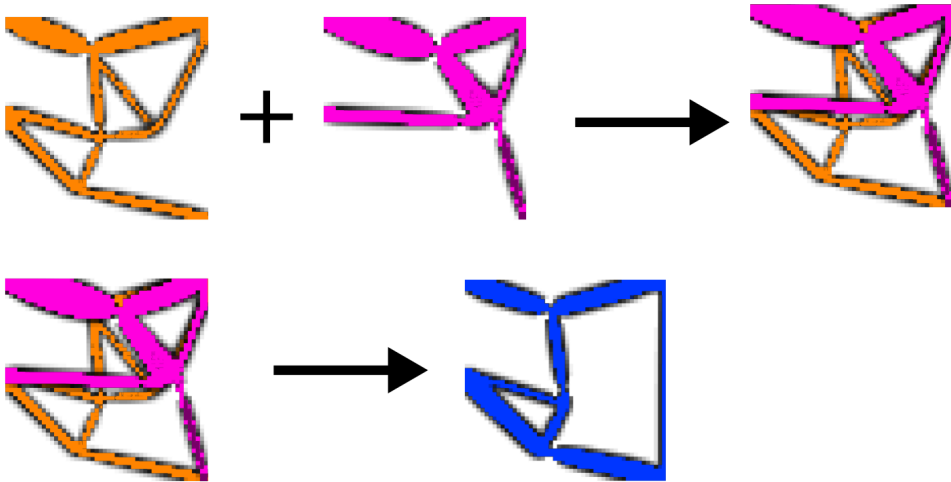


Figure 4.18: Evolution & evaluation inside the hybrid scheme

noted that the algorithm has been tested till now on single objective optimization problems. Therefore all multiobjective problems mentioned previously are transformed first into a single objective problem and then solved by this method. Nevertheless the algorithm can be extended to treat multiobjective problems and create solutions elements of the Pareto optimum.

It must be mentioned that the current hybrid scheme can be easily parallelized. Every random material distribution that is generated or evolved according to the strategy of each evolutionary algorithm must be evaluated using topology optimization. The procedure of evaluation, for every different member of population is independent from the other members. Hence, using modern computational tools like MATLAB, the evaluation procedure for every member can be assigned to each different cores of a multicore CPU, or GPU of modern workstations, and cut the computational cost very easy.

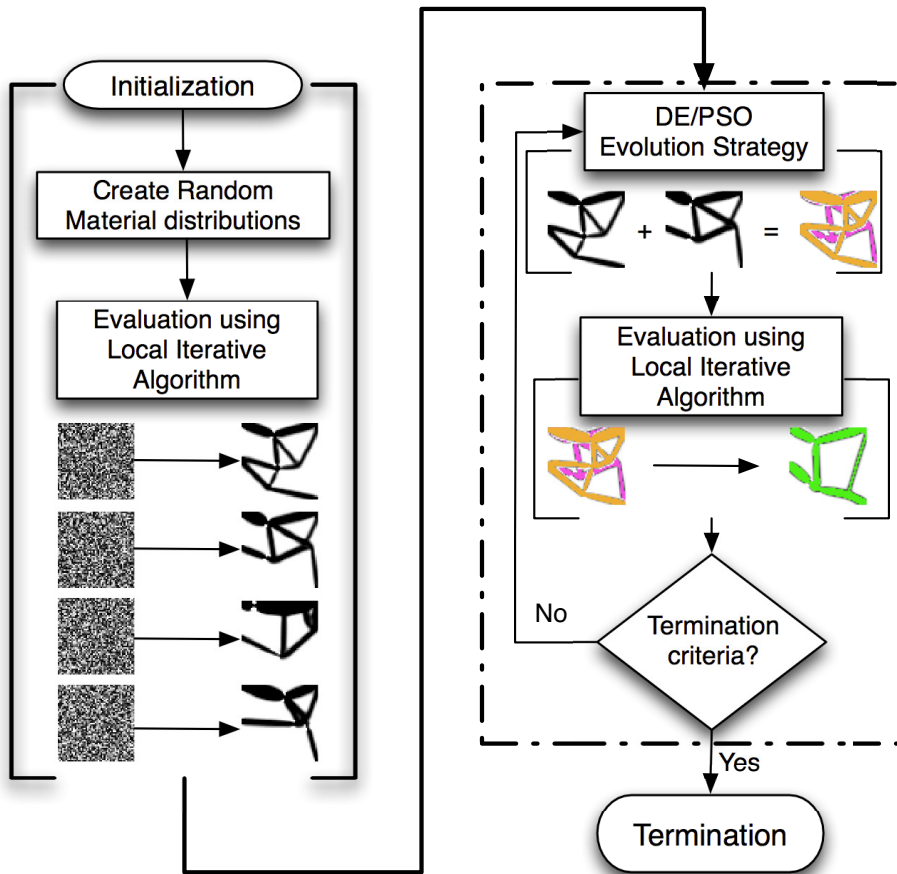


Figure 4.19: The hybrid scheme

CHAPTER 5

Case Study: Compliant mechanisms

In this chapter, numerical results for the design of compliant mechanisms using the hybrid scheme already described in the previous chapter are presented. In order to exhibit the mechanisms displacements clearly, a filter has been applied to the final material distribution, displaying only the elements with density greater than 0.6. This is used for visualization purposes only.

5.1 Classic compliant mechanisms: Single load case

The results presented in this section correspond to the an asymmetric force inverter device. There is only one load case, meaning that the compliant mechanism is configured to perform one function only.

5.1.1 Without output control

In this subsection, the results for the asymmetric force inverter compliant mechanism are presented. The problem definition is illustrated in figure 3.9 and the parameters for the topology optimization algorithm are presented in table 5.1.

5.1.1.1 Using DE

The configuration parameters for the hybrid scheme using Differential Evolution without output control are presented in the table 5.2.

Parameter	Value
Discretization	50x50
Design Variables	2500
Degrees of Freedom	5202
Local search iterations	100
SIMP penalty coefficient, p	3
Filter radius, r	2
Volume Limit	30%

Table 5.1: Topology Optimization Algorithm parameters

Parameter	Value
Population size	32
Generations	100
Crossover C_r	0.9
Mutation β	1.5
Design Variables	2500

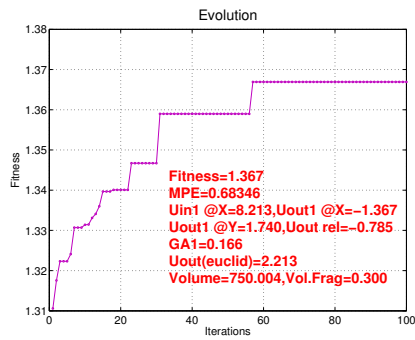
Table 5.2: Differential Evolution configuration parameters

Figure 5.1 shows the resulted material distribution for Hybrid scheme using DE for the one load case asymmetric force inverter compliant mechanism without output control.

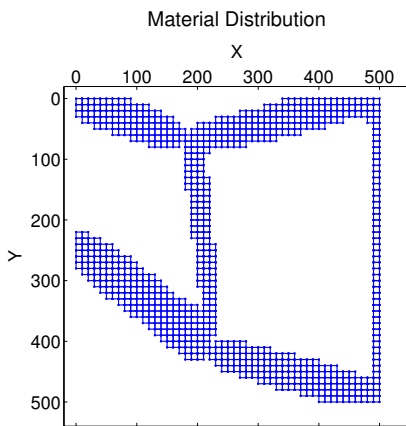
Figure 5.2 shows the resulted material distributions that represent the evolution of the hybrid scheme.



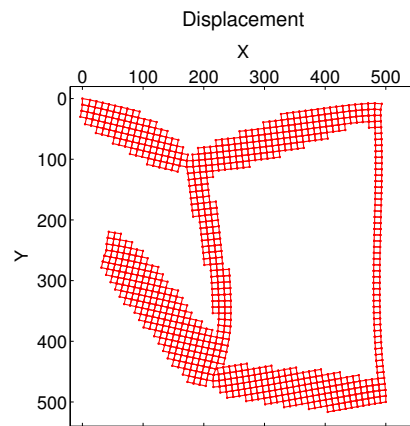
(a) Final Material Distribution



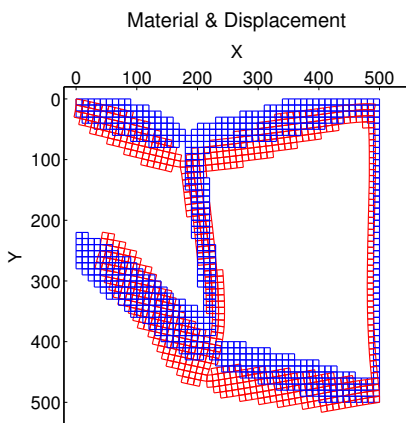
(b) Evolution of DE



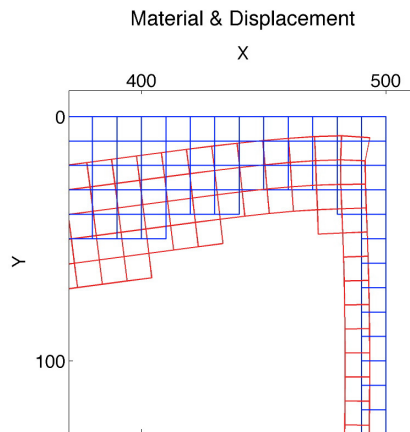
(c) Final Mat. Distribution (filtered)



(d) Displacement (filtered)



(e) Displacement & Mat. Distribution (filtered)



(f) Detail of the top right corner

Figure 5.1: Results: Hybrid Scheme, One Load Case, No output control, using DE

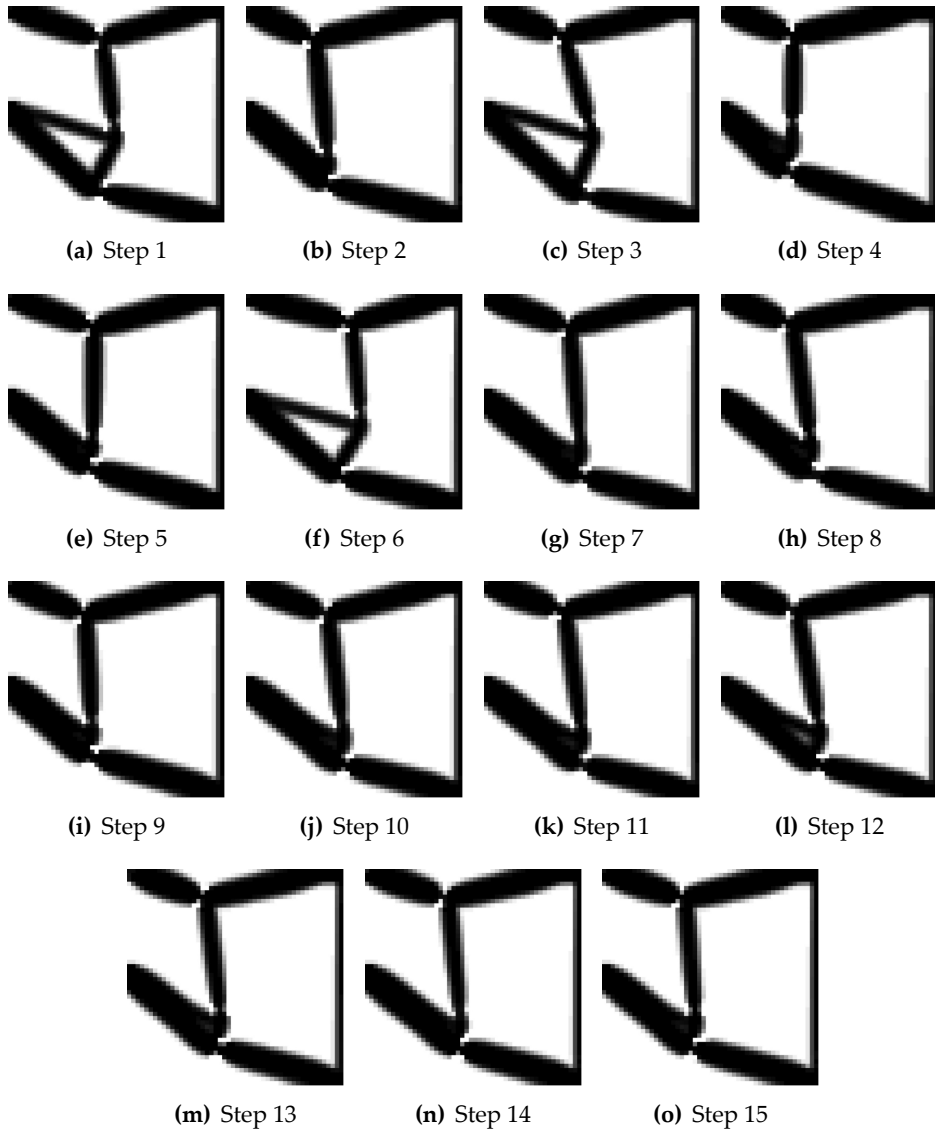


Figure 5.2: Intermediate material distributions for One load case using Differential Evolution

5.1.1.2 Using PSO

The configuration parameters for the hybrid scheme using Differential Evolution without output control are presented in the table 5.3.

Parameter	Value
Swarm size	32
Iterations	100
Acceleration parameters $c_1 = c_2$	2
Inertial parameters w_{max}, w_{min}	0.9, 0.1
Design Variables	2500

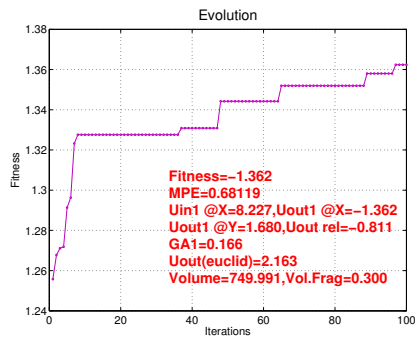
Table 5.3: Particles Swarm Optimization configuration parameters

Figure 5.3 shows the resulted material distribution for hybrid scheme using PSO for the one load case, asymmetric force inverter compliant mechanism, without output control.

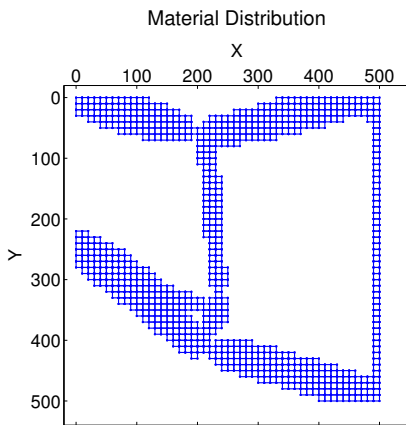
Figure 5.4 shows the resulted material distributions that represent the evolution of the hybrid scheme.



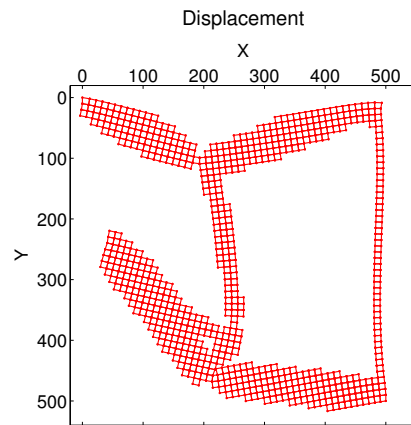
(a) Final Material Distribution



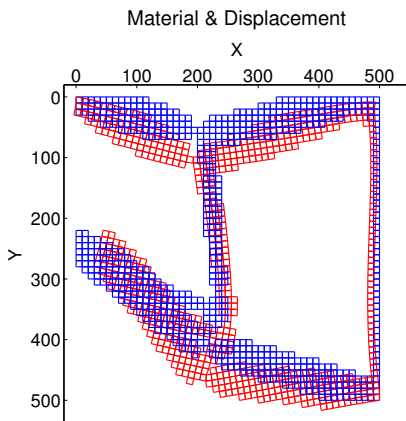
(b) Evolution



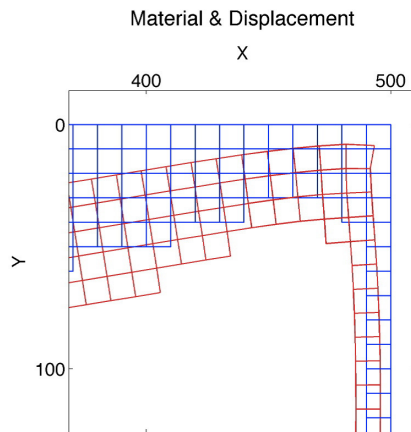
(c) Final Mat. Distribution (filtered)



(d) Displacement (filtered)



(e) Displacement & Mat. Distribution (filtered)



(f) Detail

Figure 5.3: Results for one load case using Particle Swarm Optimization

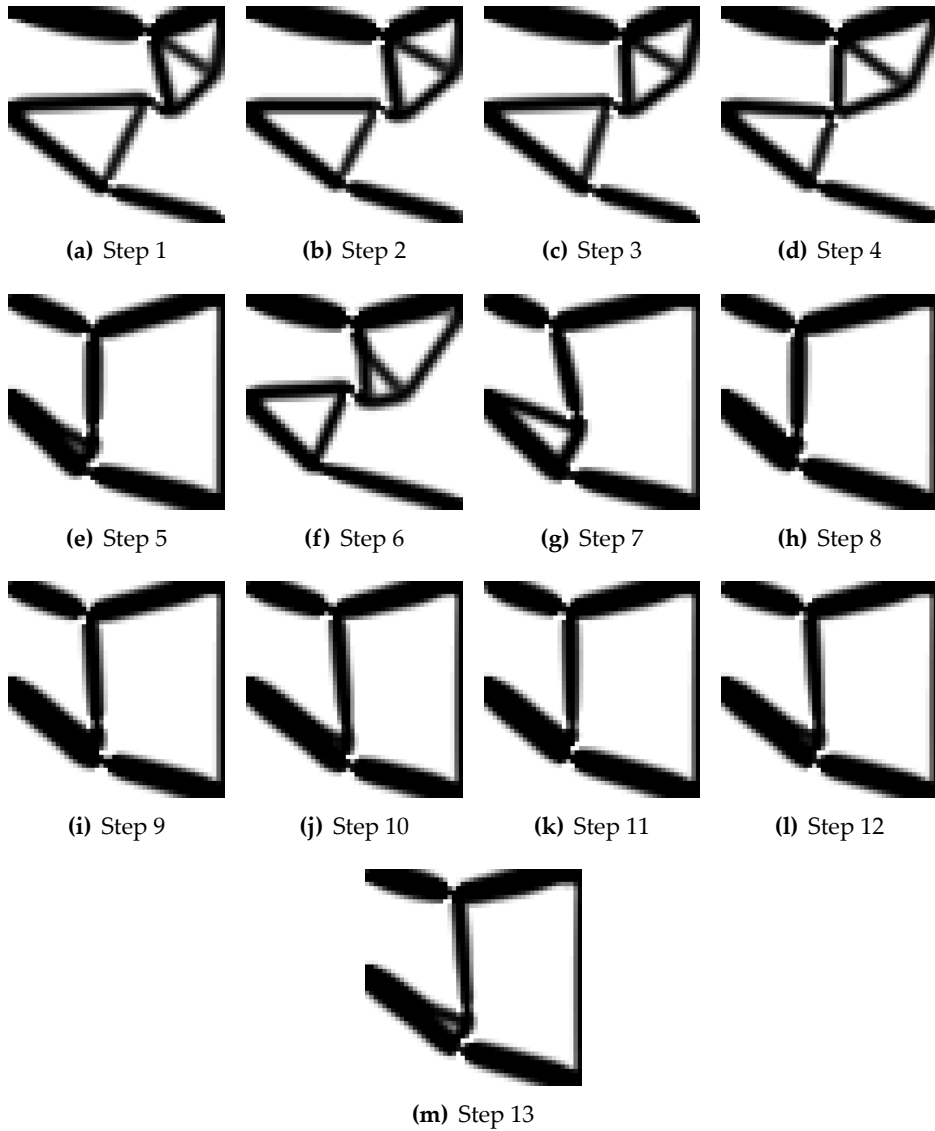


Figure 5.4: Intermediate material distributions for One load case using Particle Swarm Optimization

5.1.1.3 Repeatability of results for the one load case

Due to the stochastic nature of the DE, we run 4 different simulations in order to examine if the results are repeatable. Figures 5.5 and 5.6 demonstrates for DE and PSO respectively, the final material distributions for four different simulations of the hybrid scheme for the problem of the asymmetric force inverted compliant mechanism without output control. In all cases, the final material distributions seem to have the same shape. Tables 5.4 and 5.5 show some numerical results for each case.

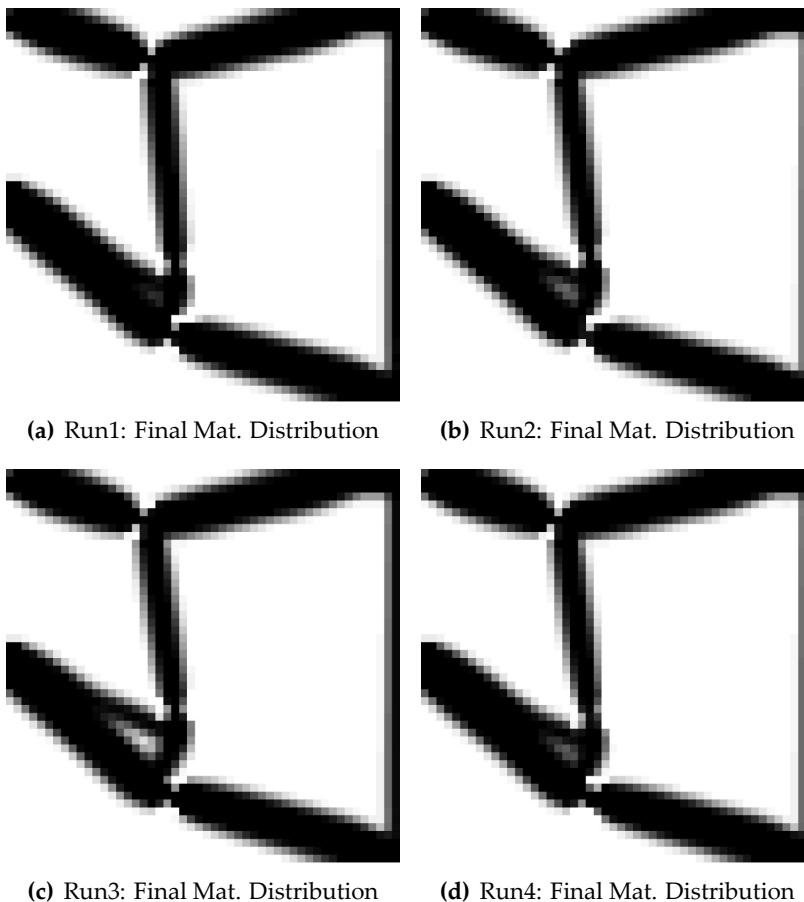


Figure 5.5: Four Final material distributions using Hybrid Scheme using Differential Evolution for one load case

Scheme	fitness	$U_{in}^{(X)}$	$U_{out}^{(X)}$	$U_{out}^{(Y)}$	U_{vec}
DE/1load					
run 1	1.367	8.123	-1.367	1.740	2.213
run 2	1.360	8.143	-1.360	1.747	2.214
run 3	1.361	8.135	-1.361	1.736	2.206
run 4	1.358	8.121	-1.358	1.746	2.212

Table 5.4: Results for One load case using Hybrid scheme with DE



(a) Run1: Final Mat. Distribution



(b) Run2: Final Mat. Distribution



(c) Run3: Final Mat. Distribution



(d) Run4: Final Mat. Distribution

Figure 5.6: Four Final material distributions using Hybrid Scheme using PSO for one load case

Scheme DE/1load	fitness	$U_{in}^{(X)}$	$U_{out}^{(X)}$	$U_{out}^{(Y)}$	U_{vec}
run 1	1.362	8.227	-1.362	1.680	2.168
run 2	1.354	8.029	-1.354	1.800	2.257
run 3	1.352	8.049	-1.352	1.802	2.258
run 4	1.349	8.099	-1.349	1.784	2.237

Table 5.5: Results for One load case using Hybrid scheme with PSO

5.1.2 With output control

In this subsection, the results for the asymmetric force inverter compliant mechanism are presented using motion control to the output point. The problem definition is illustrated in figure 3.11 and the parameters for the topology optimization algorithm are presented in table 5.6.

Parameter	Value
Discretization	30x30
Design variables	900
DOFS	1922
Local search iterations	60
SIMP penalty coefficient, p	3
Filter Radius, r	1.5
Volume fraction	30%

Table 5.6: Running parameters: topology optimization for the design of compliant mechanism using DE, and featuring output control, with a single load case.

5.1.2.1 Using DE

The configuration parameters for the hybrid scheme using Differential Evolution with output control are presented in the table 5.7.

Parameter	Value
Population size	20
Generations	50
Crossover factor C_r	0.9
Mutation factor F	1.5
Design variables	900

Table 5.7: Differential Evolution configuration parameters

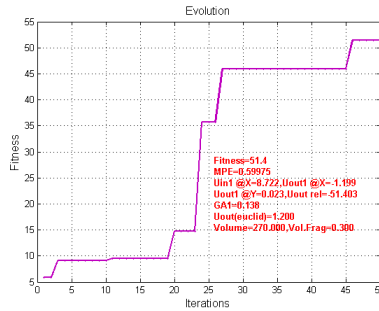
Figure 5.7 shows the resulted material distribution for Hybrid scheme using DE for the one load case asymmetric force inverter compliant mechanism with output control. The numerical results are displayed in table 5.8.

Parameter		Value
Objective function	$\left \frac{u_{out}^{@X}}{u_{out}^{@Y}} \right $	51.4
Input displacement at X,	$u_{in}^{@X}$	8.722
Output Displacement at X,	$u_{out}^{@X}$	-1.199
Output Displacement at Y,	$u_{out}^{@Y}$	-0.023
Total distance		1.200
Geometric advantage		13.8%

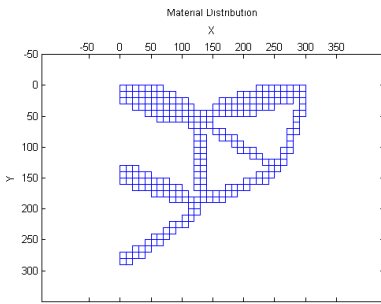
Table 5.8: Results: topology optimization for the design of compliant mechanism using DE, and featuring output control, with a single load case.



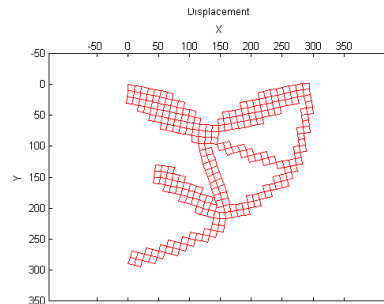
(a) Final Material Distribution



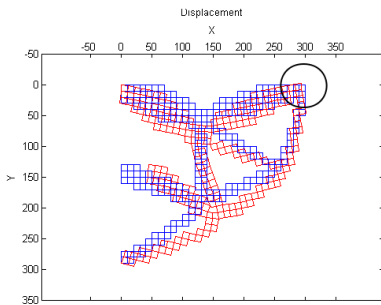
(b) Evolution



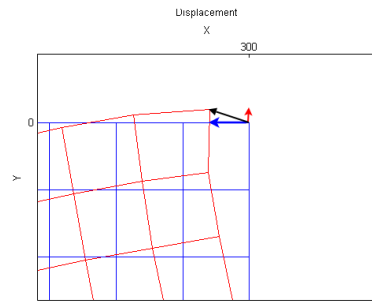
(c) Final Mat. Distribution (filtered)



(d) Displacement (filtered)



(e) Displacement & Mat. Distribution (filtered)



(f) Detail

Figure 5.7: Results for one load case using Differential Evolution and output control

5.1.2.2 Using PSO

The configuration parameters for the hybrid scheme using Particles Swarm Optimization with output control are presented in the table 5.9.

Parameter	Value
Swarm size	20
Total number of PSO local searches	50
Acceleration factors $c_1 = c_2$	2
Inertia factors w_{max} & w_{min}	0.9, 0.1
Design variables	900

Table 5.9: Particles Swarm Optimization configuration parameters

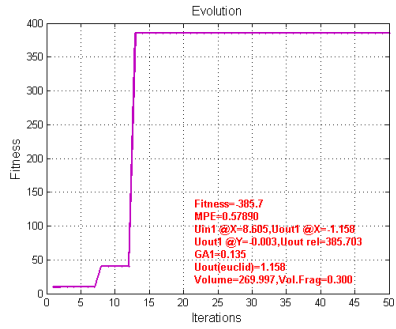
Figure 5.8 demonstrates the resulted material distribution for Hybrid scheme using DE for the one load case assymmetric force inverter compliant mechanism with output control. The numerical results are displayed in table 5.10.

Parameter	Value
Objective function	$\left \frac{u_{out}^{@X}}{u_{out}^{@Y}} \right $ 385.7
Input displacement at X,	$u_{in}^{@X}$ 8.605
Output Displacement at X,	$u_{out}^{@X}$ -1.158
Output Displacement at Y,	$u_{out}^{@Y}$ -0.003
Total distance	1.158
Geometric advantage	13.5%

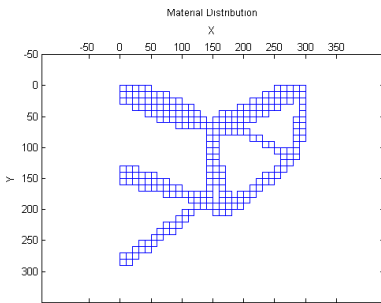
Table 5.10: Results: topology optimization for the design of compliant mechanism using PSO, and featuring output control, with a single load case.



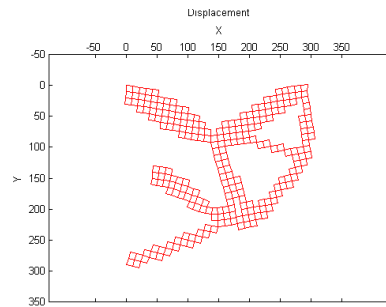
(a) Final Material Distribution



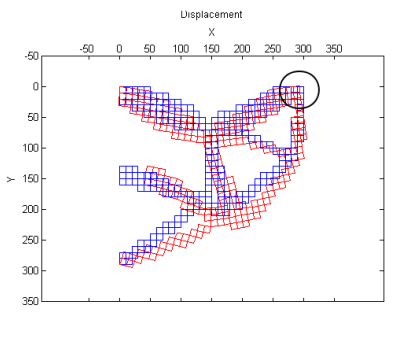
(b) Evolution



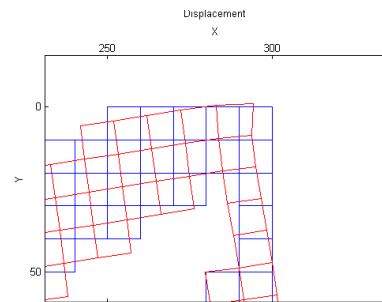
(c) Final Mat. Distribution (filtered)



(d) Displacement (filtered)



(e) Displacement & Mat. Distribution (filtered)



(f) Detail

Figure 5.8: Results for one load case using Particle Swarm Optimization and output control

5.1.2.3 Comparison of DE and PSO results for an single load case

The PSO algorithm resulted to a considerably better solution compared to the DE. The values of the objective function are 357.8 and 51.4 respectively. The displacement on the X axis in both cases is similar while in the Y axis the difference of the displacement is remarkable. In particular PSO resulted to $u_{out}^{@Y}=0.003$ while DE to $u_{out}^{@Y}=0.023$, an about 7 times higher value. The vertical displacement $u_{out}^{@Y}$ is found to the denominator of the objective function and has to be minimized. Both algorithms resulted to similar material distributions as well as volume percentage. Table 5.11 demonstrates the comparative results of the two evolutionary algorithms.

DE vs PSO		
	DE	PSO
Final material distribution		
Objective function $\left \frac{u_{out}^{@X}}{u_{out}^{@Y}} \right $	51.4	385.7
Output Displacement at X: $u_{out}^{@X}$	-1.199	-1.158
Output Displacement at Y: $u_{out}^{@Y}$	-0.023	-0.003
Geometric advantage	13.8%	13.5%

Table 5.11: Results DE vs PSO. Topology optimization for the design of compliant mechanism, featuring output control, with a single load case.

5.2 Polymorphic compliant mechanisms: Two load cases

The results presented in this section are for the a polymorphic compliant mechanism. There are two load cases, meaning that the compliant mechanism is configured to perform two functions, one each load case.

5.2.1 Without output control

In this subsection, the results for a polymorphic force inverter compliant mechanism are presented. The problem definition is illustrated in figures 3.12 and 3.13. The configuration parameters for the topology optimization algorithm are similar to the one load case example and are presented in table 5.1.

5.2.1.1 Using DE

Figure 5.9 shows the final material distribution for a two load case asymmetric force inverter compliant mechanism. Figure 5.10 illustrates the resulted material distributions that represent the evolution of the hybrid scheme.

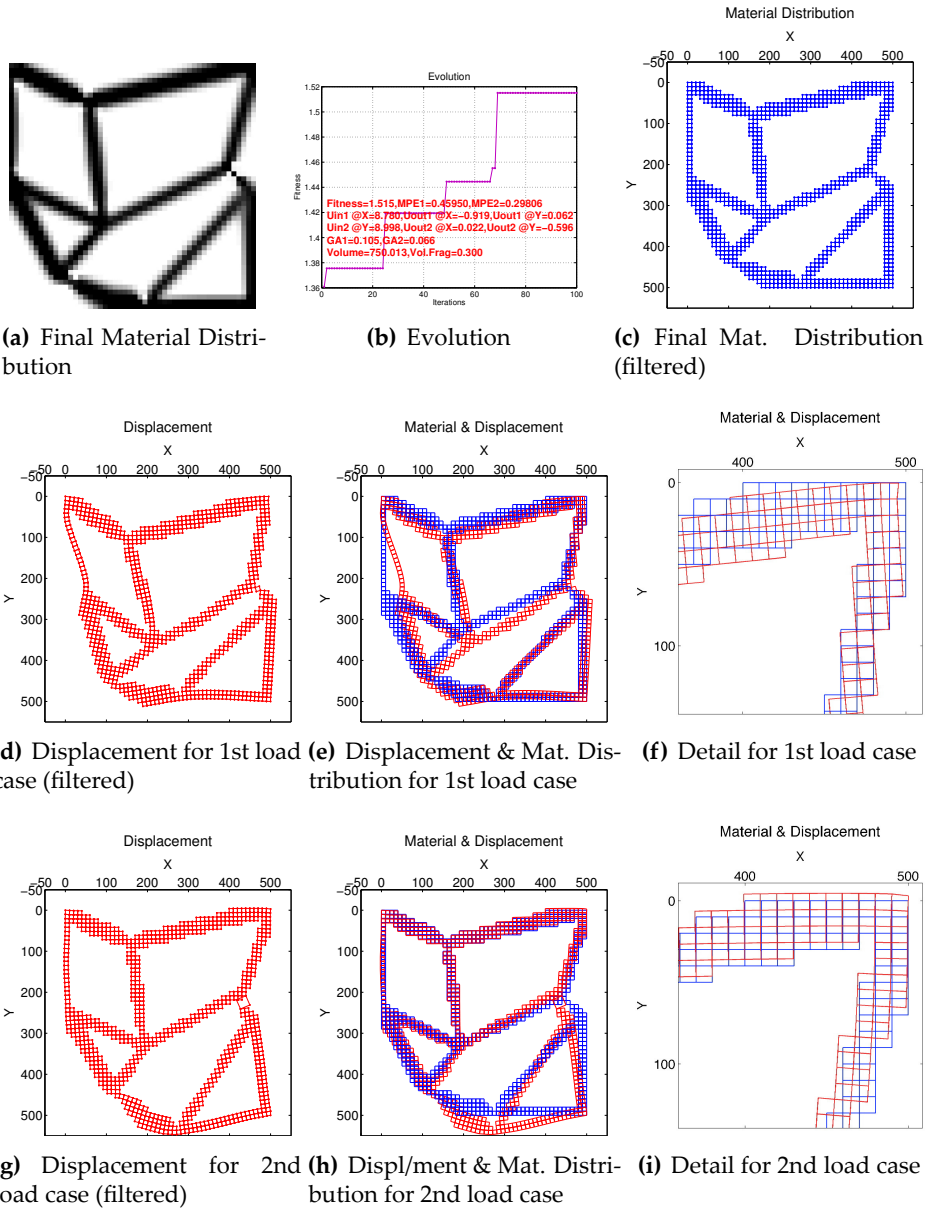


Figure 5.9: Results for two loads case using Differential Evolution

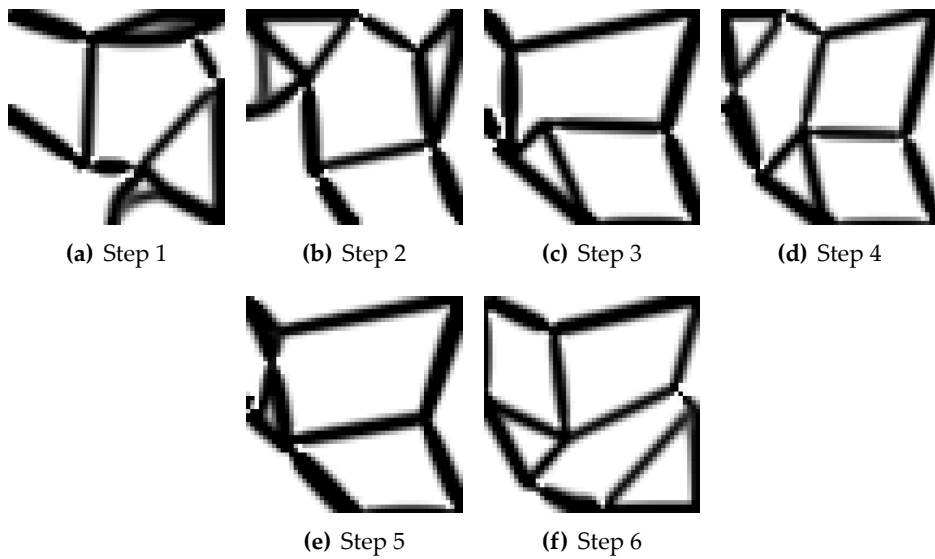


Figure 5.10: Intermediate material distributions for Two loads case using Differential Evolution

5.2.1.2 Using PSO

Figure 5.11 illustrates the final material distribution for a two load case asymmetric force inverter compliant mechanism. Figure 5.12 illustrates the resulted material distributions that represent the evolution of the hybrid scheme.

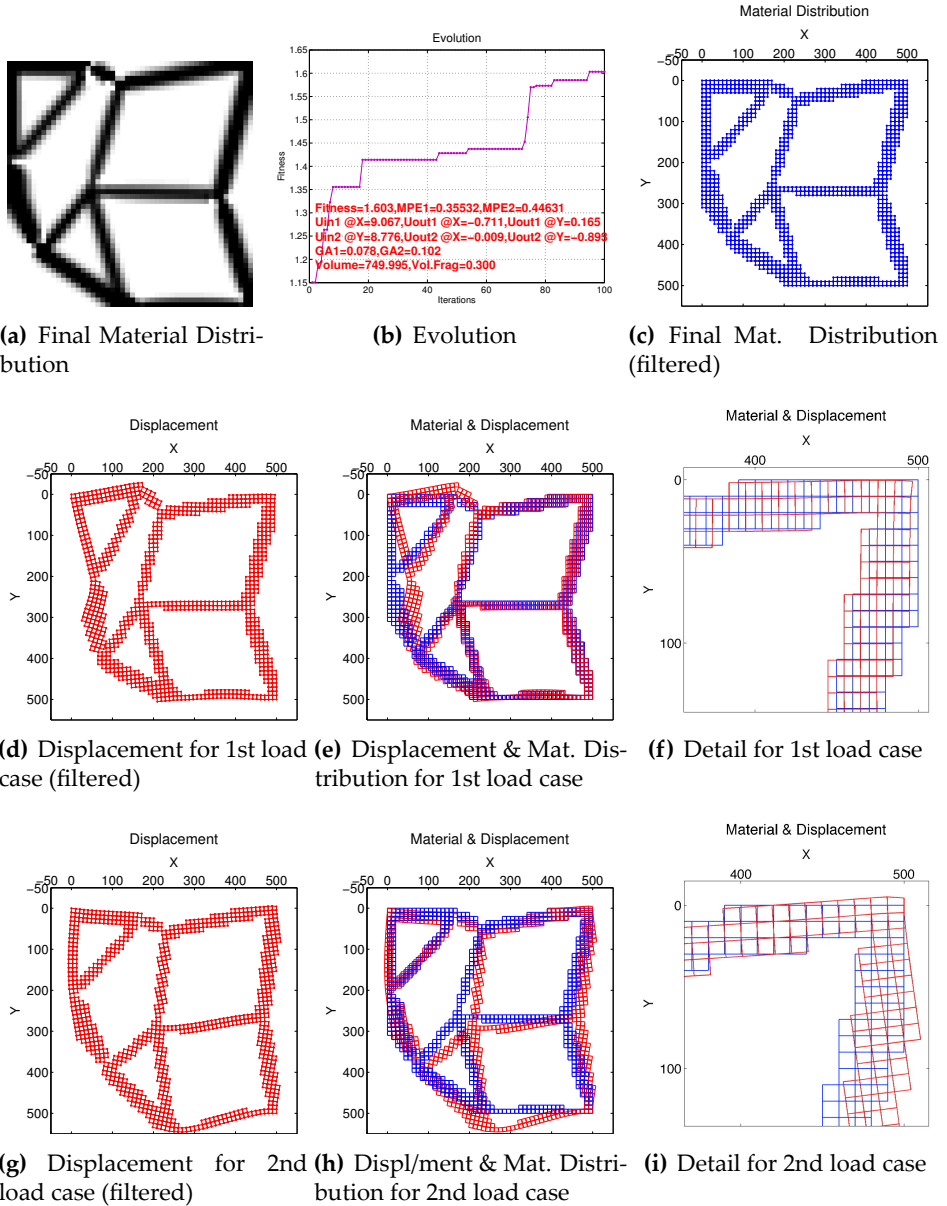


Figure 5.11: Results for two loads case using Particle Swarm Optimization

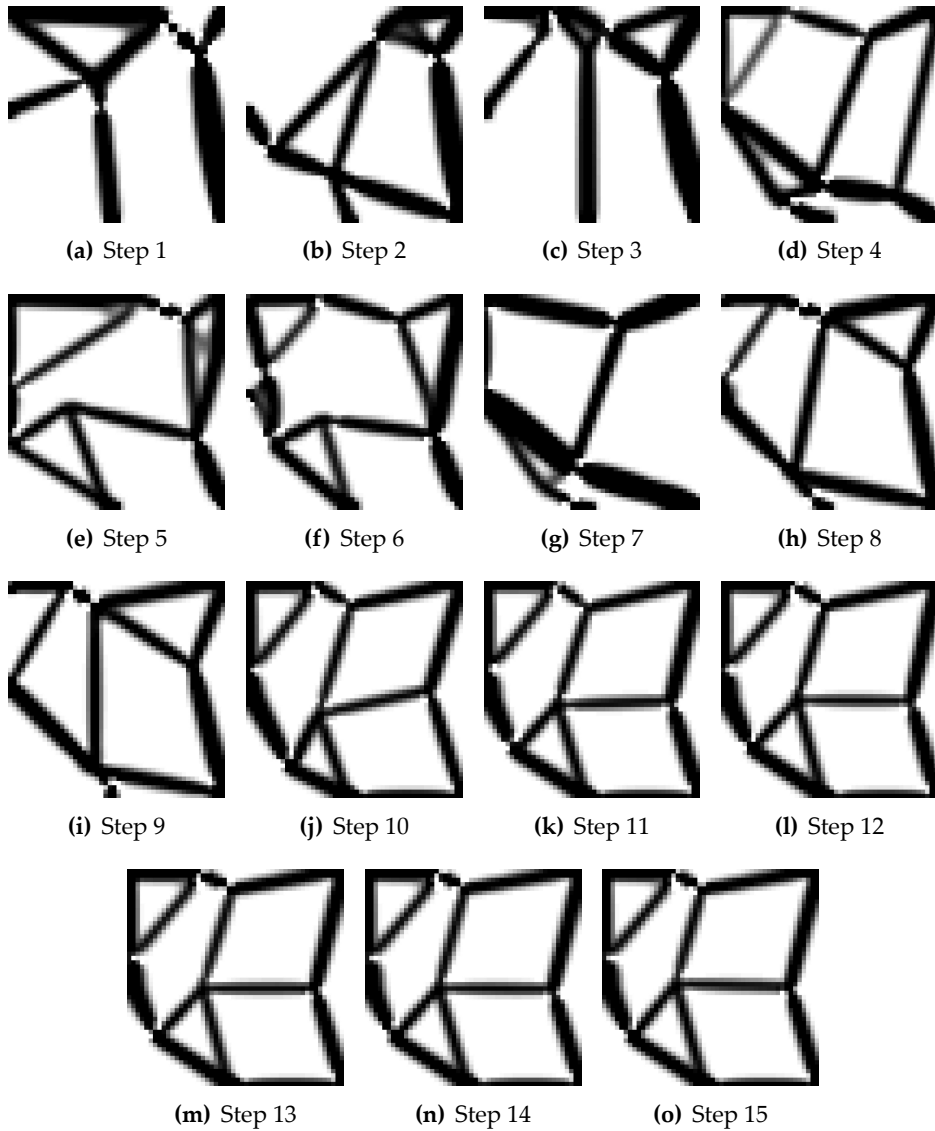


Figure 5.12: Intermediate material distributions for Two loads case using Particle Swarm Optimization

5.2.1.3 Repeatability for the polymorphic load case compliant mechanism

Figures 5.13 and 5.14 demonstrate in each evolutionary algorithm used (DE and PSO respectively), a set of four different runs of the hybrid scheme for the two load case compliant mechanism. The material distributions that are illustrated in subfigures 5.13(a), 5.13(b), 5.13(d), from the DE case and subfigure 5.14(b) from the PSO case, have almost the same configuration. The material distributions illustrated in 5.13(c) from the DE case and subfigures 5.14(c), from the PSO case are very similar to each other while material distribution illustrated in 5.14(b), 5.14(d), look very similar to each other and appear to have a diagonal axis of symmetry which passed through the top right and bottom left points of the material distribution. The numerical results for DE and PSO 4runs sets are presented in tables 5.12 and 5.13 respectively.

Runs	fitness	$U_{in,1}^X$	$U_{out,1}^X$	$U_{out,1}^Y$	$U_{in,2}^Y$	$U_{out,2}^X$	$U_{out,2}^Y$
run 1	1.486	9.390	-0.461	-0.074	8.748	0.257	-1.025
run 2	1.514	9.475	-0.498	-0.008	8.542	0.270	-1.017
run 3	1.515	8.780	-0.919	0.062	8.998	0.022	-0.596
run 4	1.510	9.517	-0.536	-0.026	8.904	0.279	-0.974

Table 5.12: Results for Two loads case using Hybrid scheme with DE

Runs	fitness	$U_{in,1}^X$	$U_{out,1}^X$	$U_{out,1}^Y$	$U_{in,2}^Y$	$U_{out,2}^X$	$U_{out,2}^Y$
run 1	1.593	8.914	-0.728	0.192	8.745	0.021	-0.865
run 2	1.579	9.223	-0.537	-0.059	8.814	0.213	-1.042
run 3	1.576	8.723	-0.890	0.009	9.106	0.172	-0.687
run 4	1.603	9.067	-0.711	0.165	8.776	-0.009	-0.893

Table 5.13: Results for Two loads case using Hybrid scheme with PSO

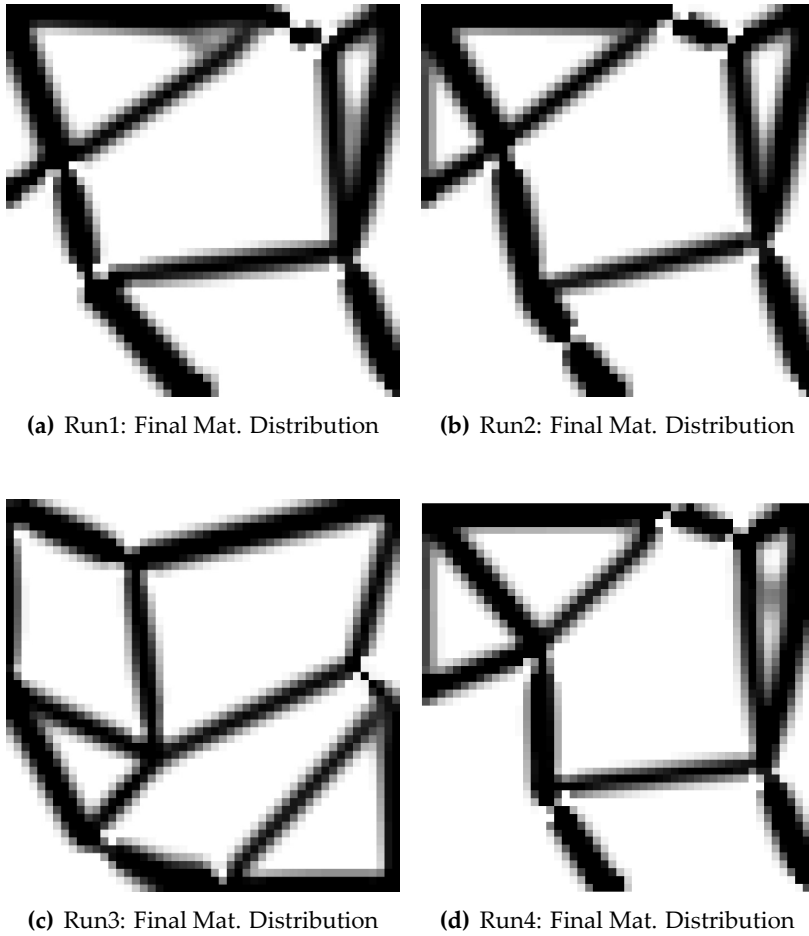


Figure 5.13: Four Final material distributions using Hybrid Scheme using Differential Evolution for two loads case

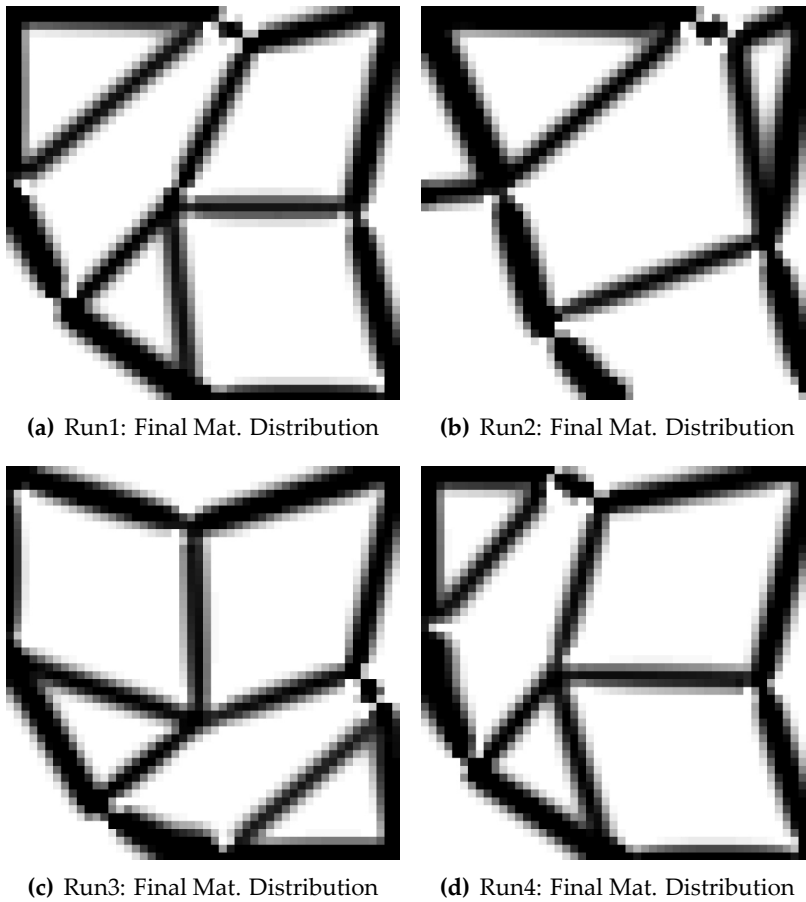


Figure 5.14: Four Final material distributions using Hybrid Scheme using PSO for two loads case

5.2.2 Results for Polymorphic Compliant Mechanism using output control

For the current problem the configuration parameters are presented in table 5.14.

Parameter	Value
Discritization	50x50
Design variables	2500
DOFS	5202
Local search iterations	80
SIMP penalty coefficient, p	3
Filter Radius, r	1.5
Volume fraction	30%

Table 5.14: Running parameters: topology optimization for the design of compliant mechanism using DE, and featuring output control, with a single load case.

5.2.2.1 Using Differential Evolution

For the selected evolutionary algorithm the configuration parameters similar to the corresponding single load case with output control but with more design variables (2500 instead of 900) and they are presented in table 5.15.

Parameter	Value
Population size	20
Generations	50
Crossover factor C_r	0.9
Mutation factor F	1.5
Design variables	2500

Table 5.15: Differential Evolution configuration parameters

The numerical results and the resulted material distribution are presented in table 5.16 and in figure 5.15 respectively.

Two load Cases, DE, output control		
Single Criteria Value		13.303
1st load case	Output Displacement at X: $u_{1,out}^{@X}$	-0.696
	Output Displacement at Y: $u_{1,out}^{@Y}$	-0.020
	Objective function $\left \frac{u_{1,out}^{@X}}{u_{1,out}^{@Y}} \right $	33.952
	Geometric Advantage	8.2%
2nd load case	Output Displacement at X: $u_{2,out}^{@X}$	0.03
	Output Displacement at Y: $u_{2,out}^{@Y}$	-0.398
	Objective function $\left \frac{u_{2,out}^{@Y}}{u_{2,out}^{@X}} \right $	13.303
	Geometric Advantage	4.3%

Table 5.16: Numerical Results for two load cases, DE and output control

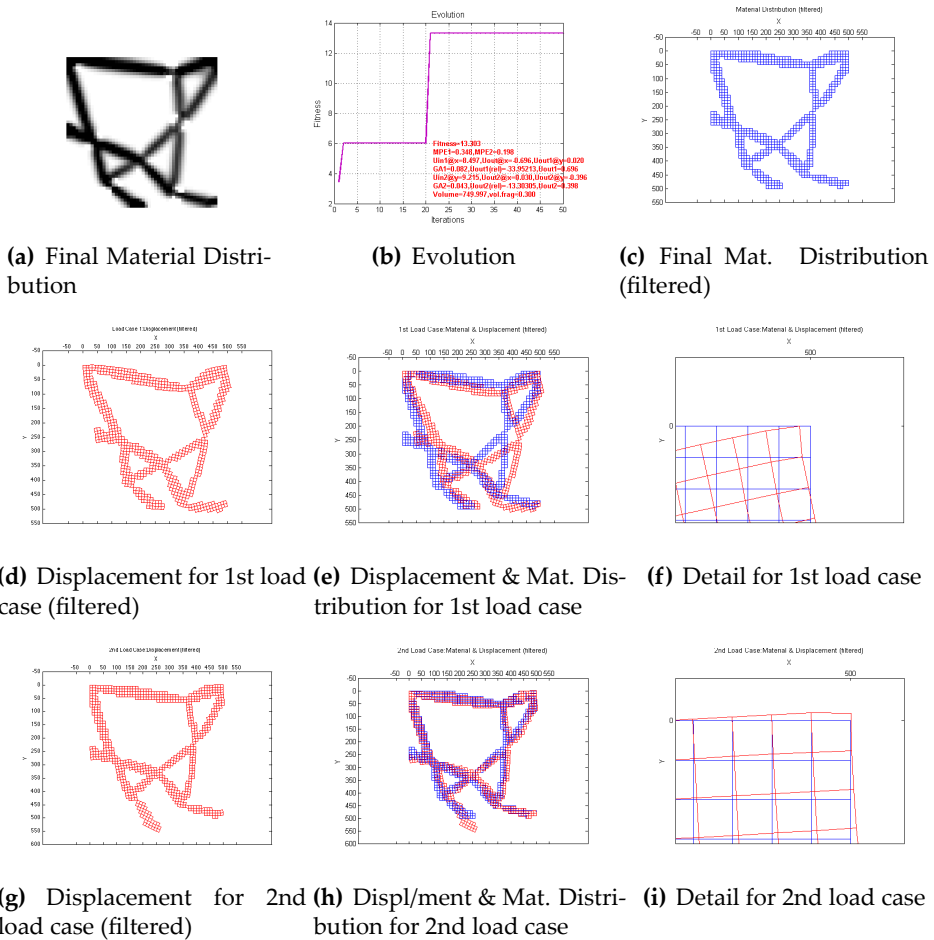


Figure 5.15: Results for two loads case using Differential Evolution and featuring output control

5.2.2.2 Using Particles Swarm Optimization

For the selected evolutionary algorithm the configuration parameters are similar to those used for corresponding single load case with output control but with more design variables (2500 instead of 900) and they are presented in table 5.17.

Parameter	Value
Population size	20
Generations	50
Acceleration factors $c_1 = c_2$	2
Inertia factors w_{max} & w_{min}	0.9 & 0.1
Design variables	2500

Table 5.17: PSO configuration parameters

The numerical results and the resulted material distribution are presented in table 5.18 and in figure 5.16 respectively.

Two load Cases, PSO, output control		
	Single Criteria Value	13.348
1st load case	Output Displacement at X: $u_{1,out}^{@X}$	-0.326
	Output Displacement at Y: $u_{1,out}^{@Y}$	-0.004
	Objective function $\left \frac{u_{1,out}^{@X}}{u_{1,out}^{@Y}} \right $	76.655
	Geometric Advantage	3.4%
2nd load case	Output Displacement at X: $u_{2,out}^{@X}$	0.043
	Output Displacement at Y: $u_{2,out}^{@Y}$	-0.580
	Objective function $\left \frac{u_{2,out}^{@Y}}{u_{2,out}^{@X}} \right $	13.348
	Geometric Advantage	6.1%

Table 5.18: Numerical Results for two load cases, PSO and output control

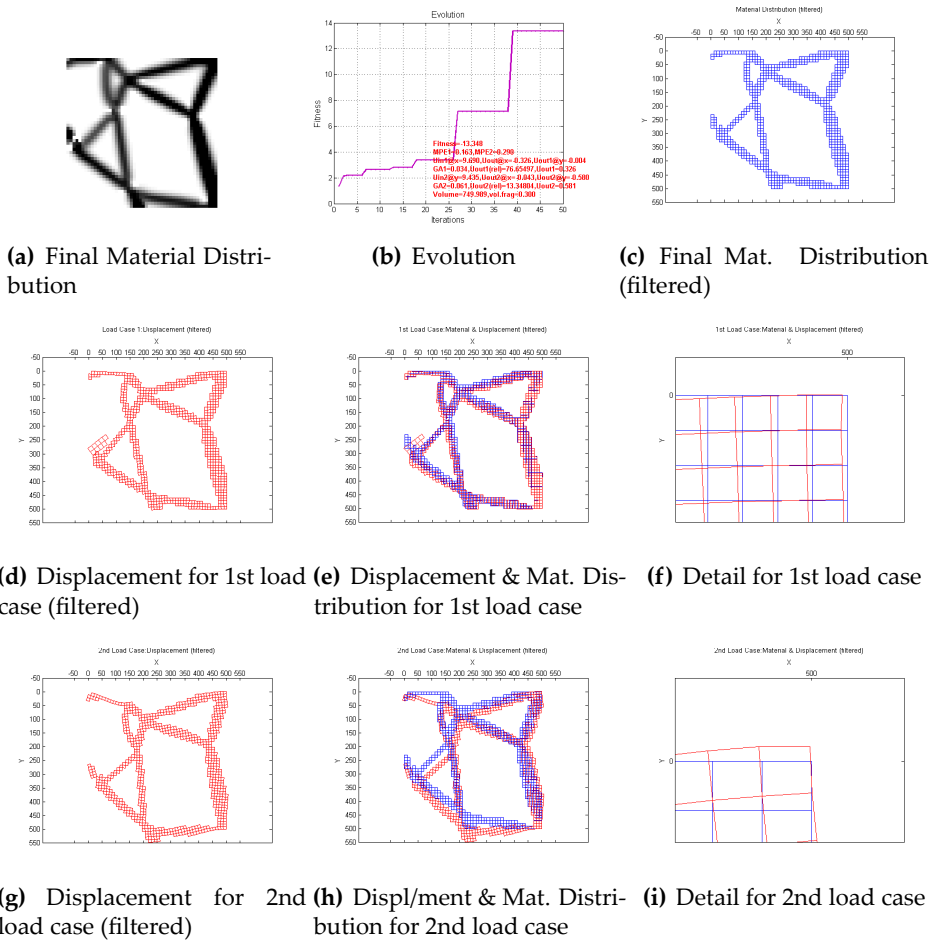


Figure 5.16: Results for two loads case using Particles Swarm Optimization and featuring output control

5.2.2.3 Comparison of DE vs PSO for the design of polymorphic compliant mechanisms using output control.

Table 5.19 represents a comparison between DE and PSO for the two load case asymmetric force inverter compliant mechanism. It seems that PSO performed better than DE but regarding the objective function and both load cases. It must be mentioned that the final material distributions look similar to each other, when applying an diagonal axis of symmetry, from bottom left to top right corner.

DE vs PSO		
	DE	PSO
Final material distribution		
Objective function		
$\left\{ \min \left\{ \left \frac{u_{1,out}^{@X}}{u_{1,out}^{@Y}} \right , \left \frac{u_{2,out}^{@Y}}{u_{2,out}^{@X}} \right \right\} \right\}$	13.303	13.348
First Load Case		
Output Displacement at X: $u_{1,out}^{@X}$	-0.696	-0.326
Output Displacement at Y: $u_{1,out}^{@Y}$	-0.020	-0.004
Objective function $\left \frac{u_{1,out}^{@X}}{u_{1,out}^{@Y}} \right $	33.952	76.655
Geometric advantage	8.2%	3.4%
Second Load Case		
Output Displacement at X: $u_{2,out}^{@X}$	0.030	0.043
Output Displacement at Y: $u_{2,out}^{@Y}$	-0.348	-0.580
Objective function $\left \frac{u_{2,out}^{@Y}}{u_{2,out}^{@X}} \right $	13.303	13.348
Geometric advantage	4.3%	6.1%

Table 5.19: Results DE vs PSO. Topology optimization for the design of compliant mechanism, featuring output control, with two load cases.

CHAPTER 6

Auxetic materials

6.1 Auxetic materials

6.1.1 General description

When a structure is under a tensile loading, shrinkage appears in directions perpendicular to the applied load, or in other words, there is a reduction to the cross-sectional area of structure. The opposite effect appears when a compressive loading is applied, thus, an increase to the cross-sectional area takes place. Poisson's ratio, which measures the change of the length of elastic material in the perpendicular direction with respect to the applied load, is usually a positive number $0 < \nu < 0.5$ and is defined as the negative fraction of transverse strain $\frac{\Delta y}{l_y}$ over the axial strain $\frac{\Delta x}{l_x}$. Materials featuring a negative

Poisson's ratio, are called auxetics. Auxetic materials can be conceptualized as microstructures, that under tensile loading, become thicker perpendicular to the direction of the applied load. This is due to artificial hinges that appear inside the microstructure and help flexing to occur. An example of an auxetic microstructure is shown in figure 6.1, where a star-shaped auxetic structure is presented [TSP97].

A body that behaves in an auxetic way is composed of a repeated pattern of identical microstructures. Each microstructure consists of a monolithic body with specific geometry, that under certain loading, delivers motion in a certain way (having a predefined deformation). Thus, it integrates all the features of a compliant mechanism. As a result, the whole body behaves in an auxetic way (see figure 6.2).

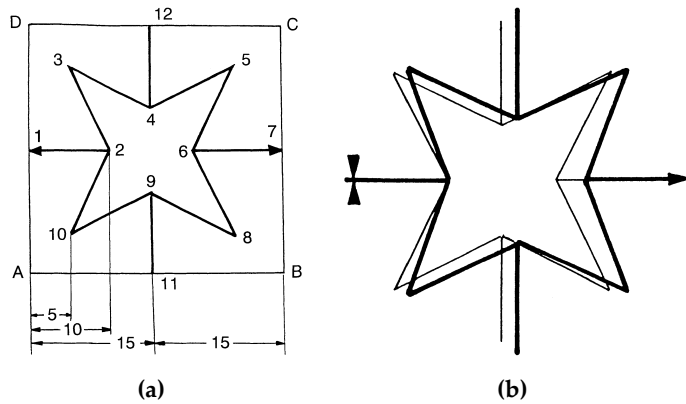
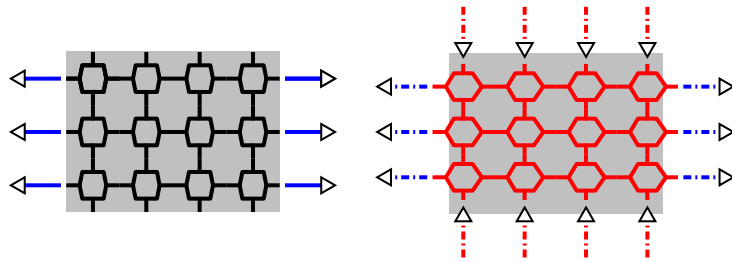
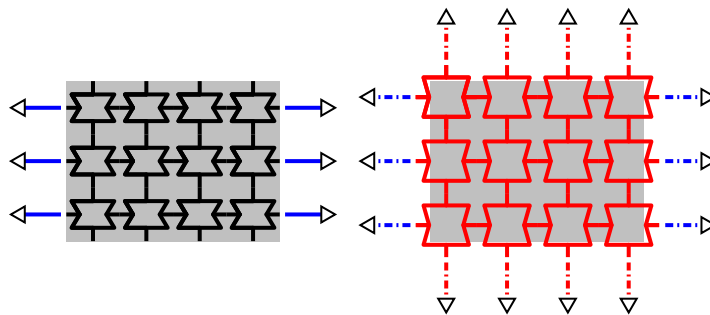


Figure 6.1: a) Star shaped, two dimensional representative cell using beam elements. Finite element discretization and node numbering. b) The star-shaped cell deformed. Thin lines represents the undeformed shape [TSP97].



(a) Regular behaviour: when longitudinal forces are applied (blue arrows), the structure shrinks



(b) Auxetic behaviour: when longitudinal forces are applied (blue arrows), the structure extends

Figure 6.2: Regular and auxetic behaviour of microstructures based on their internal substructure. Blue dotted arrows show the displacements aligned with the applied force direction, while red dotted arrows show the displacements normal to the applied force.

6.1.2 Negative Poisson's ratio definition

Subfigure 6.3(b) represents a structure that functions like a mechanism. It has been calculated using topology optimization and truss structure of subfigure 6.3(a). The structure shown in subfigure 6.3(b) presents a flexible body: when a force is applied to point A leftwards, point B moves upwards. Poisson's ratio may be defined for this specific microstructure. Using a square domain in 6.3(a) where $l_x = l_y$, the Poisson's ratio can be expressed by definition, as the negative fraction of the displacement at point B over the displacement at point A. Since both displacements are positive, Poisson's ratio is a negative number:

$$\nu = -\frac{\varepsilon_y}{\varepsilon_x} = -\frac{\frac{\Delta y}{l_y}}{\frac{\Delta x}{l_x}} = -\frac{\Delta y}{\Delta x} \left. \vphantom{\frac{\Delta y}{\Delta x}} \right\} \Rightarrow \nu < 0 \quad (6.1)$$

$\Delta x, \Delta y > 0$

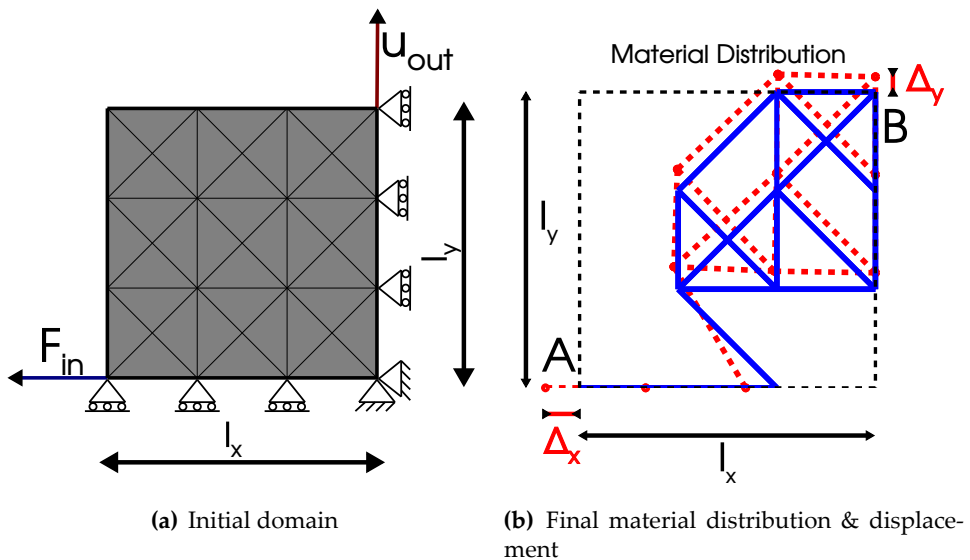


Figure 6.3: Negative Poisson's ratio resulting from topology optimization of a compliant mechanism.

6.2 Results: Trusses

6.2.1 Problem formulation for

The topology optimization problem formulated for the auxetic compliant mechanism is presented in the following equation 6.2 and illustrated in figure 6.4,

$$\begin{aligned}
 & \max_{\mathbf{u}, x_e} u_{out} = \mathbf{1}^T \mathbf{u}, \\
 & \text{subject to:} \\
 & \mathbf{K}\mathbf{u} = \mathbf{f}, \\
 & \sum_{e=1}^N l_e x_e \leq \phi V_0, \quad V_0 = \sum_{e=1}^N l_e \cdot 1 \\
 & 0 < x_{min} \leq x_e \leq 1, \quad e = 1, \dots, N, \\
 & \mathbf{K} = \left(\sum_{e=1}^N x_e^p \mathbf{K}_0 \right), \quad p \geq 3
 \end{aligned} \tag{6.2}$$

where l_e and x_e are the length and the cross section area of each element e . For the calculation of the V_0 we assume that cross section area is equal to 1.

Results of auxetic materials studied using truss elements are included in this section. The values of 30% and 40% as volume limits were chosen from experience after several numerical experiments. In order to obtain more accurate results, the mesh must be refined by adding more elements to the domain. Doubling the subcells from 3x3 to 6x6 means that the number of the design variables is increased to 156 for the case 6x6 case and to 600 for the 12x12 mesh respectively. The total volume V_0 is defined as the sum of volume of each element (see equation 6.2). In each mesh, the initial volume V_0 is changed since the number of elements is changed. In order to have comparable results with the initial 3x3 mesh, the volume fraction in the other cases must be redefined proportionally due to denser placement of structural elements in comparison with the reference 3x3 mesh. These fractions of volumes for each mesh case and initial volume fraction are represented in table 6.1.

6.2.2 Results for 3x3 cells, Volume fraction at 40%

The results for a 6x6 cells problem which was simplified to a 3x3 cell problem, representing one quarter of the representative volume cell, are shown in fig-

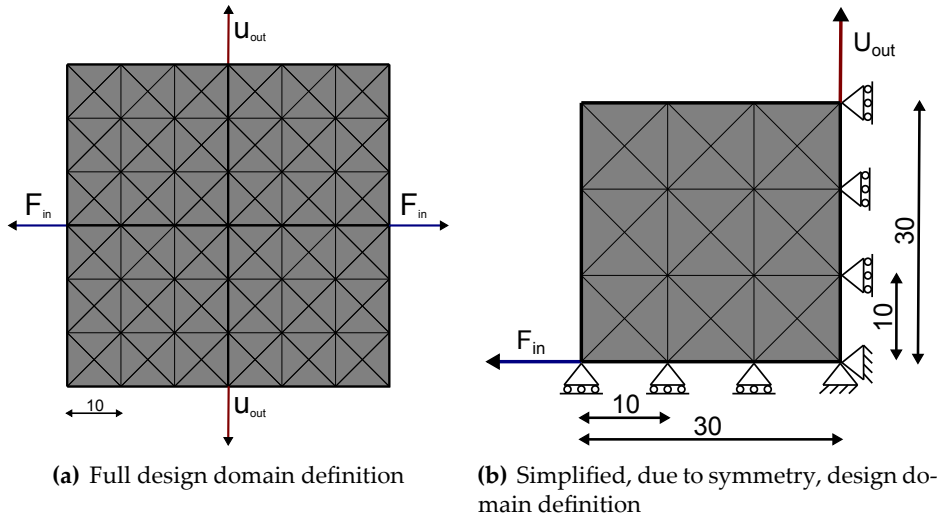


Figure 6.4: Auxetic material problem definition

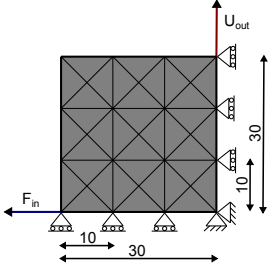
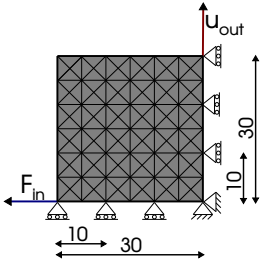
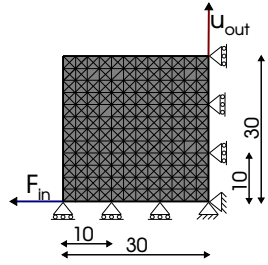
			
cells	3x3	6x6	12x12
elements	42	156	600
nodes	16	49	169
cell size	10	5	2.5
V_0	494	929	1798
$\phi\%$	40%	21.3%	11%
$V_\phi^{40\%}$	197.6	197.8	197.8
$\phi\%$	30%	15.9%	8.3%
$V_\phi^{30\%}$	148.2	147.4	149.2

Table 6.1: Numerical data for several cell configurations

ure 6.5. The number of design variables is 42 and the goal volume fraction is 40%. The Poisson's ratio is expressed as Geometric Advantage (GA) and in this case is equal to -0.481 (the absolute value of this quantity is plotted in all figures illustrating the evolution of the hybrid scheme).

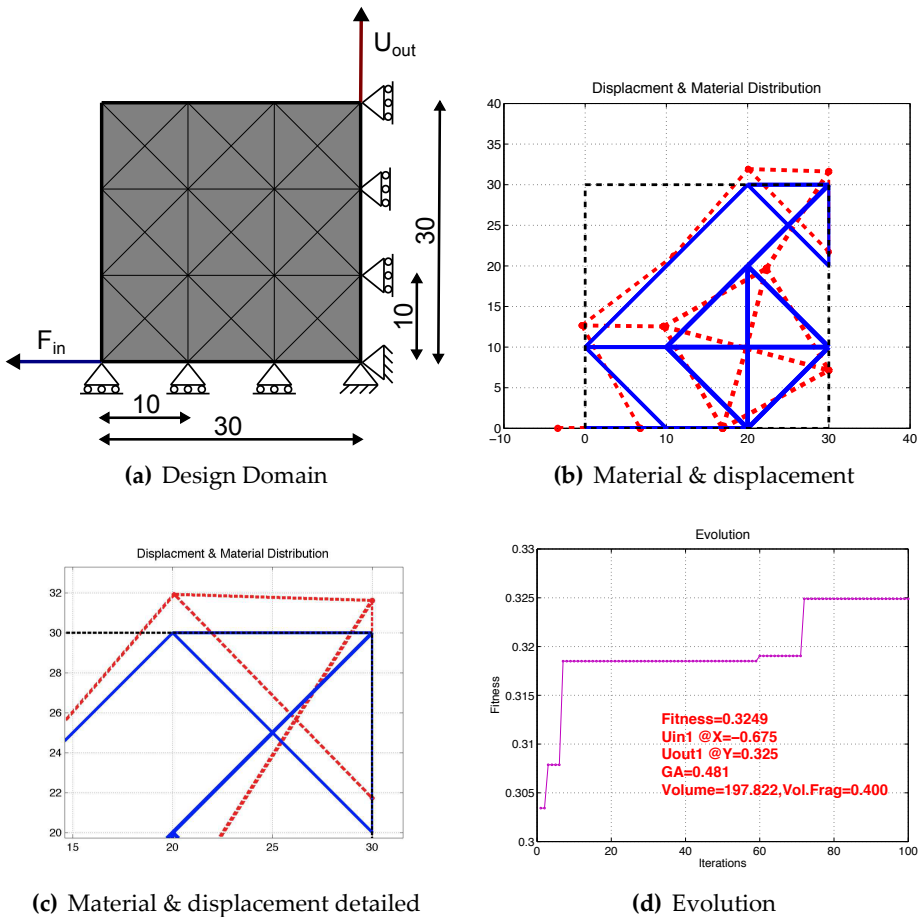


Figure 6.5: Results: 3x3 subcells, Volume fraction: 40%

6.2.3 Results for 3x3 cells, Volume fraction at 30%

Results for mesh 3x3 and volume fraction of 30% and are shown in figure 6.6. The Poisson ratio is calculated to -0.463 .

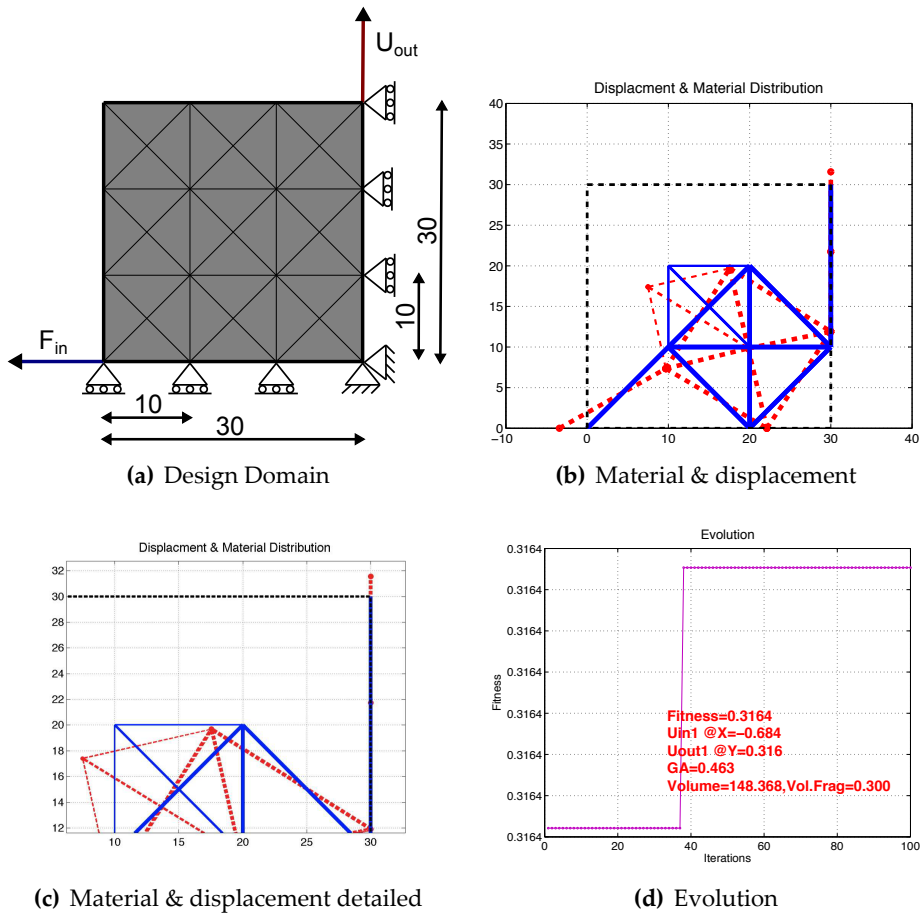


Figure 6.6: Results: 3x3 subcells, Volume fraction: 30%

6.2.5 Results for 6x6 cells, Volume fraction=15.9% (3x3: 30%)

Figure 6.8 represents the results for the 6x6 mesh with volume fraction 15.9% which corresponds to 30% of the 3x3 mesh case. The Poisson's ratio is equal to -0.612.

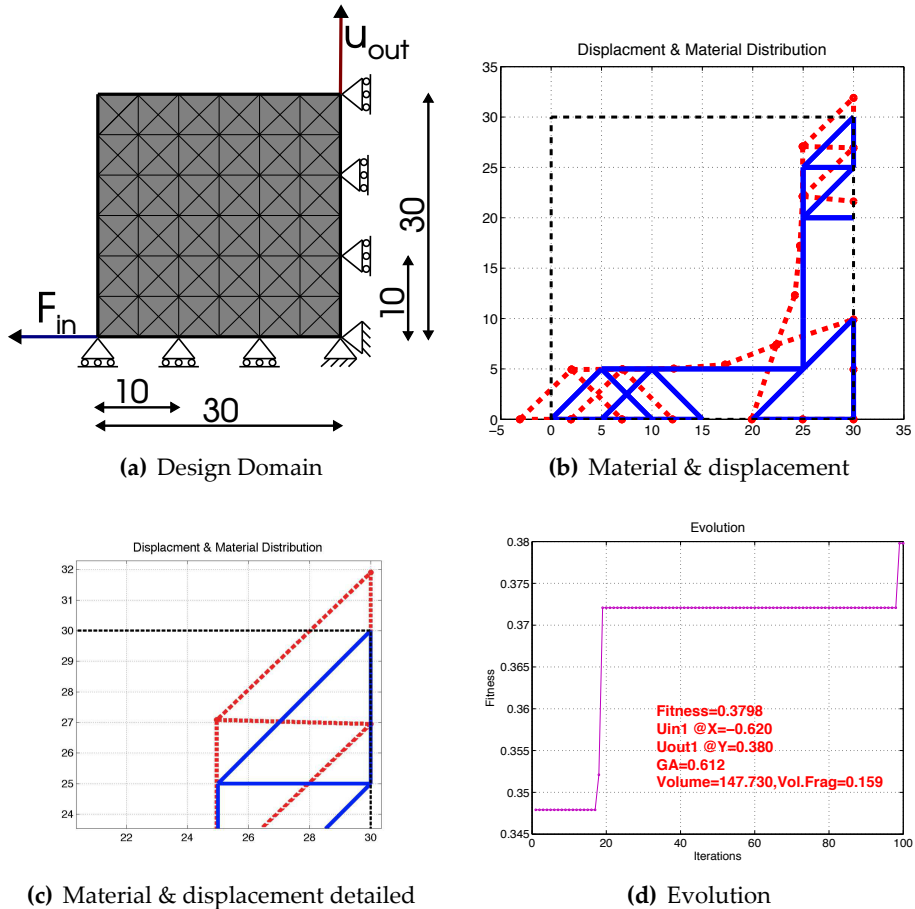


Figure 6.8: Results: 6x6 subcells, equivalent to 3x3 mesh volume 30% volume fraction: 15.9% (3x3: 30%)

6.2.6 Results for 12x12 cells, Volume fraction=11.0% (3x3: 40%)

In figure 6.9 are shown the results for the 12x12 mesh with volume fraction 11.0% which correspond to 40% of the 3x3 mesh. The Poisson's ratio is equal to -0.663.

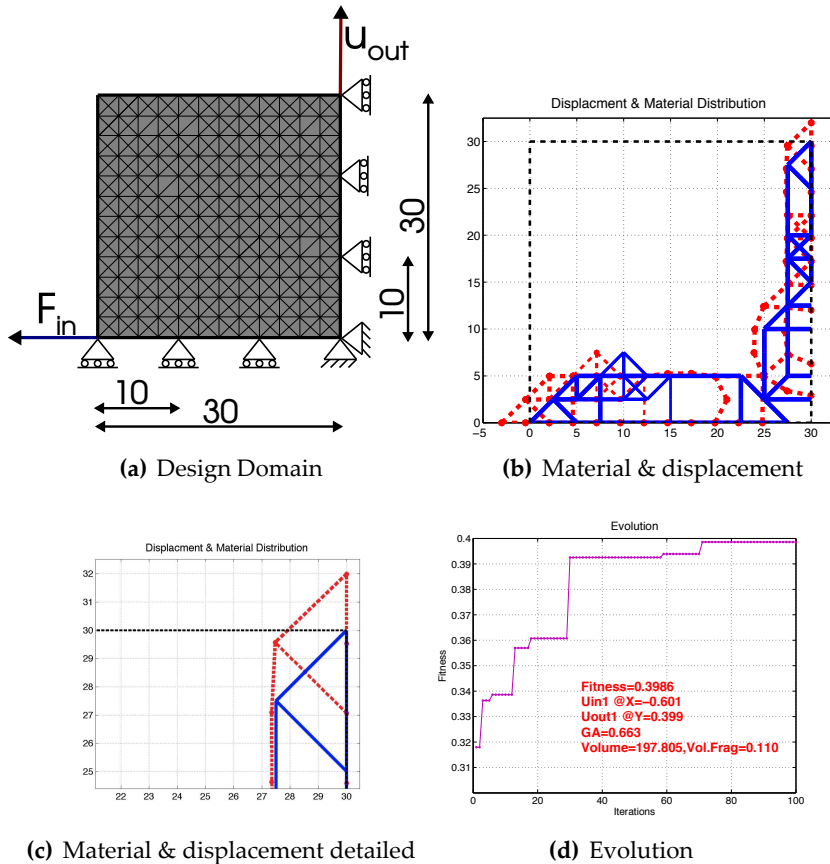


Figure 6.9: Results: 12x12 subcells, Volume fraction: 11.0% (3x3: 40%)

6.2.7 Results for 12x12 cells, Volume fraction=8.3% (3x3: 30%)

Figure 6.10 demonstrates the results for the 12x12 mesh with volume fraction 8.3% which correspond to 30% of the 3x3 mesh case. The Poisson's ratio is equal to -0.611.

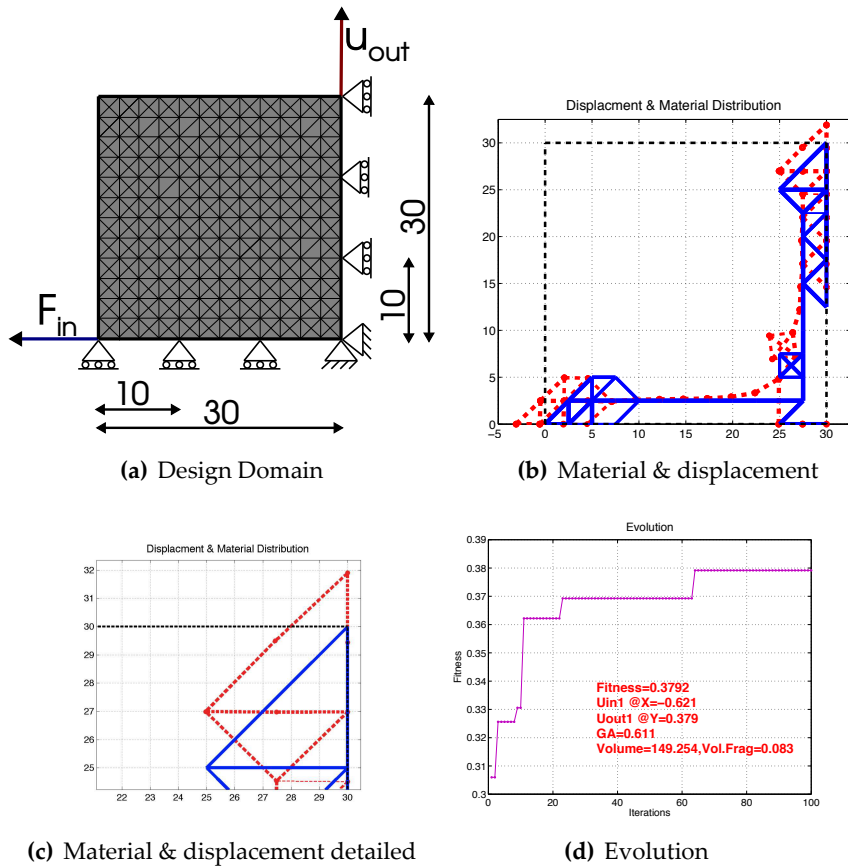


Figure 6.10: Results: 12x12 subcells, Volume fraction: 8.3% (3x3: 30%)

6.3 Results: Continuous formulation

6.3.1 Linear 2d plane stress elements

Figure 6.11 presents a continuous formulation of auxetic microstructure with 30×30 linear 2d plane stress elements with volume fraction of $\phi = 20\%$ and Poisson's ratio of $\nu = -0.192$. Subfigure 6.11(c) illustrates the final material distribution of all elements with material density ≥ 0.6 while in 6.11(d) the auxetic behaviour is clearly shown. Similar results are presented in figure 6.12 for volume fraction of $\phi = 30\%$. The black areas that appear in subfigures 6.11(a), 6.11(b), 6.12(a) and 6.12(b), represent the material that exist in the structure, while the white areas show the space that material does not exist. No connecting elements were used. The final material distribution that corresponds to the micromechanism is the result of the topology optimization procedure. Subfigures 6.11(c), 6.11(d), 6.12(c), and 6.12(d) illustrate the displacements of the specific structure.

As mentioned before, linear analysis has been used. In figures 6.11 and 6.12 a filter has been applied, in order to show the elements with density higher than 0.6. Elements with density lower than 0.6 are not shown, but have been considered in the analysis. In addition a large scale factor has been used in order to illustrate the displacements that represent the auxetic behaviour. The filter and the scale factor have been used for visualization purposes only. In areas where hinges appear, some elements seem to have big rotations as a result of the large scale factor that has been applied to the displacements. It has been noticed that by using higher mesh density, these rotations are even smaller.

The example in figure 6.12 is used as a test case for the homogenization problem. The results are, of course, valid up to the value of deformations and displacements for which the finite elements work with confidence and the assumptions of linear analysis are not violated (ca. up to deformations equal to 2%). Alternatively specialized topology optimization techniques that penalize the creation of hinges can be used [Yoo+04]. Finally, if hinges that can not be constructed easily or are prone to fatigue and extensive deformations arise, the microstructure can be modified at these areas and the homogenization technique of the next part can be used in order to verify the auxetic behaviour.

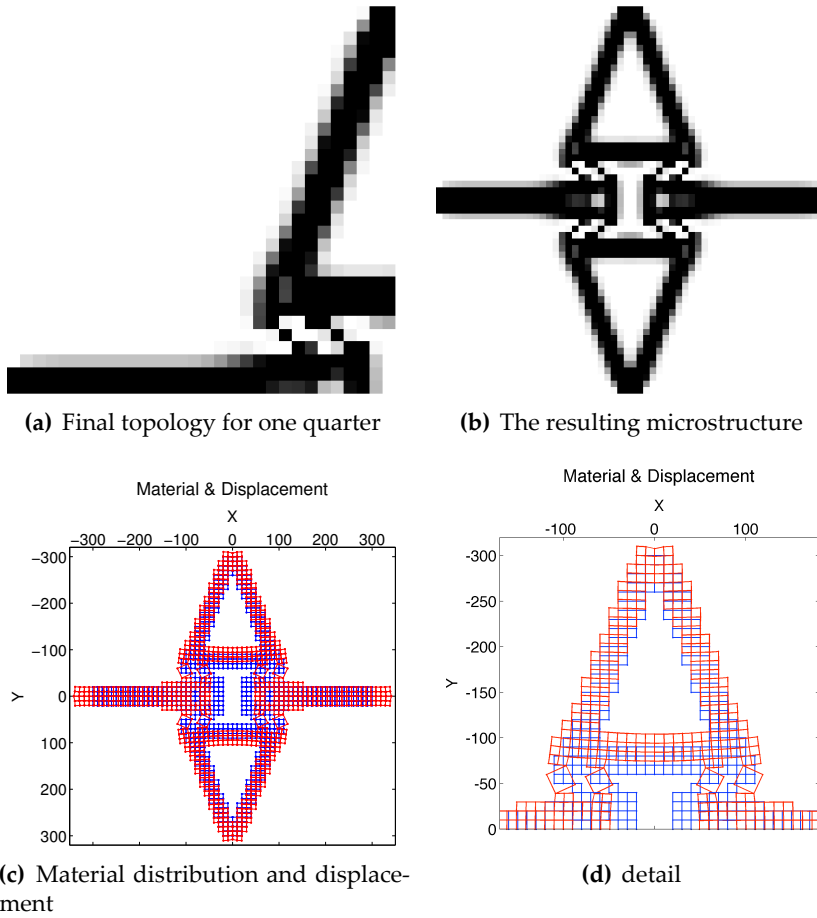


Figure 6.11: Continuous formulation with 30×30 elements and volume fraction at $\phi = 20\%$. Poisson's ratio $\nu = -0.192$.

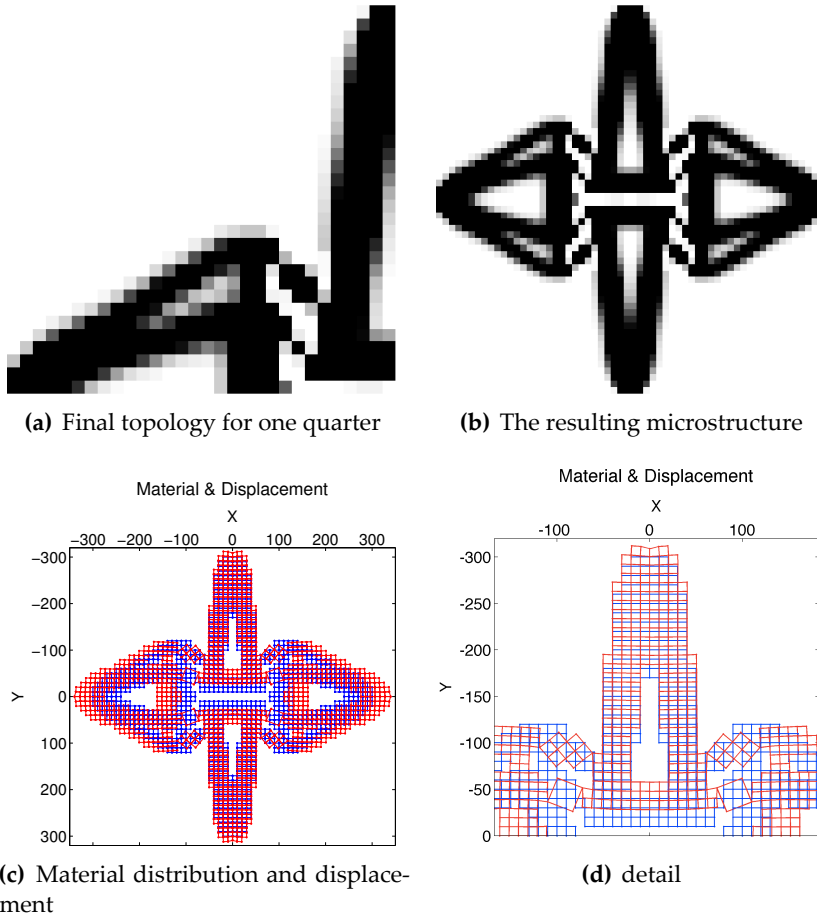


Figure 6.12: Continuous formulation with 30x30 elements and volume fraction at $\phi = 30\%$. Poisson's ratio $\nu = -0.223$.

6.4 Using homogenization to verify topology optimization

6.4.1 Homogenization principles

According to the Hill-Mandel condition or energy averaging theorem, the macroscopic volume average of the variation of work equals to the local work variation, on the RVE [Hil63]:

$$\boldsymbol{\sigma}^M : \delta \boldsymbol{\epsilon}^M = \frac{1}{V_m} \int_{V_m} \boldsymbol{\sigma}^m : \delta \boldsymbol{\epsilon}^m dV_m \quad (6.3)$$

Among others, three widely used types of loading states, which satisfy the above condition, can be applied to the RVE: a) prescribed linear displacements, b) prescribed tractions, c) periodic boundary conditions. In the present study linear displacements have been used. Thus, the loading in the boundaries of the RVE is given by the following relation:

$$\mathbf{u}|_{\partial V_m} = \boldsymbol{\epsilon}^M \mathbf{x} \quad (6.4)$$

where a loading strain $\boldsymbol{\epsilon}^M$ is applied to the boundaries ∂V_m of the RVE, and \mathbf{x} corresponds to the matrix with the undeformed coordinates of the boundary nodes of the RVE.

In order to proceed to the formulation of a homogenization scheme, the average quantities of both the microscopic strain and stress should be defined. The general averaging relations, are:

$$\langle \boldsymbol{\epsilon} \rangle_{V_m} = \frac{1}{V_m} \int_{V_m} \boldsymbol{\epsilon}^m dV_m, \langle \boldsymbol{\sigma} \rangle_{V_m} = \frac{1}{V_m} \int_{V_m} \boldsymbol{\sigma}^m dV_m \quad (6.5)$$

Equations 6.5 can be further simplified. The volume average microscopic strain is equal to the macroscopic strain which has been applied as loading to the boundaries of the RVE:

$$\langle \boldsymbol{\epsilon} \rangle_{V_m} = \boldsymbol{\epsilon}^M \quad (6.6)$$

For prescribed displacements, the following simplified formulation for the macroscopic stresses, has been chosen [Kou02]:

$$\langle \boldsymbol{\sigma} \rangle_{V_m} = \frac{1}{V_m} \mathbf{f} \mathbf{x} = \boldsymbol{\sigma}^M \quad (6.7)$$

where \mathbf{f} is the matrix of the resulting external forces in the undeformed coordinates of the boundary nodes \mathbf{x} of the RVE, after microscopic analysis has been completed.

For the completion of the homogenization procedure, the effective constitutive tensor should be calculated. In plane stress conditions, the elasticity tensor has nine unknowns, indicating that three test loading strains should be applied to the boundaries of the RVE and three equations per loading, should be formulated. In total, nine equations are formulated and the effective tensor \mathbf{E}^* is estimated, according to the following relation:

$$\langle \boldsymbol{\sigma} \rangle_{V_m} = \mathbf{E}^* \langle \boldsymbol{\epsilon} \rangle_{V_m} \quad (6.8)$$

6.4.2 Using homogenization to verify topology optimization

The main idea which is presented in this part of the study, is related to the incorporation of the final, optimized material distribution, as it is given by topology optimization, into the classical, linear, homogenization scheme described in the previous section. In this work, topology optimization is used for the design of auxetic materials, consequently the numerical homogenization procedure focuses on the effective Poisson's ratio, which is expected to be negative.

In particular, the heterogeneity imposed from the topology optimization requirement for the final configuration of the material, is considered within numerical homogenization. For the satisfaction of the objective optimization function, which here describes an auxetic behaviour, material may or may not exist at the end of the analysis. The same requirement is tested in the homogenization scheme, by considering two materials: one strong material with the initial properties (density > 0.6), and another soft material corresponding to the material that does not exist at the end of the topology optimization procedure (density < 0.6). In this framework, the effective material properties are derived and comparison with the results obtained by topology optimization, is considered.

The proposed approach offers the opportunity of verifying the results received by topology optimization. The appearance or not of the desired auxetic behaviour, will be examined from the homogenization scheme. Furthermore, a complete description of the effective material properties, will be given. The effective constitutive tensor, as it is obtained by homogenization of the hard and the soft material and a parametric investigation of the soft material parameters, will be presented as well.

6.4.3 Numerical examples

In the next sections, three numerical examples are presented. The geometry and the mesh of the structure under consideration, are shown in figure 6.13. The same structure was used in the topology optimization illustrated in figure 6.12. In the first example, a general loading is applied to the structure. In the second and the third one, linear displacement loading conditions are applied to the boundaries of the RVE within a classical homogenization framework. The developed finite element models consist of plane stress, full integration elements.

In the topology optimization, the Young's modulus and the Poisson's ratio for the hard material were considered respectively, equal to: $E^{hard} = 1$, $\nu^{hard} = 0.3$. The same properties were adopted for the hard material in the homogenization scheme. Moreover, the effective material properties are strongly influenced by the soft material characteristics. For the first and the second example, the soft material properties have been considered as follows: $E^{soft} = 0.007$, $\nu^{soft} = 0.007$. In the third example these properties are slightly changed.

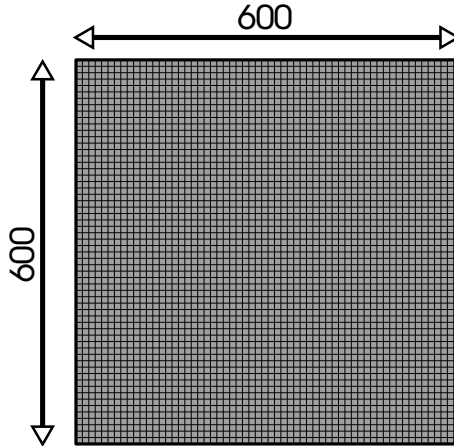


Figure 6.13: Geometry and mesh of the structure with 3600 plane stress elements.

6.4.3.1 Example 1: General loading

In this first example, a general loading shown in figure 6.14 is applied to the structure. The effective Poisson's ratio is calculate by dividing the vertical to the horizontal displacement, as it is depicted in relation 6.1. Thus, no classical homogenization procedure (boundary conditions, average stress-strain relations and estimation of the effective properties) has been considered here. The effective Poisson's ratio of the heterogeneous structure, which consists of the hard and the soft material, is estimated by applying relation 6.1.

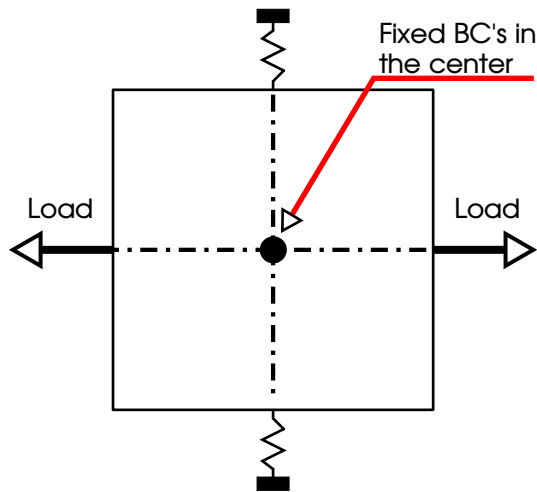


Figure 6.14: General loading and boundary conditions applied to the heterogeneous model of the first example.

According to the displacements of the hard material, which are given in figure 6.15, an auxetic behaviour is obtained for the structure. In addition, the Poisson's ratio is equal to -0.2299 , thus very close to the one given by topology optimization (see figure 6.12).

6.4.3.2 Example 2: Classical homogenization

In this example, a classical numerical homogenization procedure has been applied, for the derivation of the effective material properties of the heterogeneous material (hard-soft material). Linear displacement boundary conditions have been applied to the boundaries of the RVE. For the estimation of the effective constitutive tensor, three test loading strains have been used. In

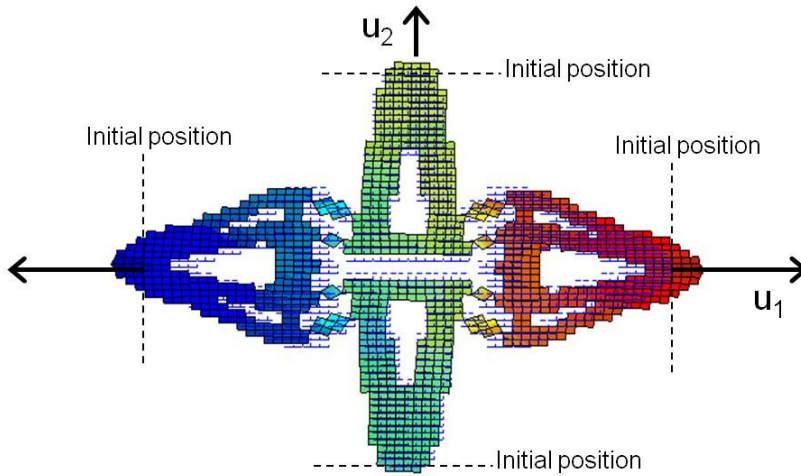


Figure 6.15: Initial and deformed position of the hard material for the loading of figure 6.14. © Appearance of auxetic behaviour.

figure 6.16, the displacements of the hard material for a test loading strain equal to $[0.06 \ 0.06 \ 0]^T$ are shown, while table 6.2 includes the effective material properties. Homogenization represents the overall effective behaviour of the structure. According to the results, the effective material property is not exactly isotropic. In addition, Poisson's ratio ν_{xy} is slightly different to ν_{yx} , however both are very close to the one given by topology optimization (-0.223).

E_{xx}^*	E_{yy}^*	ν_{xy}^*	ν_{yx}^*	G_{xy}^*
0.0660	0.0674	-0.2433	-0.2483	0.0117

Table 6.2: Effective material properties obtained by numerical homogenization, for the hard and © soft material distribution given by topology optimization.

In figure 6.17 a parametric investigation of the variation of the effective Poisson's ratio ν_{xy} versus Young's modulus of the soft material, is presented. This diagram indicates that homogenized variables and especially the auxetic behaviour depend on the properties of the soft material that is used instead of the theoretically required voids. It is noted that values of the Poisson's ratio

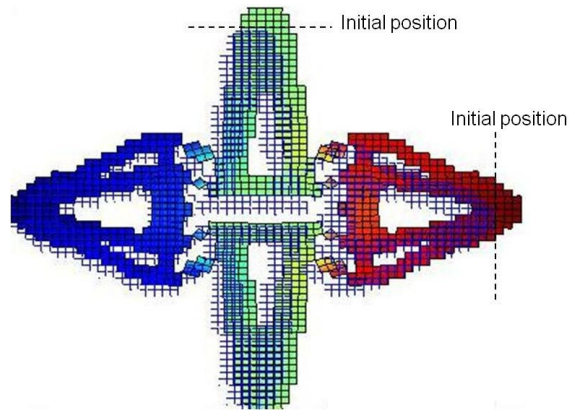


Figure 6.16: Initial and deformed position of the hard material obtained by numerical homogenization (with linear displacement boundary conditions). Appearance of auxetic behaviour.

close to limits ($-1 < \nu < 0.5$) and the respective elasticity modulus of the soft material, can also be included.

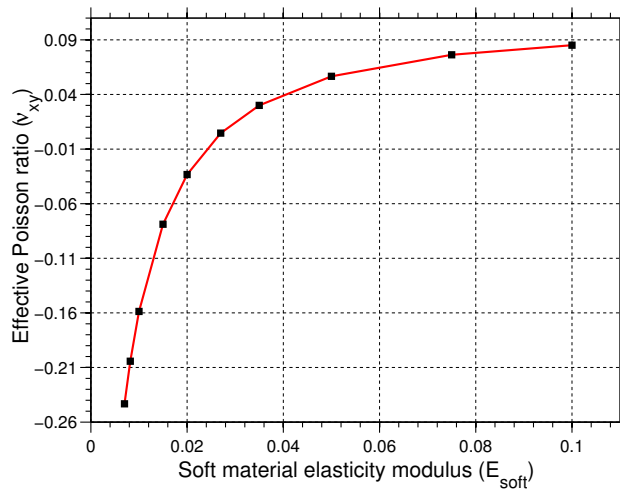


Figure 6.17: The effective Poisson's ratio versus Young's modulus of the soft material obtained from the homogenization procedure.

6.4.3.3 Example 3: Classical homogenization with slightly different boundaries

In the previous example, linear displacements have been applied to the boundaries of the structure. Moreover, in these boundaries both hard and soft material exist, according to topology optimization analysis. The idea presented here, is related to the elimination of the hard material, from the boundaries of the structure. By doing this, the hard material's movement inside the RVE will be independent of the boundary conditions, thus the hard material will be free to move and demonstrate the auxetic behaviour.

In figure 6.18 the initial and the new material configuration are shown. The circles on the top and the bottom of figure 6.18(b) indicate that the hard material is not in contact with these boundaries of the RVE.

Material properties of the hard material have been remained the same with the previous examples: $E^{hard} = 1$, $\nu^{hard} = 0.3$. For the soft material slightly different properties have been considered, in comparison with the first and the second homogenization example as follows: $E^{soft} = 0.0007$, $\nu^{soft} = 0.007$.

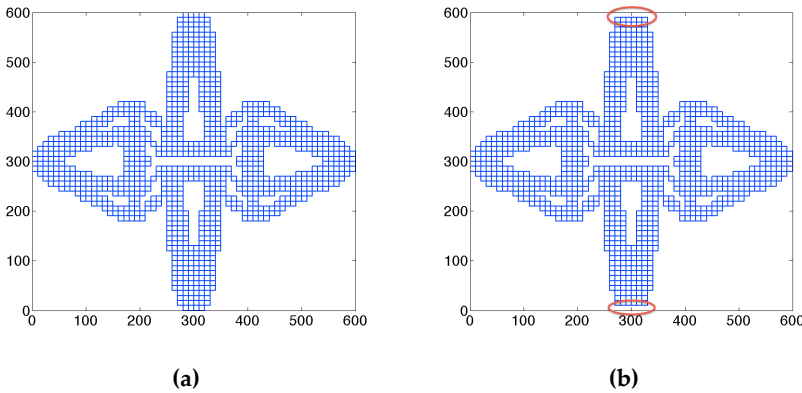


Figure 6.18: (a) Initial configuration of the hard material (b) A slightly different configuration of the hard material: The circles indicate that the hard material is not in contact with these boundaries.

The values of the effective Poisson's ratio which are obtained from the homogenization approach, are close to the value received by topology optimization: $\nu_{xy} = -0.163$ and $\nu_{yx} = -0.193$. In addition, in figure 6.19 the RVE with both the hard and the soft material, as well as the RVE with the hard material only, are shown. Auxetic behaviour appears for the two loading di-

rections which have been adopted during simulations. For the second loading direction (presented in figures 6.19(c), 6.19(d)) the hard material crosses the boundaries of the RVE.

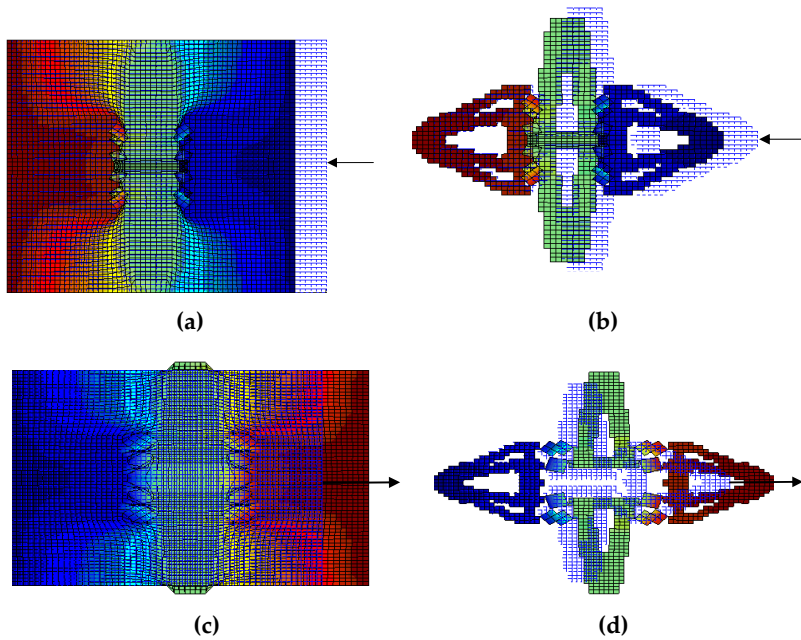


Figure 6.19: Initial and deformed position for the case of figure 6.18(b) Top left figure: the hard and the soft material - load direction 1. Top right figure: hard material only - load direction 1. Bottom left figure: hard and soft material - load direction 2. Bottom right figure: hard material only - load direction 2.

6.5 CAD-CAE Verification

6.5.1 Motivation

Usually the outcome of topology optimization is either a two dimensional black-white image that illustrates the optimum layout, or a group of three dimensional elements (tetrahedrons or hexahedrons) that describe the optimum geometry. In none of the above cases the resulted topology is ready to be used for manufacturing and a relative post-process is required. The post process consists of creating a 2d or 3d parametric geometry based on 2d

curves or 3d surfcases and describes nicely the resulted layout from topology optimization. Besides manufacturability must be taken into account. There are automated procedures (in 2d, borrowed from the image processing) that may help to accelerate this process, but there is always the need to tweak the final design by hand. In addition, the new parametric geometry needs to be verified that satisfies all the constraints that set firstly in the definition of the topology optimization problem. These comments are in accordance with published works [PC90; Bre+91; Chi+94].

In order to verify that the auxetic behaviour indeed occurs, a more detailed sample needed to be constructed and tested using modern CAE application. To achieve this the discretization had to be more detailed, hence increased to a mesh of 120×120 elements. The resulted material distribution was imported into a CAD software and a 2d NURBS model was drafted. The outcome was simulated with FEA, to verify the auxetic behaviour.

6.5.2 Configuration parameters

Differential Evolution was used for the hybrid scheme. The configuration parameters are presented in tables 6.3 and 6.4.

Parameter	Value
Discretization	120x120
Design Variables	14400
Degrees of Freedom	29282
Local search iterations	150
SIMP penalty coefficient, p	3
Filter radius, r	4.8
Volume Limit	30%

Table 6.3: Topology Optimization Algorithm configuration parameters for the auxetic mechanism problem with mesh 120×120 .

6.5.3 Mesh 120×120 : Numerical Results and material distributions

The hybrid scheme was used twice and the numerical results are presented in table 6.5. The final material distributions are presented in figure 6.20

Parameter	Value
Population size	8
Generations	100
Crossover C_r	0.9
Mutation β	1.5
Design Variables	14400

Table 6.4: Differential Evolution configuration parameters for the auxetic mechanism problem with mesh 120×120 .

	$u_{in}^{@X}$	$u_{out}^{@Y}$	$\nu = -\frac{u_{out}^{@Y}}{u_{in}^{@X}}$
case 1	1.606	7.425	-0.216
case 2	1.636	7.918	-0.207

Table 6.5: Comparison between

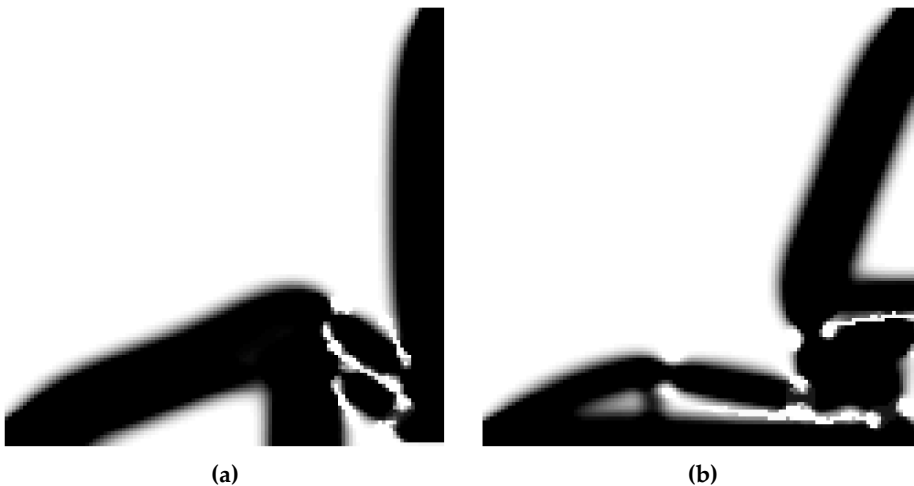


Figure 6.20: Final material distributions for run1 and run2 respectively

Figures 6.21 and 6.22 illustrates the displacements for the $\frac{1}{4}$ of the design domain and for the whole for each run respectively. Elements with density greater than 0.6 are shown only and a factor $\times 2$ scale has been applied to the displacements. The auxetic behaviour is clearly illustrated.

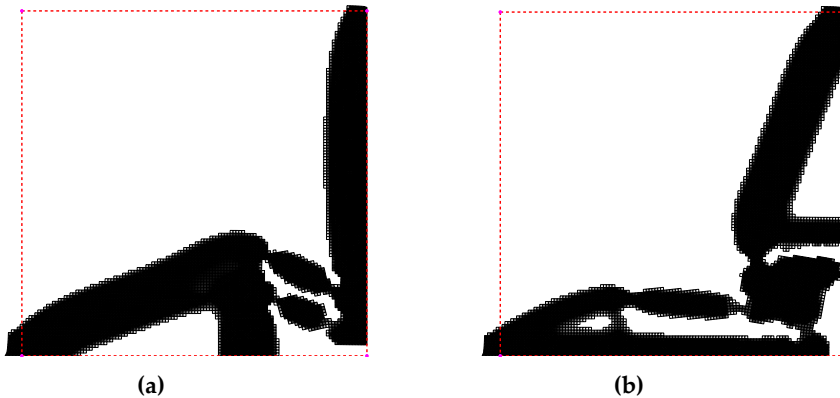


Figure 6.21: Displacements for run1 and run2 respectively

6.5.4 3D CAD modeling

The resulted material distributions were imported into the mechanical CAD software CREO 3.0 of Parametric Technology Corporation (www.ptc.com) in order to create a 3D CAD model for further analysis. The 2D bitmap image that illustrates material distributions was imported into the software, and NURBS curves were drafted by hand around the black and white areas. A 2d flat surface model was modeled that later was thickened. The size of the design domain (since the image is dimensionless) was set to a square of 300×300 mm, of thickness is 3mm. The resulted CAD models for each case are illustrated in figure 6.23.

6.5.5 FEA implementation

The 2d CAD models were analysed using the embedded to CREO©3.0, simulation software, Creo Simulate. The material used is a common aluminum alloy AL6061-T6. Its mechanical material properties are presented in table 6.6.

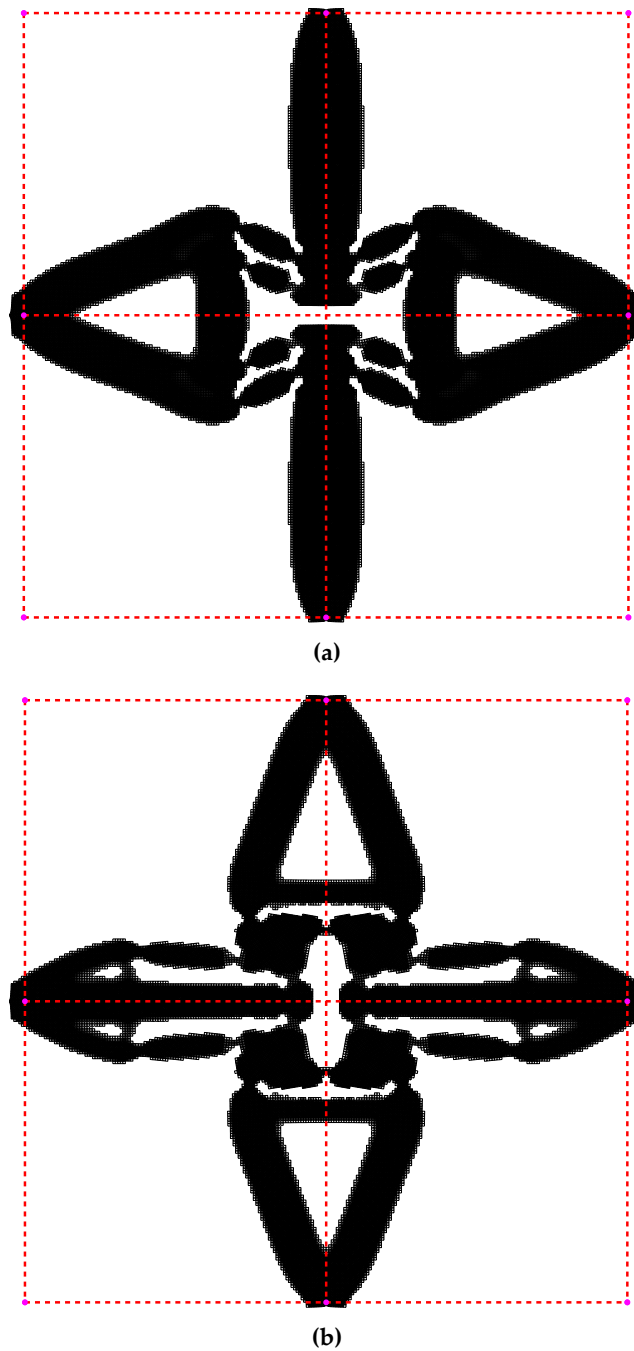


Figure 6.22: Displacements for case 1 and case 2 respectively

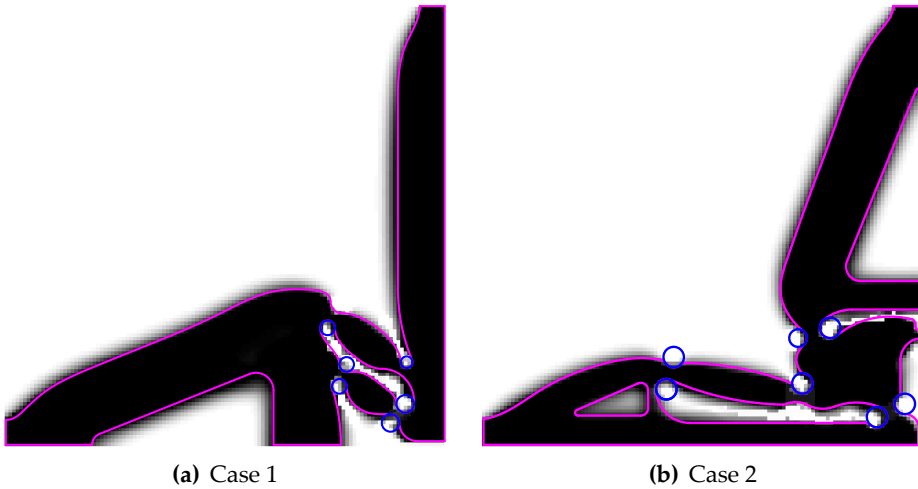


Figure 6.23: 2d CAD models created in Mechanical CAD softwareCreo 3.0

Mechanical Parameters	Value
Density	$2.71 \text{ g}^r/\text{cm}^3$
Poisson's ratio ν	0.33
Ultimate Tensile Strength	310 MPa
Tensile Yield Strength	276MPa

Table 6.6: Aluminum Alloy AL6061-T6 mechanical properties.

The boundary conditions used for the auxetic mechanism is used here as well. A load of 50 kilograms has been applied to the lower right edge with direction to the left. The setup of the model for the first case is presented in figure 6.24.

6.5.6 FEA results

Both cases were simulated using the same material and loads and relative same boundary conditions, and both verified their auxetic behaviour. Custom measures were defined at the lower left and upper right corners of the structure, for measuring the displacement of each point. The numerical results for each cases are presented in table 6.7. It must be noticed that in case 1, according to the definition for the negative Poisson's ratio given in equa-

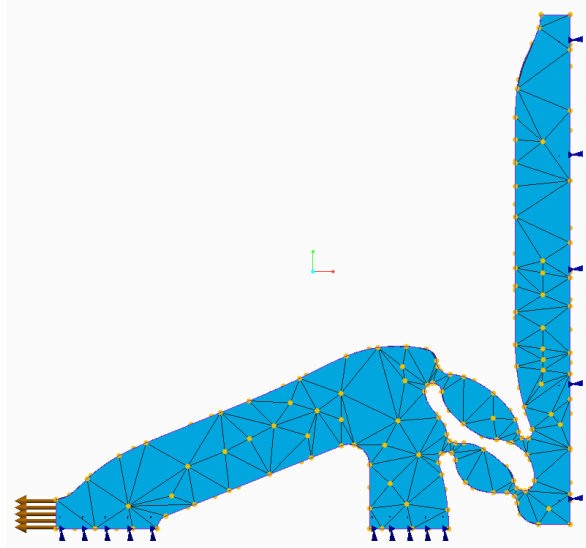


Figure 6.24: Finite element setup of case 1

tion 6.1, the poisson's ratio for the first cases exceeded -1. In both analysis the maximum stress exceeded the ultimate tensile strength. Even though the software continued the analysis until convergence, a warning has been noticed. Nevertheless for further analysis geometric nonlinearities must be taken into account.

	$u_{in}^{@X}$	$u_{out}^{@Y}$	$\nu = -\frac{u_{out}^{@Y}}{u_{in}^{@X}}$
case 1	0.327	0.413	-1.263
case 2	0.429	0.390	-0.909

Table 6.7: Numerical results for each case FEA study.

Figures 6.25, 6.26 and illustrates the coresponding stress and displacement results for each case respectively while figure 6.27 illustrates the mesh used.

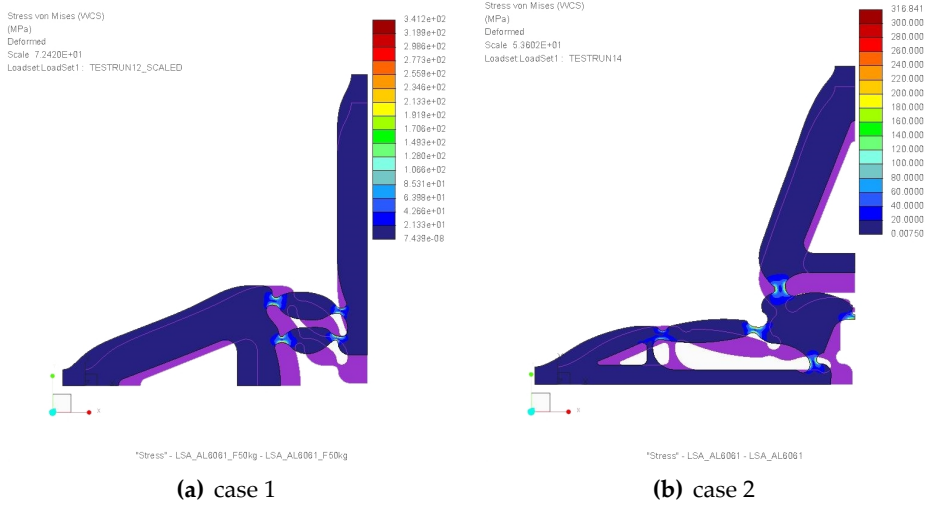


Figure 6.25: Stress results for each case

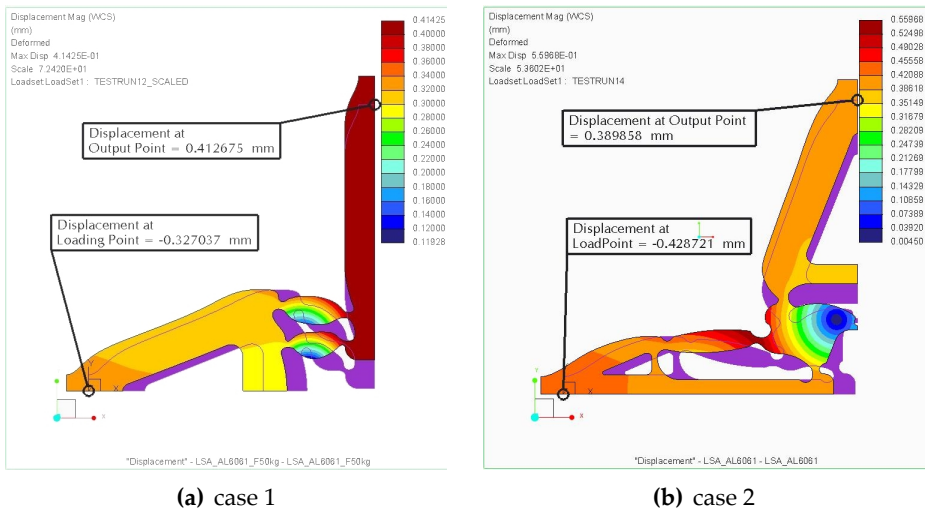


Figure 6.26: Displacement results for each case

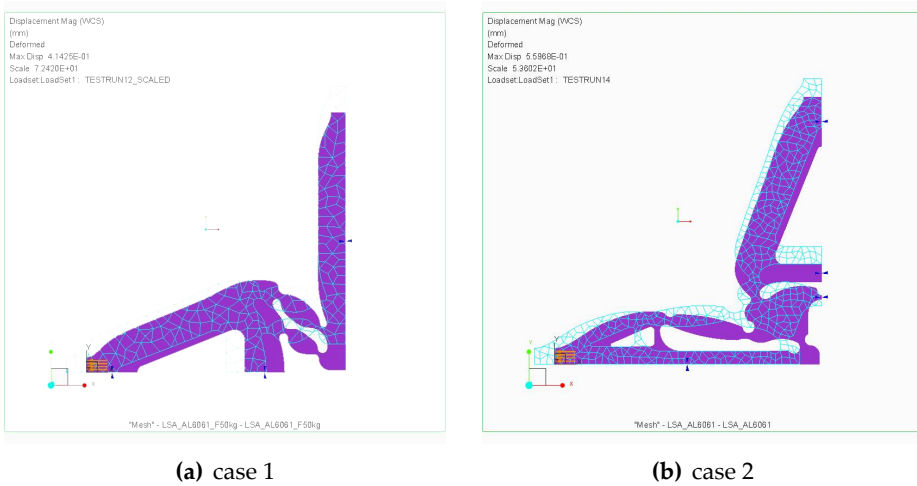


Figure 6.27: Meshes for each case

6.6 Mechanical behaviour of auxetic structures using nonlinearities

In this section, the effect of geometrical, contact and material nonlinearities on one of the above pre-mentioned auxetic structures is demonstrated [Dro+15]. In particular non-linear finite element analysis show how the auxetic behaviour is influenced by unilateral contact between the constituent materials, large displacements and elastoplasticity. The example selected is the one described in *case 1*, in subsections 6.5.3 and 6.5.4 and it is represented by a 120x120 representative volume element (RVE).

6.6.1 Linear verification

The auxetic behaviour of the structure presented in subfigure 6.23(b) is verified. The CAD model for *case 1* was imported into CAE software ABAQUS and linear 2d plane stress finite elements were used using the same loading and boundary conditions used during topology optimization. The mesh is represented in figure 6.28 and the resulted Von Mises stresses are illustrated in figure 6.29. The negative Poisson's ratio obtained from Abaqus is $\nu = -0.2064$, a value very close to $\nu = -0.211$ calculated from the hybrid scheme.

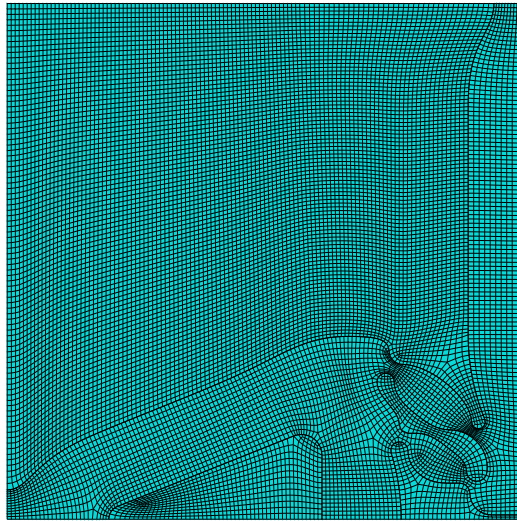


Figure 6.28: Mesh of the auxetic material distribution

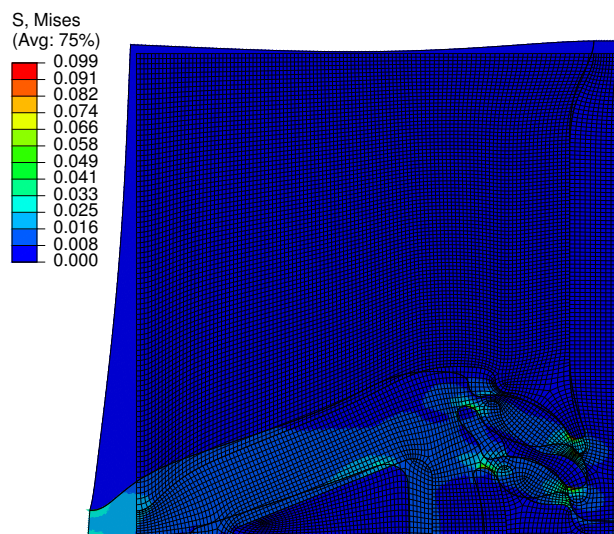


Figure 6.29: Auxetic behaviour obtained by linear analysis - von Mises stress distribution (MPa)

6.6.2 Geometrical and material non-linearities effects

However, in case non-linear geometric analysis is considered, the Poisson's ratio does not remain constant during analysis. Instead, a non-linear (bilinear) variation is obtained, according to the solid line of the Poisson's ratio - external force diagram which is shown in figure 6.30.

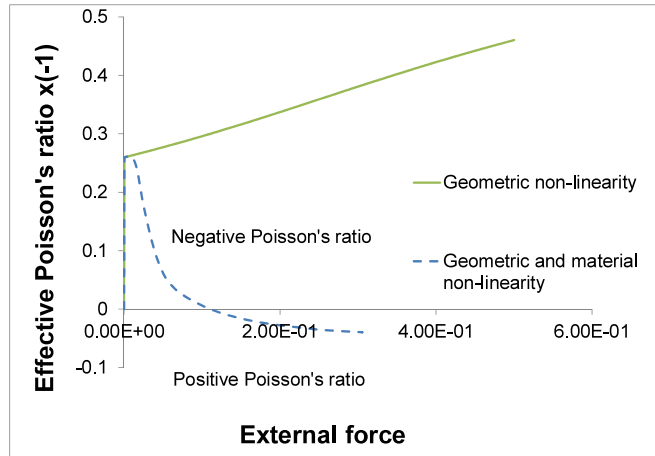


Figure 6.30: Effective Poisson's ratio-external force diagram for non-linear finite element analysis of the auxetic microstructure

If an elastoplastic, von Mises constitutive law with a bilinear stress-strain relation is added to the hard material, then the diagram shown with the dash line in figure 6.30 is obtained. Thus, there is a branch, in which the auxetic behaviour gradually decreases. At the end of the analysis, the effective Poisson's ratio eventually takes positive values. It is noted that for clarity reasons, the negative values of the Poisson's ratio correspond to the positive vertical axis of the diagram. By a careful examination of the elastoplastic analysis of the auxetic microstructure, three phases regarding variation of the effective Poisson's ratio are clearly developed:

- phase 1: The absolute value of the effective (negative) Poisson's increases which results in increase of the auxetic behaviour. This is the case just before yielding in the hard material appears.
- phase 2: The absolute value of the effective (negative) Poisson's ratio is reduced which results in reduction of the auxetic behaviour. In this

phase, yielding of the hard material begins and expands until the vertical branch of it (figure 6.31).

- phase 3: The effective Poisson's ratio takes positive values which are gradually increased. No auxetic behaviour is observed in this phase. In addition, yielding of the hard material expands in the vertical branch of it (figure 6.32).

These observations depend strongly on the chosen microstructure [DFJ12; GA13].

Extended description on the effects of contact and self-contact nonlinearities over the auxetic structures is presented in the paper [Dro+15] (accepted for publication) where a "meiotic" (instead of an auxetic) behavior is presented.

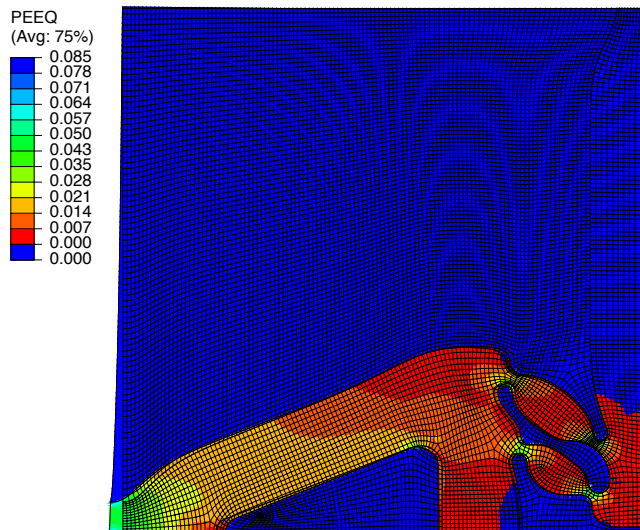


Figure 6.31: Equivalent plastic strain at the end of the auxetic behaviour

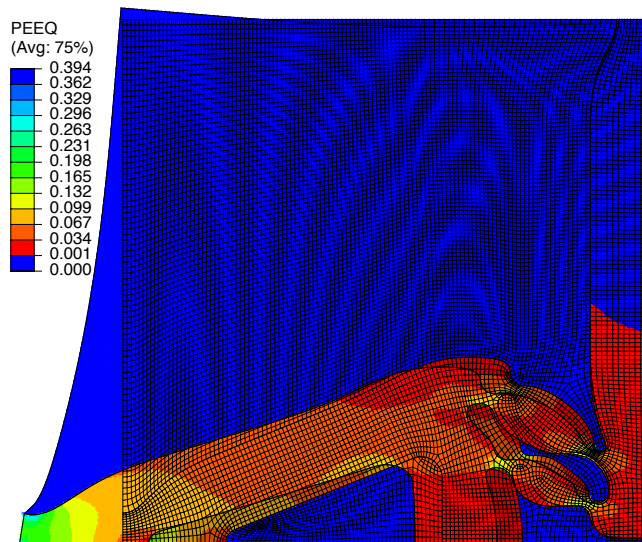


Figure 6.32: Equivalent plastic strain at the end of analysis (no auxetic behaviour)

CHAPTER 7

Conclusions & Future work

7.1 Achievements of the thesis

The proposed hybrid scheme can provide applicable solutions to complex topology optimization problems such as the multi-functional compliant mechanism. For this kind of complex problems, topology optimization may produce a number of different solutions. Due to the iterative nature of topology optimization depending on the starting point of the process, it cannot be clear which of these solutions is the optimum. The use of the hybrid scheme can, in most cases, overcome this problem by combining the advantages of topology optimization and evolutionary algorithms. Hence, relatively optimal solution (close to the global optimum) can be provided. Having the above mentioned advantages, the hybrid scheme can be used as excellent conceptual design tool for any design application.

7.2 Conclusions

It is clear that topology optimization algorithm is a very powerful tool for the design of compliant mechanisms and microstructures. This tool can be extended with evolutionary algorithms in order to overcome the local minima appearing from the single application of topology optimization. The presented results indicates that the Hybrid Scheme algorithm proposed here leads to solutions for very large scale topology optimization problems that classical or stochastic based optimization tools are unable to find solutions due to huge amount of design variables.

Two different applications were presented: the design of compliant mechanisms and auxetic materials. As it was mentioned before the design of auxetic materials is an extension of the methodology that used for the design of compliant mechanisms. The hybrid scheme used for design of compliant mechanisms, was applied with and without motion control on the output point. It was clear that motion control leads to multiobjective criteria prob-

lems with collateral constraints. Including all the criteria and constraints inside the topology optimization problem it might be very difficult. The Method of Moving Asymptotes might be used. Another way is to just set the overall objective function (the multicriteria problem converted to a single criteria) outside the topology optimization iterative process as the objective function for the evolutionary algorithm. This has the advantage of use any other evolutionary algorithm other than Differential Evolution or PSO.

For the design of auxetic materials two different methods have been used using truss and plane stress elements. In the later case classical numerical homogenization has been used, for the verification of the results obtained by topology optimization. The auxetic behaviour, as well as the effective Poisson's ratio have been verified. Furthermore, homogenization offers the information for the variation of the soft material mechanical properties, until the desired effective behaviour arises. This is considered independently of the optimization procedure. An implementation where the auxetic behaviour appears independently from the boundary conditions applied to the RVE, has also been presented to indicate auxetic behaviour. It is clear that the arising microstructures lead to auxetic phenomena. Furthermore, they are automatically generated and one cannot find them by intuition like the relatively simple microstructures of figures 6.1 and 6.2. These complicated microstructures have much more flexibility to allow fine tuning of the homogeneous parameters than any convectional microstructure.

7.3 Future work

The present work can be extended to the design of compliant mechanisms with more than two load cases, leading to more complex shapes and structures. Non-linear elasticity can be applied as well. Another area of research, could be on the design of structures with optimum homogenized properties in multiphysics (thermoelasticity, piezoelectricity). In order to improve the computational efficiency, the hybrid algorithm can be extended, by fine-tuning the DE's and PSO's running parameters, or using other techniques from the global optimization portfolio like Ant colony optimization, Simulated annealing, Genetic Algorithms to name few of them. The hybrid scheme can be easily extended to use alternative to topology optimization methods like ESO and BESO or level set methods. Since the optimization problems arising might be multi objective, multi-objective versions of DE and PSO may be used.

The results presented demonstrate that the hybrid algorithm proposed here delivers solutions for large scale topology optimization problems. Therefore topology optimization for structures and flexible mechanisms can be used as a design tool for the design of the microstructure of tailored materials. It is clear that other microstructures different than the star-shaped ones lead to the desired auxetic behaviour and can be found by using topology optimization.

Within the area of elasticity the present work can be extended to the design of anisotropic materials using linear or non-linear elasticity (load-dependent Poisson's ratio). In order to improve the computational efficiency, the hybrid algorithm can be extended, by fine-tuning the DE's running parameters, or using other global optimization techniques like Particle Swarms Optimization (PSO), genetic algorithms and others. Depending on the dimensions of the structures, for more accurate solutions plane elasticity or beam elements instead of trusses can be used.

A complete design procedure for the creation of novel auxetic microstructures has been presented here. The method can be extended to cover the design of metamaterials in multiphysics applications, like the design of thermoelastic microstructures with negative thermal expansion rate, in magneto-electronics etc. Further extensions of this work include the study of nonlinear instantaneous negative Poisson's effect.

The design of auxetics can be transferred to reality by using 3d printing (in two dimensions with constant thickness) to construct one of the final material distributions shown in figures 6.11 and 6.12. As a first step one should transfer the final quarter topology into a CAD system and create a two dimensional model using splines. Special attention should be given where hinges appear. Later a special CAD oriented optimization tool can be used in order to model and optimize the hinge geometry and may take into account material fatigue issues. Finishing this step, a 2d pattern of the final CAD optimized topology can be modelled and 3d printed in a rapid prototyping machine. A very good example of a 3d auxetic material is described in [ALS14].

Further research towards coupling topology optimization and homogenization in nonlinear problems with large deformations, material nonlinearity and contact mechanics are left for future investigation.

7.3.1 Publications

During the funding program HERACLITOUS II the following journal and conference papers were published:

- journal papers:
 - Kaminakis, N., Stavroulakis, G.E. (2012). "*Topology optimization for compliant mechanisms, using evolutionary algorithms and application on the design of auxetic materials*", JCOMB Composites Part B: Engineering (Elsevier), vol. 43(6), pp. 2655-2668.
 - Kaminakis, N., Stavroulakis, G.E. (2012). "*Design of auxetic microstructures using topology optimization*", Structural Longevity, vol. 8(1), pp. 1-6.
 - Kaminakis N., Drosopoulos G.A. and Stavroulakis G.E. (2014). "*Design and verification of auxetic microstructures using topology optimization and homogenization*", Archive of Applied Mechanics. September 2015, Volume 85, Issue 9, pp. 1289-1306
 - G.A. Drosopoulos, N. Kaminakis, N. Papadogianni and G.E. Stavroulakis (2015). "*Mechanical behaviour of auxetic microstructures using contact mechanics and elastoplasticity*", Key Engineering Materials, vol. 681, pp. 110-116.
- conference papers:
 - Stavroulakis G.E., Kaminakis N. and Drosopoulos G.A. (2013). "*Auxetic Microstructures: Topology Optimization and Numerical Homogenization*". **8th German – Greek – Polish Symposium: "Recent Advances in Mechanics"**, 9-13 September 2013, Goslar, Germany.
 - Kaminakis, N., Stavroulakis, G.E. (2013). "*Topology Optimization of multi-functional structures and mechanisms using global and multicriteria optimization.*". Poster Presentation in **Summer School: Topology Optimization - Theory, Methods and Applications**, organized by: Dep. of Mechanical Engineering, Dep. of Applied Mathematics and Computer Science, Dep. of Wind Energy. Technical University of Denmark (DTU), 19-25 June 2003, Lyngby, Denmark.
 - Fetsi V., Kaminakis N., Stavroulakis G.E. (2013). "*Design and Topology optimization of Horizontal axis wind turbine rotor*". **10th HSTAM International Congress on Mechanics**", 25 - 27 May 2013, Chania, Crete, Greece.
 - Kaminakis, N., Stavroulakis, G. (2012). "*Design of Auxetic Materials using Topology Optimization of Flexible mechanisms and Hybrid –*

Evolutionary Algorithms". **International Conference of Computational and Experimental Engineering and Sciences ICCES12**, 30 April – 4 May 2012, Chania, Greece.

- Kaminakis, N., Stavroulakis, G. (2012). *“Design of Auxetic Materials using Topology Optimization of Flexible mechanisms and Hybrid – Evolutionary Algorithms”*. **International Conference of Computational and Experimental Engineering and Sciences ICCES12**, 30 April – 4 May 2012, Chania, Greece.
- Kaminakis, N., Stavroulakis, G.E. (2011). *“Topology Optimization & Evolutionary Algorithms for the design of flexible mechanisms: Design/Synthesis of Auxetic Material”*. **2nd World Congress on Global Optimization**, July 2011, Chania, Greece.

Bibliography

- [AJM04] G. Allaire, F. Jouve, and H. Maillot. Topology optimization for minimum stress design with the homogenization method. In: *Structural and Multidisciplinary Optimization*, **28**:2-3 (2004), 87–98 (cited on page 12).
- [AKK94] GK Ananthasuresh, Sridhar Kota, and Noboru Kikuchi. Strategies for systematic synthesis of compliant MEMS. In: *Proceedings of the 1994 ASME winter annual meeting*, (1994), 677–686 (cited on page 33).
- [Alo+13] Cristina Alonso et al. “Design of multi-input-multi-output compliant mechanisms”. In: *6th ECCOMAS Conference on Smart Structures and Materials, SMART2014*. 2013 (cited on page 11).
- [ALS14] Erik Andreassen, Boyan S. Lazarov, and Ole Sigmund. Design of manufacturable 3D extremal elastic microstructure. In: *Mechanics of Materials*, **69**:1 (2014), 1–10 (cited on pages 12, 136).
- [Ame14] Scientific American. *First Flexible Airplane Wing Takes Flight*. 2014. URL: <http://blogs.scientificamerican.com/observations/first-flexible-airplane-wing-takes-flight/> (cited on page 10).
- [ASM06] ASME. *Guide for verification and validation in computational solid mechanics*. American Society of Mechanical Engineers, 2006 (cited on page 12).
- [Ban+98] Wolfgang Banzhaf et al. *Genetic Programming: An Introduction: on the Automatic Evolution of Computer Programs and Its Applications*. San Francisco, CA, USA: Morgan Kaufmann Publishers Inc., 1998 (cited on page 45).
- [Ben89] M. P. Bendsøe. Optimal shape design as a material distribution problem. In: *Structural and Multidisciplinary Optimization*, **1**:4 (1989), 193–202 (cited on pages 8, 16).

- [Ben95] M. P. Bendsøe. *Optimization of structural topology, shape, and material*. Springer, 1995 (cited on page 10).
- [BK88] Martin Philip Bendsøe and Noboru Kikuchi. Generating optimal topologies in structural design using a homogenization method. In: *Computer Methods in Applied Mechanics and Engineering*, 71:2 (November 1988), 197–224 (cited on pages 8, 10, 27).
- [Bre+91] M. Bremicker et al. Integrated Topology and Shape Optimization in Structural Design®. In: *Mechanics of Structures and Machines*, 19:4 (1991), 551–587 (cited on page 122).
- [BRS08] R. Balamurugan, C.V. Ramakrishnan, and Nidur Singh. Performance evaluation of a two stage adaptive genetic algorithm (TSAGA) in structural topology optimization. In: *Applied Soft Computing*, 8:4 (2008). *Soft Computing for Dynamic Data Mining*, 1607–1624 (cited on page 41).
- [BRS11] R. Balamurugan, C.V. Ramakrishnan, and N. Swaminathan. A two phase approach based on skeleton convergence and geometric variables for topology optimization using genetic algorithm. English. In: *Structural and Multidisciplinary Optimization*, 43:3 (2011), 381–404 (cited on page 41).
- [BS03] M. P. Bendsøe and Ole Sigmund. *Topology Optimization – Theory, methods and applications*. 2nd edition. Springer, 2003 (cited on pages 10, 11, 30, 33).
- [BW89] G. Beni and J. Wang. “Swarm intelligence in cellular robotic systems”. In: *NATO Advanced Workshop on Robotics and Biological Systems*. June 1989 (cited on page 56).
- [Car+13] Alessandro Cardillo et al. Multi-objective topology optimization through GA-based hybridization of partial solutions. In: *Engineering with Computers*, 29:3 (2013), 287–306 (cited on page 64).
- [CF00] S. Canfield and M. Frecker. Topology optimization of compliant mechanical amplifiers for piezoelectric actuators. In: *Structural and Multidisciplinary Optimization*, 20:4 (4 2000), 269–279 (cited on page 10).
- [Chi+94] M. Chirehdast et al. Structural Configuration Examples of an Integrated Optimal Design Process. In: *Journal of Mechanical Design*, 116:4 (December 1994), 997–1004 (cited on page 122).

- [Cre15] Encyclopedia of Creation Science. *Genetic algorithm*. 2015. URL: http://creationwiki.org/Genetic_algorithm (cited on page 46).
- [DBA08] C. Dascalu, G. Bilbie, and E. K. Agiasofitou. Damage and size effects in elastic solids: A homogenization approach. In: *Int J Solids Struct*, **45**:2 (2008), 409–430 (cited on page 12).
- [DFJ12] J. Dirrenberger, S. Forest, and D. Jeulin. Elastoplasticity of auxetic materials. In: *Computational Materials Science*, **64**: (2012). Proceedings of the 21st International Workshop on Computational Mechanics of Materials (IWCMM 21), 57–61 (cited on page 132).
- [Dro+15] Georgios A. Drosopoulos et al. Mechanical Behaviour of Auxetic Microstructures Using Contact Mechanics and Elastoplasticity. In: *Key Engineering Materials*, **681**: (2015), 110–116 (cited on pages 129, 132).
- [DS95] A. Díaz and O. Sigmund. Checkerboard patterns in layout optimization. In: *Structural optimization*, **10**:1 (1995), 40–45 (cited on page 23).
- [DWS13a] Georgios A. Drosopoulos, Peter Wriggers, and Georgios E. Stavroulakis. “Contact analysis in multi-scale computational homogenization”. In: *Proceedings of 3rd international conference on computational modeling of fracture and failure of materials and structures (CFRAC)*. Edited by M. Jirásek et al. Prague, Czech Republic, 2013, 226 (cited on page 12).
- [DWS13b] Georgios A. Drosopoulos, Peter Wriggers, and Georgios E. Stavroulakis. “Incorporation of contact mechanics in multi-level computational homogenization for the study of composite materials”. In: *Proceedings of 3rd international conference on computational contact mechanics (ICCCM)*. Lecce, Italy, 2013 (cited on page 12).
- [EK95] R. Eberhart and J. Kennedy. “A new optimizer using particle swarm theory”. In: *Micro Machine and Human Science, 1995. MHS '95., Proceedings of the Sixth International Symposium on*. 1995, 39–43 (cited on page 57).
- [ES03] Agoston E. Eiben and J. E. Smith. *Introduction to Evolutionary Computing*. SpringerVerlag, 2003 (cited on page 45).
- [Feo06] Vitaliy Feoktistov. *Differential Evolution: In search of solutions*. Secaucus, NJ, USA: Springer-Verlag New York, Inc., 2006 (cited on page 48).

- [FKK99] M. Frecker, N. Kikuchi, and S. Kota. Topology optimization of compliant mechanisms with multiple outputs. In: *Structural optimization*, **17**:4 (1999), 269–278 (cited on page 10).
- [Fle15] FlexSys. *Compliant mechanisms advantages*. 2015. URL: <http://www.flxsys.com/compliant> (cited on page 10).
- [FOW66] L.J. Fogel, A.J. Owens, and M.J. Walsh. *Artificial intelligence through simulated evolution*. Chichester, WS, UK: Wiley, 1966 (cited on page 44).
- [GA13] Rivka Gilat and Jacob Aboudi. Behavior of Elastoplastic Auxetic Microstructural Arrays. In: *Materials*, **6**:3 (2013), 726–737 (cited on page 132).
- [Gal38] Galilei Galileo. *Discorsi e Dimostrazioni Matematiche Intorno a Due Nuove Scienze*. 1638 (cited on page 5).
- [GKB10] M. G. D. Geers, V. Kouznetsova, and W. A. M. Brekelmans. Multi-scale computational homogenization: Trends and challenges. In: *J Comput Appl Math*, **234**:7 (2010), 2175–2182 (cited on page 12).
- [Gol02] David E. Goldberg. *The Design of Innovation: Lessons from and for Competent Genetic Algorithms*. Norwell, MA, USA: Kluwer Academic Publishers, 2002 (cited on page 44).
- [Gol89] David E. Goldberg. *Genetic Algorithms in Search, Optimization and Machine Learning*. 1st. Boston, MA, USA: Addison-Wesley Longman Publishing Co., Inc., 1989 (cited on page 44).
- [Gor78] J.E. Gordon. *Structures or Why Things Don't Fall Down*. Penguin Books, 1978 (cited on page 5).
- [Hil63] R. Hill. Elastic properties of reinforced solids: Some theoretical principles. In: *J Mech Phys Solids*, **11**:5 (1963), 357–372 (cited on page 114).
- [Hol62] John H. Holland. Outline for a logical theory of adaptive systems. In: *JACM*, **9**:3 (1962), 297–314 (cited on page 44).
- [Hol92] John H. Holland. *Adaptation in Natural and Artificial Systems*. Cambridge, MA, USA: MIT Press, 1992 (cited on page 44).
- [JH96] Chandrashekhar S. Jog and Robert B. Haber. Stability of finite element models for distributed-parameter optimization and topology design. In: *Computer Methods in Applied Mechanics and Engineering*, **130**:3–4 (1996), 203–226 (cited on page 23).

- [Jia+11] Haipeng Jia et al. Evolutionary level set method for structural topology optimization. In: *Computers & Structures*, **89**:5–6 (2011), 445–454 (cited on page 8).
- [JS10] Chandini Jain and Anupam Saxena. An Improved Material-Mask Overlay Strategy for Topology Optimization of Structures and Compliant Mechanisms. In: *Journal of Mechanical Design*, **132**:6 (May 2010), 061006–061006 (cited on page 41).
- [KA08] Girish Krishnan and G. K. Ananthasuresh. Evaluation and design of displacement-amplifying compliant mechanisms for sensor applications. In: *J Mech Design*, **130**:10 (2008) (cited on page 10).
- [Kan+09] P. Kanouté et al. Multiscale methods for composites: A review. In: *Archives of Computational Methods in Engineering*, **16**:1 (2009), 31–75 (cited on page 12).
- [Kav+08] A. Kaveh et al. Structural topology optimization using ant colony methodology. In: *Engineering Structures*, **30**:9 (2008), 2559–2565 (cited on page 42).
- [KDS15] Nikos T. Kaminakis, Georgios A. Drosopoulos, and Georgios E. Stavroulakis. Design and verification of auxetic microstructures using topology optimization and homogenization. In: *Archive of Applied Mechanics*, **85**:9-10 (2015), 1289–1306 (cited on page 8).
- [KE01] James Kennedy and Russell C. Eberhart. *Swarm Intelligence*. San Francisco, CA, USA: Morgan Kaufmann Publishers Inc., 2001 (cited on page 57).
- [KE95] J. Kennedy and R. Eberhart. “Particle swarm optimization”. In: *Neural Networks, 1995. Proceedings., IEEE International Conference on*. Volume 4. 1995, 1942–1948 (cited on page 57).
- [Kot+03] Sridhar Kota et al. *Design and application of compliant mechanisms for morphing aircraft structures*. 2003 (cited on page 10).
- [Kou02] V.G. Kouznetsova. *Computational homogenization for the multi-scale analysis of multi-phase materials*. PhD thesis. The Netherlands: Technical University Eindhoven, 2002 (cited on pages 12, 114).
- [Koz92] John R. Koza. *Genetic Programming: On the Programming of Computers by Means of Natural Selection*. Cambridge, MA, USA: MIT Press, 1992 (cited on page 45).
- [Koz94] John R. Koza. *Genetic Programming II: Automatic Discovery of Reusable Programs*. Cambridge, MA, USA: MIT Press, 1994 (cited on page 45).

- [KS12] Nikolaos T. Kaminakis and Georgios E. Stavroulakis. Topology optimization for compliant mechanisms, using evolutionary-hybrid algorithms and application to the design of auxetic materials. In: *Composites Part B: Engineering*, **43**:6 (2012), 2655–2668 (cited on pages [8](#), [10](#), [12](#), [13](#)).
- [Liu06] Q. Liu. *Literature Review: Materials with negative Poisson's ratios and potential applications to aerospace and defence*. Technical report DSTO-GD-0472. Air Vehicles Division, Defence Science and Technology Organisation, Department of Defence, Australian Government, 2006 (cited on page [11](#)).
- [LL09] Guan-Chun Luh and Chun-Yi Lin. Structural topology optimization using ant colony optimization algorithm. In: *Applied Soft Computing*, **9**:4 (2009), 1343–1353 (cited on page [42](#)).
- [LLL11] Guan-Chun Luh, Chun-Yi Lin, and Yu-Shu Lin. A binary particle swarm optimization for continuum structural topology optimization. In: *Applied Soft Computing*, **11**:2 (2011), 2833–2844 (cited on page [42](#)).
- [LSB97] U.D. Larsen, Ole Sigmund, and S. Bouwstra. Design and fabrication of compliant mechanisms and material structures with negative Poissons ratio. In: *J MicroElectroMech S*, **6**:2 (1997), 99–106 (cited on pages [10](#), [13](#)).
- [MA07] N. D. Mankame and G. K. Ananthasuresh. Synthesis of contact-aided compliant mechanisms for non-smooth path generation. In: *International Journal for Numerical Methods in Engineering*, **69**:12 (2007), 2564–2605 (cited on page [10](#)).
- [Mar97] Frecker Mary. *Optimal design of compliant mechanisms*. PhD thesis. Department of Mechanical Engineering, University of Michigan, Ann Arbor; 1997 (cited on page [33](#)).
- [MCE04] A.G.M. Michell M.C.E. The limits of economy of material in frame-structures. In: *Philosophical Magazine Series 6*, **8**:47 (1904), 589–597 (cited on page [8](#)).
- [Mic96] Zbigniew Michalewicz. *Genetic Algorithms + Data Structures = Evolution Programs (3rd Ed.)* London, UK, UK: Springer-Verlag, 1996 (cited on page [44](#)).

- [MLF09] Vipul Mehta, George A. Lesieutre, and Mary Frecker. Stress relief in contact-aided compliant cellular mechanisms. In: *Journal of Mechanical Design*, **131**:9 (August 2009), 091009–091009 (cited on page 10).
- [MPG07] T. J. Massart, R. H. J. Peerlings, and M. G. D. Geers. Structural damage analysis of masonry walls using computational homogenization. In: *Int J Damage Mech*, **16**:2 (2007), 199–226 (cited on page 12).
- [MPR10] J.F.Aguilar Madeira, H.L. Pina, and H.C. Rodrigues. GA topology optimization using random keys for tree encoding of structures. English. In: *Structural and Multidisciplinary Optimization*, **40**:1–6 (2010), 227–240 (cited on page 41).
- [MRP06] J.Aguilar Madeira, H.C. Rodrigues, and H. Pina. Multiobjective topology optimization of structures using genetic algorithms with chromosome repairing. In: *Structural and Multidisciplinary Optimization*, **32**:1 (2006), 31–39 (cited on pages 11, 42).
- [NTN13] P. B. Nakshatrala, D. A. Tortorelli, and K. B. Nakshatrala. Non-linear structural design using multiscale topology optimization. Part I: Static formulation. In: *Comput Methods Appl Mech Eng*, **261–262**: (2013), 167–176 (cited on page 12).
- [OS88] Stanley Osher and James A Sethian. Fronts propagating with curvature–dependent speed: Algorithms based on Hamilton–Jacobi formulations. In: *Journal of Computational Physics*, **79**:1 (1988), 12–49 (cited on page 8).
- [Pap+96] Manolis Papadrakakis et al. Advanced solution methods in topology optimization and shape sensitivity analysis. In: *Engineering Computations*, **13**:5 (1996), 57–90 (cited on page 64).
- [Pap+98] Manolis Papadrakakis et al. Advanced solution methods in structural optimization based on evolution strategies. In: *Engineering Computations*, **15**:1 (1998), 12–34 (cited on page 64).
- [PBS01] Claus B. Wittendorf Pedersen, Thomas Buhl, and Ole Sigmund. Topology synthesis of large-displacement compliant mechanisms. In: *Int J Numer Methods Eng*, **50**:12 (2001), 2683–2706 (cited on page 11).

- [PC90] Panos Y. Papalambros and Mehran Chirehdast. An Integrated Environment for Structural Configuration Design. In: *Journal of Engineering Design*, **1:1** (1990), 73–96 (cited on page 122).
- [Pin+09] M. J. Pindera et al. Micromechanics of spatially uniform heterogeneous media: A critical review and emerging approaches. In: *Comp Part B: Eng*, **40:5** (2009), 349–378 (cited on page 12).
- [PLT98] Manolis Papadrakakis, Nikos D. Lagaros, and Yiannis Tsompatakis. Structural optimization using evolution strategies and neural networks. In: *Computer Methods in Applied Mechanics and Engineering*, **156:1–4** (1998), 309–333 (cited on page 64).
- [PS00] H. E. Pettermann and S. Suresh. A comprehensive unit cell model: A study of coupled effects in piezoelectric 1–3 composites. In: *Int J Solids Struct*, **37:39** (2000), 5447–5464 (cited on page 12).
- [PSL05] Kenneth V. Price, Rainer M. Storn, and Jouni A. Lampinen. *Differential Evolution – A practical approach to global optimization*. Natural Computing Series. Berlin, Germany: Springer-Verlag, 2005 (cited on pages 48, 54).
- [PW00] Panos Y. Papalambros and Douglass J. Wilde. *Principles of Optimal Design*. Second. Cambridge Books Online. Cambridge University Press, 2000 (cited on page 5).
- [QSX00] O.M. Querin, G.P. Steven, and Y.M. Xie. Evolutionary structural optimisation using an additive algorithm. In: *Finite Elements in Analysis and Design*, **34:3–4** (2000), 291–308 (cited on page 8).
- [Que+00] O.M. Querin et al. Computational efficiency and validation of bi-directional evolutionary structural optimisation. In: *Computer Methods in Applied Mechanics and Engineering*, **189:2** (2000), 559–573 (cited on page 8).
- [Rec73] I. Rechenberg. *Evolutionsstrategie - Optimierung technischer Systeme nach Prinzipien der biologischen Evolution*. Fromman-Holzboog, 1973 (cited on page 44).
- [Roz09] G. Rozvany. A critical review of established methods of structural topology optimization. In: *Structural and Multidisciplinary Optimization*, **37:3** (January 2009), 217–237 (cited on page 16).
- [Roz89] George I. N. Rozvany. *Structural design via optimality criteria*. Kluwer Academic Publishers, 1989 (cited on page 22).

- [RS05] S. Rahmatalla and C. C. Swan. Sparse monolithic compliant mechanisms using continuum structural topology optimization. In: *International Journal for Numerical Methods in Engineering*, **62**:12 (2005), 1579–1605 (cited on page 33).
- [RZB92] G.I.N. Rozvany, M. Zhou, and T. Birker. Generalized shape optimization without homogenization. In: *Structural optimization*, **4**:3–4 (1992), 250–252 (cited on page 8).
- [San80] E. Sanchez-Palencia. *Non-homogeneous media and vibration theory*. Lecture notes in physics. Berlin: Springer, 1980 (cited on page 12).
- [SB11] Mathias Stolpe and Martin P. Bendsøe. Global optima for the Zhou–Rozvany problem. In: *Structural and Multidisciplinary Optimization*, **43**:2 (2011), 151–164 (cited on page 41).
- [Sch93] Hans-Paul Schwefel. *Evolution and Optimum Seeking: The Sixth Generation*. New York, NY, USA: John Wiley & Sons, Inc., 1993 (cited on page 44).
- [Sig01] Ole Sigmund. A 99 line topology optimization code written in matlab. In: *Struct Multidisc Optim*, **21**:2 (2001), (cited on page 11).
- [Sig11] Ole Sigmund. On the usefulness of non-gradient approaches in topology optimization. In: *Struct Multidisc Optim*, **43**:5 (2011), 589–596 (cited on pages 11, 42).
- [Sig96] Ole Sigmund. *Some inverse problems in topology design of materials and mechanisms*. In: *Proc. of the IUTAM Symposium on Optimization of Mechanical Systems*. Kluwer, 1996, 277–284 (cited on page 10).
- [SP70] Richard T. Shield and William Prager. Optimal structural design for given deflection. In: *Zeitschrift für angewandte Mathematik und Physik ZAMP*, **21**:4 (1970), 513–523 (cited on page 33).
- [SP95] Rainer Storn and Kenneth Price. *Differential Evolution - A simple and efficient adaptive scheme for global optimization over continuous spaces*. 1995 (cited on page 48).
- [SP98] Ole Sigmund and J. Petersson. Numerical instabilities in topology optimization: A survey on procedures dealing with checkerboards, mesh-dependencies and local minima. In: *Struct Optimization*, **16**: (1998), 68–75 (cited on page 24).

- [SSB85] P.M. Suquet, A. Sawczuk, and G. Bianchi. *Local and global aspects in the mathematical theory of plasticity, plasticity today: Modelling, methods and applications*. London: Elsevier, 1985, 279–310 (cited on page 12).
- [ST99] Ole Sigmund and S. Torquato. Design of smart composite materials using topology optimization. In: *Smart Mater Struct*, 8: (1999), 365–379 (cited on page 10).
- [Sto03] Mathias Stolpe. *On Models and Methods for Global On Models and Methods for Global Optimization of Structural Topology*. PhD thesis. Optimization and Systems Theory, Department of Mathematics, Royal Institute of Technology, 2003 (cited on page 41).
- [Sva87] Krister Svanberg. The method of moving asymptotes—a new method for structural optimization. In: *International Journal for Numerical Methods in Engineering*, 24:2 (1987), 359–373 (cited on page 32).
- [SZ99] J. Sokolowski and A. Zochowski. On the Topological Derivative in Shape Optimization. In: *SIAM J Control Optim*, 37:4 (April 1999), 1251–1272 (cited on page 8).
- [TSP97] P. S. Theocaris, G. E. Stavroulakis, and P. D. Panagiotopoulos. Negative Poisson’s ratios in composites with star-shaped inclusions: a numerical homogenization approach. In: *Arch Appl Mech*, 67:4 (1997), 274–286 (cited on pages 100, 101).
- [WT05] S.Y. Wang and K. Tai. Structural topology design optimization using Genetic Algorithms with a bit-array representation. In: *Computer Methods in Applied Mechanics and Engineering*, 194:36–38 (2005), 3749–3770 (cited on pages 11, 42).
- [WT10] Chun-Yin Wu and Ko-Ying Tseng. Topology optimization of structures using modified binary differential evolution. English. In: *Structural and Multidisciplinary Optimization*, 42:6 (2010), 939–953 (cited on page 42).
- [XS93] Y.M. Xie and G.P. Steven. A simple evolutionary procedure for structural optimization. In: *Computers & Structures*, 49:5 (1993), 885–896 (cited on pages 8, 11).
- [Yoo+04] G.H. Yoon et al. Hinge-free topology optimization with embedded translation-invariant differentiable wavelet shrinkage. In: *Structural and Multidisciplinary Optimization*, 27:3 (2004), 139–150 (cited on page 111).

- [ZW08] T. I. Zohdi and Peter Wriggers. *An introduction to computational micromechanics*. The Netherlands: Springer, 2008 (cited on pages 12, 13).

